

Quantum Position Verification with Remote Untrusted Devices

Gautam A. Kavuri,^{1,2,*} Yanbao Zhang,^{3,†} Abigail R. Gookin,^{4,2} Soumyadip Patra,⁵ Joshua C. Bienfang,⁶ Honghao Fu,⁷ Yusuf Alnawakhtha,⁸ Dileep V. Reddy,^{1,2} Michael D. Mazurek,^{1,2} Carlos Abellán,⁹ Waldimar Amaya,⁹ Morgan W. Mitchell,^{10,11} Sae Woo Nam,^{1,12} Carl A. Miller,^{13,8} Richard P. Mirin,¹² Martin J. Stevens,¹² Scott Glancy,^{14,1} Emanuel Knill,^{14,1,15} and Lynden K. Shalm^{1,12,16,‡}

¹*Department of Physics, University of Colorado, Boulder, CO, 80309, USA*

²*Associate of the National Institute of Standards and Technology, Boulder, CO, 80305, USA*

³*Quantum Information Science Section,*

Computational Sciences and Engineering Division,

Oak Ridge National Laboratory, Oak Ridge, TN, 37831, USA

⁴*Department of Electrical, Computer, and Energy Engineering, University of Colorado, Boulder, CO, 80309, USA*

⁵*Department of Mathematics, University of New Orleans, New Orleans, LA, 70148, USA*

⁶*Joint Quantum Institute, National Institute of Standards and Technology and University of Maryland, 100 Bureau Drive, Gaithersburg, MD, 20899, USA.*

⁷*Concordia Institute for Information Systems Engineering, Concordia University, Montreal, QC, H3G 1M8, Canada*

⁸*Joint Center for Quantum Information and Computer Science, University of Maryland, College Park, MD, 20742, USA*

⁹*Quside Technologies S.L., Castelldefels (Barcelona), Spain*

¹⁰*ICFO-Institut de Ciències Fotoniques,*

The Barcelona Institute of Science and Technology, 08860 Castelldefels (Barcelona), Spain.

¹¹*ICREA - Institució Catalana de Recerca i Estudis Avançats, 08010, Barcelona, Spain*

¹²*Physical Measurement Laboratory, National Institute of Standards and Technology, Boulder, CO, 80305, USA*

¹³*Computer Security Division, National Institute of Standards and Technology, Gaithersburg, MD, 20899, USA*

¹⁴*Applied and Computational Mathematics Division, National Institute of Standards and Technology, Boulder, CO, 80305, USA*

¹⁵*Center for Theory of Quantum Matter,*

University of Colorado, Boulder, CO, 80305, USA

¹⁶*Quantum Engineering Initiative, Department of Electrical, Computer, and Energy Engineering, University of Colorado, Boulder, CO, 80309, USA*

(Dated: January 26, 2026)

Many applications require or benefit from being able to securely localize remote parties. In classical physics, adversaries can in principle have complete knowledge of such a party's devices, and secure localization is fundamentally impossible. This limitation can be overcome with quantum technologies, but proposals to date require trusting vulnerable hardware. Here we develop and experimentally demonstrate a protocol for device-independent quantum position verification that guarantees security with only observed correlations from a loophole-free Bell test across a quantum

network. The protocol certifies the position of a remote party against adversaries who, before each instance of the test, are weakly entangled, but otherwise have unlimited quantum computation and communication capabilities. Our demonstration achieves a one-dimensional localization that is 2.47(2) times smaller than the best, necessarily non-remote, classical localization protocol. Compared to such a classical protocol having identical latencies, the localization is 4.53(5) times smaller. This work anchors digital security in the physical world.

INTRODUCTION

Knowing where something is located forms the basis of position, navigation, and timing applications. However, proving or authenticating that information is processed at a particular location remains an open challenge. Classical localization protocols use the timing of signals to determine a position, but in principle it is always possible for adversaries to intercept and manipulate classical signals to spoof a location they do not occupy [1–4]. Using the speed of light, these protocols can then at best bound the maximum distance (proximity) to a processing node but not its location [5–7]. To remedy this, some approaches authenticate position by relying on cryptographic keys or hardware devices to avoid spoofing [5, 8]. However, these methods are insecure if secret keys are leaked or copied, if hardware security is broken, or if cryptographic hardness assumptions fail. This leaves a wide range of sensitive systems that depend on position, navigation, and timing vulnerable to location spoofing attacks. Conversely, the ability to securely verify the physical location of network participants would allow increased levels of trust in financial transactions, legal agreements, critical infrastructure, and other sensitive applications [9–12].

A viable approach to secure position verification is to use quantum signals that cannot be cloned [1, 13, 14]. However, existing protocols have stringent experimental requirements such as a low tolerance to loss [15] or make unrealistic theoretical assumptions [16] that have so far prevented an unconditional demonstration of quantum position verification [17, 18]. Furthermore, many of these schemes rely on quantum hardware that must be trusted, and not have been tampered with [19, 20]. This introduces opportunities that adversaries could exploit to compromise the security of the protocol [21–23].

Here we introduce and experimentally demonstrate a new secure quantum position verification protocol for remote parties that overcomes these limitations by utilizing loophole-free Bell tests [24, 25] across a quantum network. The protocol solves the problem of verifying that a specified target region contains a quantum device, making minimal assumptions about the internal workings of the quantum devices and achieving device-independent [26, 27] security based on analysis of inputs to and outputs from the experimental devices. We implement the protocol with two verifiers separated by 195.1(3) m, performing 335 experimental protocol instances over two days. Each protocol instance consists of a sequence of trials. Measurement outcomes and messages from the trials are recorded and determine whether the instance successfully verified position.

While we do not limit the computation or communication power of adversaries during each experimental trial, our security analysis requires a limit on the amount of entanglement

* gautam.kavuri@colorado.edu

† zhangy2@ornl.gov

‡ krister.shalm@nist.gov

shared between adversaries prior to the trial. Throughout this work, we refer to such pre-shared entanglement as prior entanglement. A basic version of the protocol is secure against adversaries who share no prior entanglement. An extended protocol demonstrates security against adversaries possessing limited prior entanglement, bounded from above by a 8×10^{-6} average robustness of entanglement [28] over the trials of a protocol instance. The security of our protocol is derived from the impossibility of faster-than-light signaling and constraints on the shareability of three-party non-signaling correlations [29]. To this end, we establish that no adversary strategy without prior entanglement can outperform strategies based on three-party non-signaling correlations.

Conditional on successfully passing our protocol, we can be confident that a prover must have performed a quantum operation in a localized target spacetime region E . Ideally, the localization could approach arbitrary precision, independent of verifier separation. In practice, it is constrained by communication and processing latencies. Using low-latency processing and communication, we are able to certify the position of a prover to a volume 4.53(5) smaller than that achievable by a comparable classical protocol that is constrained by the same latencies. Our results establish a new cryptographic primitive for quantum networks, allowing access to a secure physical location to be used to authenticate a network user. This bridges physical and network security and opens new directions for position-based cryptography and computation [1, 2].

POSITION VERIFICATION

Position verification is a cryptographic protocol that involves two or more verifiers working together to ensure that only provers with access to a target region E can pass the protocol. A key requirement is that the target region must scale favorably with increased verifier separation, remaining small and allowing position verification to be performed over large distances. In this work, we consider two verifiers **A** and **B** who rely on a version of time-of-flight ranging. Provers are allowed to move freely in spacetime. Provers with access to the target region E are called honest provers, while adversaries are provers that are trying to pass the protocol from outside the target region. Adversaries are assumed to be able to control all untrusted hardware, have access to instantaneous and unlimited computation, and have their communication constrained only by causality during a trial. However, adversaries are assumed to share limited entanglement before each trial of the protocol.

To benchmark our demonstration’s performance, we compare the size of the target region in our demonstration to the smallest achievable target region with a comparable classical protocol. In the classical protocol illustrated in Fig. 1 A, verifiers **A** and **B** start by broadcasting challenge bits u_A and u_B at times s_A and s_B , timed to arrive simultaneously at some position between them. Appropriately positioned provers are assumed to have access to these bits as soon as they are released. An honest prover **P**, or adversaries, can receive the challenge bits and use them as inputs to a predetermined function $f(u_A, u_B)$ that is publicly known. The value of this function determines the specific measurement to be performed. The measurement outcome is then sent back to **A** and **B**, who receive z_A and z_B , respectively, and jointly validate the results.

The verifiers choose the target region by deciding when they send challenges and accept responses. There are four relevant times: s_A and s_B are the times when **A** and **B** send their challenge bits, and r_A and r_B are the latest times when the verifiers accept the responses. This procedure is repeated multiple times to build confidence in the honest running of the

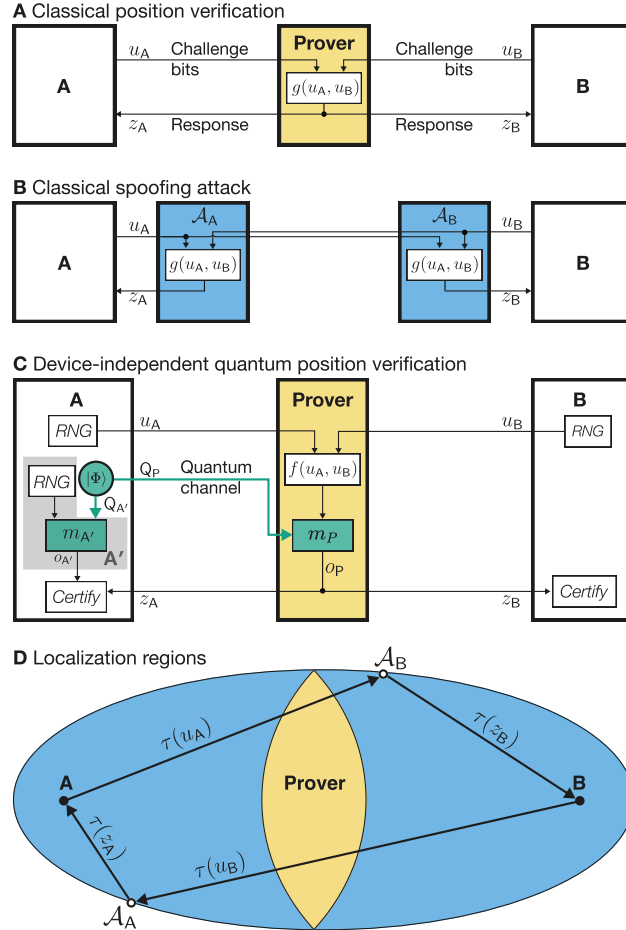


FIG. 1. Schematic representations of position verification protocols and possible attacks. Subfigure A shows an (insecure) classical protocol for position verification that tries to enforce the target region in yellow with classical challenges from the verifiers A and B. The verifiers desire that the computation $g(u_A, u_B)$ is localized to the target region. Subfigure B sketches a specific attack on the classical protocol, with adversaries \mathcal{A}_A and \mathcal{A}_B , situated in the blue regions outside the target regions, each performing the computation locally. By communicating the challenge bits to one another, they can spoof a successful pass of the classical protocol. To ensure security against general attacks perpetrated by unentangled or weakly entangled adversaries, we introduce our quantum protocol, sketched in subfigure C. Here, the honest prover P and a quantum measurement station A' located at A share an entangled state $|\Phi\rangle$. The state is measured using untrusted quantum hardware, with the measurement basis at A decided by a local random number generator and the basis at P decided by the output of $f(u_A, u_B)$. Subfigure D is a schematic of the spatial extents of the target regions enforceable by the classical (blue and yellow) and quantum (yellow) protocols, projected into two-dimensions for the specific case of a realistic two-verifier protocol.

protocol. Repeated late responses, or trials where $z_A \neq z_B$ will result in failure with high likelihood. We show in the Supplementary Information Sect. V A that target regions for the classical protocol and our quantum protocol are determined by the speed of light c and the

four time intervals

$$\Delta\tau_1 = (r_A - s_A)/2, \quad (1)$$

$$\Delta\tau_2 = (r_B - s_B)/2, \quad (2)$$

$$\Delta\tau_3 = r_A - s_B, \quad (3)$$

$$\Delta\tau_4 = r_B - s_A. \quad (4)$$

For intuition, consider that the impossibility of superluminal signaling constrains the locations from which a stationary prover can receive u_A and reply to verifier **A** to points in a sphere $S(\mathbf{A}, c\Delta\tau_1)$ of radius $c \times \Delta\tau_1$ centered on **A**. Similarly, $c \times \Delta\tau_2$ is the radius of an analogous sphere $S(\mathbf{B}, c\Delta\tau_2)$ centered on **B**. The set of all locations from which a stationary prover can receive u_B (released at s_B) and respond to verifier **A** is a prolate ellipsoid $E(\mathbf{A}, \mathbf{B}; c\Delta\tau_3)$ with the verifier **A** and **B** locations as foci, and major axis $c \times \Delta\tau_3$. Prolate ellipsoids are the set of all points such that the sum of the distances from the verifiers is less than or equal to the major axis. This means any prover outside this shape could not receive u_B and reply to **A** within r_A . An analogous ellipsoid $E(\mathbf{A}, \mathbf{B}; c\Delta\tau_4)$ constrains receiving u_A and replying to **B**.

If the verifiers can ensure that they only ever interact with a single prover, the target region is the intersection of all the regions listed above, $S_{\text{single}} = S(\mathbf{A}, c\Delta\tau_1) \cap S(\mathbf{B}, c\Delta\tau_2) \cap E(\mathbf{A}, \mathbf{B}; c\Delta\tau_3) \cap E(\mathbf{A}, \mathbf{B}; c\Delta\tau_4)$. A projection of this region to a 2-D plane for a particular choice of release and receive times is indicated in yellow in Fig. 1 d). This single-prover target region could be made arbitrarily small if one could approach zero-latency processing and direct speed-of-light transmission. However, the verifiers have no way to enforce the single-prover assumption in practice, and must allow for multiple interacting provers. As we show in the Supplementary Information Sect. V A, multiple adversaries can use the ‘‘classical spoofing’’ protocol, shown in Fig. 1 B, to pass the protocol, provided they have access to the larger region $S_{\text{multi}} = \left(S(\mathbf{A}, c\Delta\tau_1) \cap E(\mathbf{A}, \mathbf{B}; c\Delta\tau_3) \right) \cup \left(S(\mathbf{B}, c\Delta\tau_2) \cap E(\mathbf{A}, \mathbf{B}; c\Delta\tau_4) \right) \supseteq S_{\text{single}}$. This spoofing is indistinguishable from an honest single-prover strategy from the verifiers’ point of view. A 2-D projection of S_{multi} is indicated with blue in Fig. 1. The target region for the classical protocol S_{multi} precludes remote position verification because the target region includes the verifier positions themselves. While arbitrarily small target regions that include the verifier positions are always possible with straightforward ranging [30], no classical protocols admit remote position verification [2].

Our device-independent quantum position verification protocol is based on the honest prover and verifiers jointly violating a loophole-free Bell inequality as shown in Fig. 1. In addition to the previously introduced ranging capabilities, additional quantum resources are required for success. The verifiers require an entangled photon source as well as a quantum measurement station, denoted \mathbf{A}' . In principle, the measurement station \mathbf{A}' and the entangled source hardware need not be co-located at **A**, but may act as separate parties. Here we treat them as being a part of **A**’s station. A quantum channel connects **A** to the prover station that is capable of making quantum measurements on qubits. The second verifier station, **B**, does not require additional quantum capabilities. As in the classical protocol, both verifiers send classical challenge bits to the prover. In addition, the quantum verifier also sends half of an entangled photonic Bell state to the prover (\mathbf{Q}_P) while locally storing the other half $\mathbf{Q}_{A'}$. The honest prover uses the challenge bits to compute a measurement basis, which they measure the photon in. The honest prover then sends the measurement outcome to the verifiers. The verifiers record the round-trip time from when the challenge bits are sent to

when they receive the responses. While the prover is measuring their photon, the station A also performs a measurement on its half of the entangled photon state in a basis determined by a random number generator. This procedure is repeated many times in a series of trials.

The target region E and A's quantum measurements are space-like separated from one another, meaning that no information about the setting choice or outcome at A' reaches the target region before the prover's measurement is completed. The target region E for the quantum protocol is determined in the Supplementary Information Sect. V A and is the same as the single-prover target region S_{single} in the classical protocol above. In principle, the quantum protocol's target region could be made arbitrarily small with instantaneous processing and direct, speed-of-light communication.

While the preceding discussion has focused on the target region in the three spatial dimensions, it can be specified in all four dimensions including time, see Sect. V A in the Supplementary Information. Given that our experiment is performed as a series of trials, the localization has a periodic structure in time.

THEORY

The security analysis (see Supplementary Information Sect. V) involves reducing general adversary strategies without prior entanglement to a simplified three-party non-signaling game. For each trial, the verifiers compute a non-negative statistic W from the trial record for this game, where W defines an optimized Bell-like inequality [31] in the following sense: in each trial, the expectation of W is guaranteed to be at most 1 for all considered adversaries, whereas its expectation is larger than 1 for an honest prover located in the target region. Intuitively, if the empirical average of W across the trials exceeds 1 by a sufficient amount, this can be taken as evidence that the prover is in the target region. To more effectively account for finite statistics, even in the presence of adversaries employing non-independent and non-identical strategies across the trials, we use the product P of the trial-wise values of W . The probability that $P \geq 1/\delta$ for adversaries outside the target region is at most δ , where δ is the soundness or security parameter which is fixed before the protocol runs; we choose $\delta = 2^{-64}$.

In a real-world setting, adversaries interacting with the verifiers A and B could be positioned at arbitrary spacetime locations and employ general coordinated strategies to appear to be in the target region [2]. Constructing a protocol that achieves a low soundness error against such adversarial strategies with untrusted, near-term, quantum hardware is a central contribution of our work. The security assumptions for the protocol include secure classical computing, known verifier laboratory locations, and physical security of the laboratories. The main additional assumption is that there is no or limited prior adversary entanglement. The detailed protocol and its assumptions are in Supplementary Information Sect. II.

To deal with arbitrary positioning of any number of non-stationary adversaries in the security analysis, we divide the spacetime region of a trial into a collection of subregions [16]. Because the experiment consists of a series of periodic trials, all relevant subregions repeat periodically in time. When focusing on a single trial, the boundaries of these subregions are fully specified by the four times introduced above (s_A , s_B , r_A , and r_B) and the locations of the verifiers. In a one-dimensional slice, these subregions are bounded by the grey lines in Fig. 2 a), see also Fig. 9 in the Supplementary Information. In each subregion that may contain adversaries, adversarial actions can be treated as a single quantum operation that takes input from causally earlier regions and delivers output to later regions.

The subregions can be combined into a pair of regions \mathcal{M}_A and \mathcal{M}_B with corresponding adversary actions \mathcal{A}_A and \mathcal{A}_B , so that any general adversary strategy can be effectively implemented by two collaborating adversaries. Region \mathcal{M}_A is close to verifier A, and adversary actions located here can receive Q_P , u_A and u_B , process them, and respond to A before r_A . Similarly, \mathcal{M}_B corresponds to the region close to B from which \mathcal{A}_B can receive all inputs (Q_P , u_A and u_B), and respond to B before time r_B . Refer to Fig. 10 and Fig. 11 in Supplementary Information for details. The adversary actions \mathcal{A}_A and \mathcal{A}_B map to two coordinating point adversaries in simplified one-dimensional treatments of position verification in the literature, such as Ref. [1]. Restrictions on the amount of prior entanglement under which our protocol remains secure can be stated in terms of the joint state available to \mathcal{A}_A and \mathcal{A}_B at the beginning of the trial. Although the source is in the secure lab of verifier A in our demonstration, our security analysis allows for adversary control of the source. Because the entanglement generated by the source has the potential to contribute to prior entanglement, it is desirable for the source emissions to be controlled to ensure that Q_P does not reach the prover location before the challenge from B as discussed in Supplementary Information Sect. II.

The timing constraints of the protocol allow only one round of communication between \mathcal{A}_A and \mathcal{A}_B , which in principle can help the adversaries coordinate their responses. However, as we show in the Supplementary Information Sect. VB, any adversary strategy without prior entanglement that makes use of this communication round can do no better in terms of maximizing the expectation of the non-negative statistic W than an appropriately modified three-party non-signaling strategy. Here, the three parties are A' , \mathcal{A}_A , and \mathcal{A}_B with inputs $m_{A'}$, m_P , and m_P and outputs $o_{A'}$, z_A , and z_B . Consequently, to ensure that the expectation of W for all adversary strategies without prior entanglement is at most 1, it suffices to verify that its maximum expectation according to all three-party non-signaling strategies does not exceed 1. Moreover, these non-signaling strategies can be further restricted to those that are symmetric in \mathcal{A}_A and \mathcal{A}_B . As shown in Ref. [29], this symmetry implies that the two-party marginals for A' and \mathcal{A}_A (or \mathcal{A}_B) must be local realistic. In contrast, the honest prover strategy is designed to produce a correlation between the prover and A' that violates local realism. These observations allow us to construct the non-negative statistic W that excludes adversary strategies with high confidence, using a rigorous formalism inspired by analysis of data from loophole-free tests of local realism [31, 32]. We also extend the security analysis to upper bound the expectation of W achievable by adversaries who pre-share limited entanglement as quantified by robustness of entanglement, and we show that our implemented honest prover can violate these bounds see Supplementary Information Sect. VD.

EXPERIMENT

In our experiment, we demonstrate successful instances of the quantum position verification protocol using two verifier stations, A and B, and a prover station, P. Each verifier is equipped with a random number generator to produce challenge bits and a time-tagging device to record detection events. Verifier A also houses an entangled photon source and a polarization measurement apparatus A' . As shown in Fig. 3, verifier stations A and B are separated by 195.1(3) m. The prover station is 92.8(1) m from verifier B. All three stations are arranged approximately collinearly, and much of our hardware is similar to past device-independent experiments [33, 34].

The protocol requires the accumulation of statistics over many trials. At the beginning of each trial, the quantum verifier A attempts to generate a pair of polarization-entangled

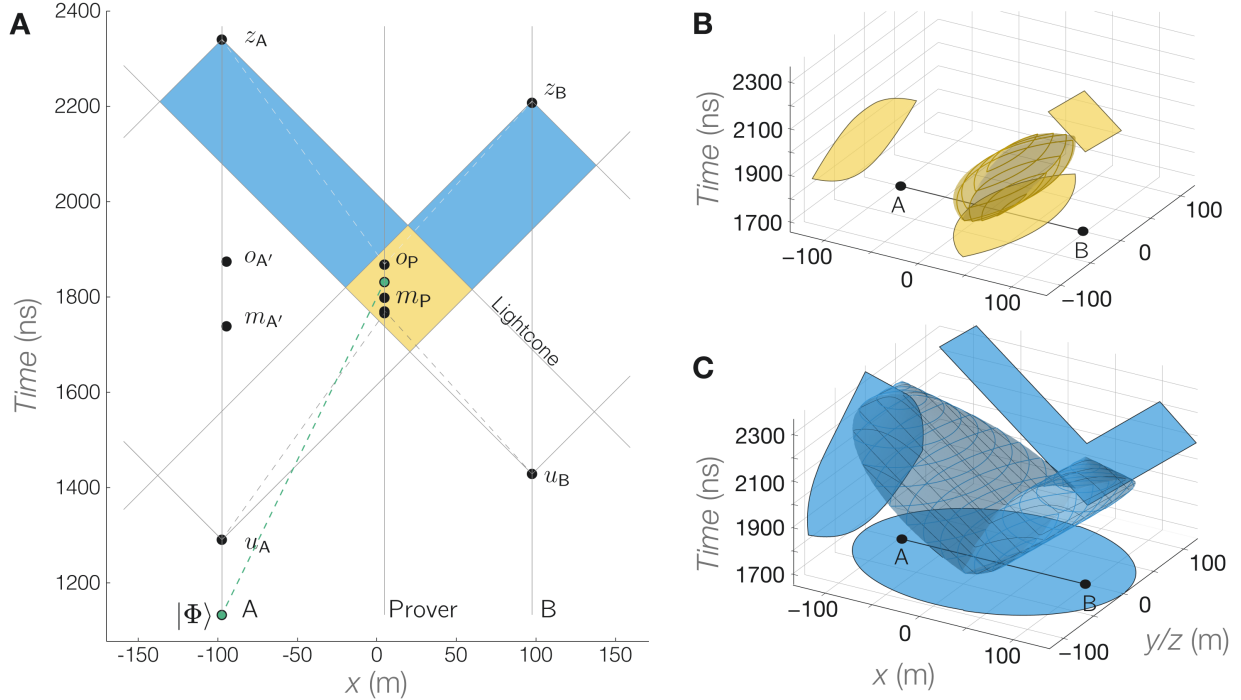


FIG. 2. Figure depicting the spacetime target regions in our protocol. Subfigure A depicts a two-dimensional spacetime slice, where the spatial dimension is along the line joining the provers, here assigned the x -axis. Both the quantum (yellow), and comparable classical (blue) regions are completely defined by forward and backward lightcones from the spacetime events corresponding to the release of u_A and u_B and the last moments when z_A and z_B are accepted. Events $o_{A'}$ and $m_{A'}$ occur at A' , which is slightly displaced from A . Subfigures B and C show three-dimensional projections of the quantum and classical target regions, with the time dimension vertically up on the page, and the spatial dimensions parallel and perpendicular to the verifier axis depicted in the other two directions. The regions are all rotationally symmetric about the verifier axis, and so are identical in the spatial dimensions (y and z) perpendicular to the verifier axis.

photons in a state close to $0.383 |HH\rangle + 0.924 |VV\rangle$, where $|H\rangle$ and $|V\rangle$ represent horizontal and vertical polarizations respectively. The target state was chosen based on a simulation numerically maximizing Bell violation. One photon is delayed locally via a fiber loop, while the other is transmitted to the prover in fiber. Each verifier then sends a randomly generated challenge bit to the prover. The challenge bits are timed to arrive at the prover station within $3(2)$ ns of each other and are transmitted using specialized coaxial cables with signal transmission speeds about 86% the speed of light.

When the challenge bits u_A, u_B arrive at the prover station, an XOR circuit is used to compute a settings bit $m_P = u_A \oplus u_B$. The prover selects their polarization measurement bases, defined as $\cos(\theta_P) |H\rangle + \sin(\theta_P) |V\rangle$, by using this bit to choose between two angles, $\theta_P \in \{6.7^\circ, -29.5^\circ\}$. The selection is implemented using a Pockels cell to rotate the polarization of the incoming photon, followed by a polarizer to perform a polarization measurement, see Fig. 3. The output of the polarizer is coupled into a single-mode fiber and incident on a superconducting nanowire detector. The result of the single-photon measurement (click

or no-click) is sent back to the verifier stations via another set of coaxial cables, where the arrival times are recorded on time tagging devices. As depicted in Fig. 2 A, the incoming photon arrives just in time for the measurement. The timing is assured by the speed of light in the fiber, which could help prevent source contributions to adversaries' prior entanglement. The source emits photon pairs in pulses at a rate much larger than the trial rates. In future experiments, it is desirable to block these unneeded photon pairs so that they cannot be utilized by adversaries to establish prior entanglement.

At nearly the same time that the prover performs its quantum measurement (see Fig. 2 a)), verifier A measures the polarization of the stored local photon $Q_{A'}$ using a similar setup. The verifier uses a local random number generator to select $m_{A'}$, which sets the polarization measurement basis $\cos(\theta_{A'}) |H\rangle + \sin(\theta_{A'}) |V\rangle$ to the angle $\theta_{A'}$ to either -6.7° or 29.26° .

The setting choice and outcome are recorded on a local time tagger. The quantum verifier and prover locations are sufficiently separated to ensure space-like separation of measurement settings and measurement outcomes at the other station, see Fig. 2.

The system operates at a rate of approximately 250,000 trials per second, limited by the operating rate of the Pockels cells. Data was recorded in 60 s intervals over two days. At the start of each day, an automated calibration routine was performed to correct for polarization drifts in the optical fiber and to ensure high coupling efficiency for the entangled photons. The measured system detection efficiency was $> 81\%$ for both verifier A and the prover station P, sufficient for an analysis that does not rely on any fair-sampling assumptions. The efficiency threshold for our protocol is $2/3$, the same as a two-party Bell test [35, 36], see Supplementary Information Sect. V B.

ANALYSIS AND RESULTS

To test our protocols, we first collected calibration data to set key parameters in our analysis. We then performed a series of quantum position verification experiments on two separate days, with data collected in 60 s chunks with each chunk containing about 15 million experimental trials. Approximately eight hours of data was collected on September 20, 2024 (day 1) and seven hours of data on October 7, 2024 (day 2). The day 1 data was reserved for testing the basic protocol against adversaries without prior entanglement, while the day 2 data was used to test the extended protocol against adversaries with prior entanglement whose robustness averaged over trials is limited by a threshold r_{th} . Based on the calibration data, the soundness parameter for both protocols was chosen to be $\delta = 2^{-64}$, and the targeted completeness, or success rate, was set to $\epsilon = 0.97725$, corresponding to a Gaussian 2σ probability of a particular protocol run successfully passing. For the extended protocol the robustness threshold was fixed at $r_{\text{th}} = 8 \times 10^{-6}$. For comparison, 2×10^{-3} is the robustness per trial of the entangled state designed to be emitted by the source, accounting for the probability of about $1/350$ that a photon pair is emitted in a trial (see Supplementary Information Sect. III B). The robustness of entanglement of a Bell state is 1. Using the calibration data, we also determined that to reach the above protocol parameters, 30 million trials (two minutes of data) were required per run of the basic protocol, and 60 million trials (four minutes of data) were needed per run of the extended protocol.

After collection, the data were compressed and placed in blind storage prior to analysis. Occasional errors where our single-photon nanowire detectors failed to properly reset, and therefore were off for one or more of the trials during a chunk were flagged. On both day 1 and day 2, the first 10 minutes of data free of detector errors were used to construct the initial

non-negative statistic W . The trials from the subsequent two or four minutes, depending on whether running the basic or extended protocol, and irrespective of detector errors, were then un-blinded and analyzed to determine the product P of the values of W witnessed by each trial record. A product $P \geq 2^{64}$ results in a pass; otherwise, that instance is considered a fail. Subsequent instances were processed sequentially using the next two or four minutes of data if available. To track long-term drifts in the experiment, we updated the non-negative statistic W before each subsequent instance, using the preceding 10 minutes of processed data without detector errors. This yielded 232 runs of the basic protocol on day 1 and 103 runs of the extended protocol on day 2. Of the 232 evaluated for the basic analysis, 224 passed (96.5%), and of the 103 evaluated for the extended analysis, 102 succeeded (99.0%). Both of these agree well with the expected completeness of $\epsilon = 0.97725$, and are shown in Fig. 4.

In each of the successful instances, the target three-dimensional volume in which a prover must perform a quantum operation is 4.53(5) times smaller than the volume they would need to be in to pass a comparable classical protocol. This is a measure of our quantum position verification advantage (QA). This comparison can also be made in two-dimensions, $\text{QA}_{\text{area}} = 4.02(3)$, and in one-dimension, $\text{QA}_{\text{length}} = 4.48(2)$. Finally, we can also compare with the ideal classical protocol in one dimension where the target region is the line segment between the two verifiers. In this case the advantage is $\text{QA}_{\text{length-ideal}} = 2.47(2)$. See Sect. IV B in the Supplementary Information for more details. Prior theory works [2, 15] often consider an ideal version of this protocol, with $\Delta\tau_1 = \Delta\tau_2 = d_{\text{AB}}/2c$ and $\Delta\tau_3 = \Delta\tau_4 = d_{\text{AB}}/c$, where d_{AB} is the verifier separation, and the other symbols are defined in Eqs. 1-4. In this case, the quantum target region reduces to a point, the best classical target region reduces to the line joining the verifiers, and the QA tends to infinity. In our experimental demonstration, processing and signal transmission latencies increase the time intervals relative to the ideal scenario, so that $\Delta\tau_1 \approx 1.6 (d_{\text{AB}}/2c)$, $\Delta\tau_2 \approx 1.2 (d_{\text{AB}}/2c)$, and $\Delta\tau_3 \approx \Delta\tau_4 \approx 1.4 (d_{\text{AB}}/c)$.

CONCLUSION

This work presents the first complete demonstration of a quantum position verification protocol—a major step forward in the development of secure quantum cryptographic primitives. Our implementation achieves strong localization guarantees and rules out powerful classes of adversaries without relying on assumptions about the internal functioning of the quantum devices involved. While the protocol as demonstrated already offers robust security within minutes, there are desirable feasible improvements: The localization can be improved by improving transmission speeds to approach the speed of light, and by reducing prover processing and measurement latencies. To improve the time required for a protocol instance, we can increase the trial rates, the probability of emitting photon pairs and the efficiencies. It is desirable to exclude adversaries with entanglement greater than that prepared by the source. A demonstrated method toward excluding adversaries with more entanglement is to increase the number of bits in the challenges $u_{\text{A}}, u_{\text{B}}$ and the complexity of the function $f(u_{\text{A}}, u_{\text{B}})$ [15, 37]. More work is required to determine whether this method can be applied to our protocol. More generally, work remains to be done to construct position-based cryptography protocols that are secure in real-world conditions [38]. We believe our protocol and demonstration will spur research in this field. Because our protocol can be run with untrusted devices, a compelling direction would be to explore protocols that can be run with

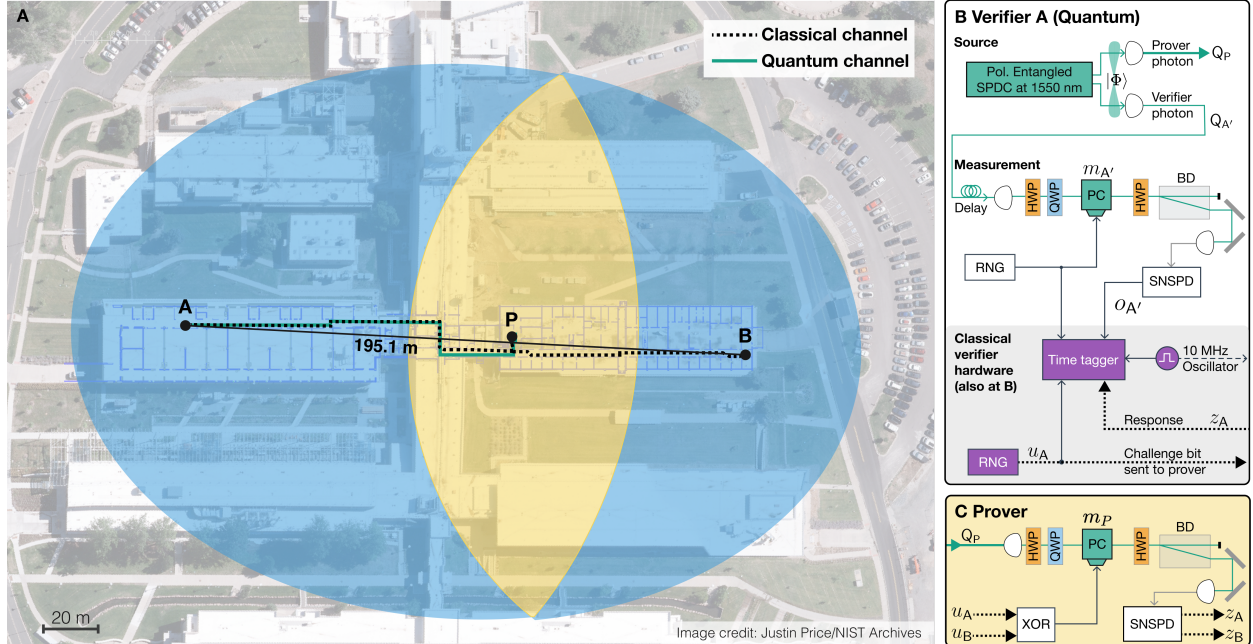


FIG. 3. Figure depicting the experimental setup and verifier and prover stations used for our demonstration. Subfigure A depicts the quantum target region E of our protocol in yellow, and the classical target region of a comparable classical protocol in blue overlaid on an aerial photograph of the NIST building, where the experiment is housed. Subfigure B shows a schematic of the hardware at verifier A. From an entangled photon pair source, one photon of the pair is sent to prover P, and the other to the measurement station A' . At measurement station A' , the incoming photon is delayed in a fiber loop and measured by a superconducting nanowire detector in a polarization basis determined by a fast Pockels cell and waveplates. The setting is chosen via a random number generator (RNG), and the outcome is recorded on a time-tagger. Subfigure C depicts the measurement station at the prover P. The choice of measurement basis here is set via an XOR of the bits u_A and u_B from the verifiers. The outcome of this measurement is sent back to both verifiers, who record it on their timetagers. SNSPD: Superconducting nanowire single photon detector; XOR: Exclusive OR; PC: Pockels cell; HWP: Half-wave plate; QWP: Quarter-wave plate.

both the entangled photon source and the measurement station A' being untrusted and located far from the verifiers. This would allow verifiers A and B to be entirely classical. Such a protocol with classical verifiers that is secure against adversaries with limited computational power is studied in Ref. [39]. Our protocol also has deep connections to device-independent random number generation [33, 34, 40, 41] protocols, another direction that merits further exploration [42].

A key challenge in modern cryptographic systems, both classical and quantum, involves authenticating the identity of parties involved. Quantum position verification protocols, like the ones presented here, offer a new paradigm for secure communications where digital authentication is directly anchored to a known physical location. This approach has the potential to profoundly reshape how trust is established in distributed systems and enables a new class of cryptographic protocols, such as position-based cryptography and computation [1, 2, 42], that increase trust in both classical and quantum communication networks.

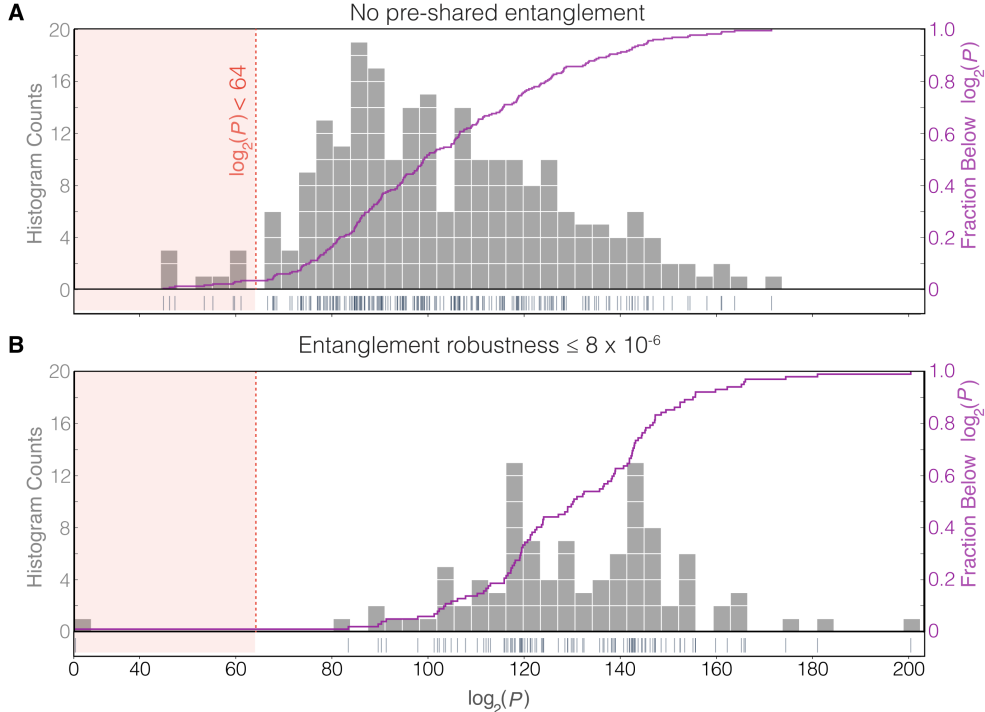


FIG. 4. Plots of results from our experimental runs. Two sets of protocol instances were run as part of our demonstration: subfigure A is day 1, analyzed for security against adversaries pre-sharing no entanglement; and subfigure B is day 2, analyzed against adversaries pre-sharing entanglement such that the average robustness over an instance’s trials is upper bounded by $r_{\text{th}} = 8 \times 10^{-6}$. The soundness target for all instances was $\delta = 2^{-64}$. Plotted are histograms of the data binned based on their calculated $\log_2(P)$ value. The $\log_2(P)$ value of each protocol instance is indicated with a tick directly above the x -axis and below the histograms on both plots. Any instances with a $\log_2(P)$ less than $-\log_2(\delta) = 64$ are declared failures, and correspond to ticks inside the red regions. Also plotted in purple is the experimental fraction of instances below $\log_2(P)$ as a function of $\log_2(P)$. At a higher $\log_2(P)$, which corresponds to a stricter choice for the soundness, a larger fraction of the data would be considered a failure, reducing success probability. The plots both share the same x -axis.

ACKNOWLEDGMENT

The authors would like to thank Peter Bierhorst and Michael Grayson for useful discussions, Yi-Kai Liu, Adam McCaughan and Aneesh Ramaswamy for close reading of the manuscript, and Daniel Sorensen for help with cable routing. The authors acknowledge support from the National Science Foundation QLCI OMA-2016244, National Science Foundation NQVL:QSTD:Pilot 2435378, the National Science Foundation ECCS 2330228, the National Science Foundation OSI 2328800, the University of Colorado Quantum Engineering Initiative, the National Institute of Standards and Technology, and the U.S. Department of Energy, Office of Science, Advanced Scientific Computing Research (Field Work Proposal ERKJ381). Yusuf Alnawakhtha acknowledges support from the Crown Prince International Scholarship Program and the Arabian Gulf University.

DISCLAIMER

Any mention of commercial products within the manuscript is for information only; it does not imply recommendation or endorsement by NIST. This work includes contributions of the National Institute of Standards and Technology, which are not subject to U.S. copyright. The U.S. Government is authorized to reproduce and distribute reprints for governmental purposes notwithstanding any copyright annotation thereon.

Additionally, this manuscript has been co-authored by UT-Battelle, LLC, under contract DE-AC05-00OR22725 with the US Department of Energy (DOE). The US government retains and the publisher, by accepting the article for publication, acknowledges that the US government retains a nonexclusive, paid-up, irrevocable, worldwide license to publish or reproduce the published form of this manuscript, or allow others to do so, for US government purposes. DOE will provide public access to these results of federally sponsored research in accordance with the DOE Public Access Plan (<http://energy.gov/downloads/doe-public-access-plan>).

DISCLOSURES

The authors declare no conflicts of interest.

AUTHOR CONTRIBUTIONS

Conceptualization: G.A.K., L.K.S., E.K. Y.Z., S.G., M.J.S., H.F., C.A.M., Y.A., A.R.G., S.P., J.C.B.; Investigation: G.A.K., A.R.G., L.K.S., M.J.S., M.D.M; Methodology: Y.Z., G.A.K., L.K.S, E.K., S.G.; Software: G.A.K., Y.Z., L.K.S., S.W.N.; Formal analysis: Y.Z., S.P., E.K., G.A.K., S.G.C., L.K.S.; Funding acquisition: L.K.S., S.W.N., R.P.M., M.J.S.; Project administration: L.K.S., E.K., M.J.S.; Resources: D.V.R., J.C.B., C.A., W.A., M.W.M.; Supervision: L.K.S., E.K., S.G., M.J.S., R.P.M.; Visualization: G.A.K., L.K.S., E.K., Y.Z.; Writing – original draft: G.A.K, E.K., L.K.S., Y.Z., S.G.; Writing – review & editing: G.A.K, E.K., Y.Z., S.G, L.K.S., S.P., A.R.G., H.F., Y.A., M.W.M., C.A.M.

-
- [1] H. Buhrman, N. Chandran, S. Fehr, R. Gelles, V. Goyal, R. Ostrovsky, and C. Schaffner, Position-Based Quantum Cryptography: Impossibility and Constructions, *SIAM Journal on Computing* **43**, 150 (2014).
 - [2] N. Chandran, V. Goyal, R. Moriarty, and R. Ostrovsky, Position-Based Cryptography, *SIAM Journal on Computing* **43**, 1291 (2014).
 - [3] N. O. Tippenhauer, K. B. Rasmussen, C. Pöpper, and S. Čapkun, Attacks on public WLAN-based positioning systems, in *Proceedings of the 7th International Conference on Mobile Systems, Applications, and Services* (ACM, Kraków Poland, 2009) pp. 29–40.
 - [4] J. Paay, J. Kjeldskov, D. Internicola, and M. Thomasen, Motivations and practices for cheating in Pokémon GO, in *Proceedings of the 20th International Conference on Human-Computer Interaction with Mobile Devices and Services* (ACM, Barcelona Spain, 2018) pp. 1–13.

- [5] G. Hancke and M. Kuhn, An RFID Distance Bounding Protocol, in *First International Conference on Security and Privacy for Emerging Areas in Communications Networks (SECURECOMM'05)* (IEEE, Athens, Greece, 2005) pp. 67–73.
- [6] S. Capkun and J.-P. Hubaux, Secure positioning in wireless networks, *IEEE Journal on Selected Areas in Communications* **24**, 221 (2006).
- [7] G. Hancke, Design of a secure distance-bounding channel for RFID, *Journal of Network and Computer Applications* **34**, 877 (2011).
- [8] S. Drimer and S. J. Murdoch, Keep your enemies close: Distance bounding against smart-card relay attacks, in *Proceedings of 16th USENIX Security Symposium on USENIX Security Symposium*, SS'07 (USENIX Association, USA, 2007) pp. 1–16.
- [9] A. Alabdulatif, R. Samarasinghe, and N. N. Thilakarathne, A Novel Robust Geolocation-Based Multi-Factor Authentication Method for Securing ATM Payment Transactions, *Applied Sciences* **13**, 10743 (2023).
- [10] D. E. Denning and P. F. MacDoran, Location-based authentication: Grounding cyberspace for better security, *Computer Fraud & Security* **1996**, 12 (1996).
- [11] F. Zhang, A. Kondoro, and S. Muftic, Location-Based Authentication and Authorization Using Smart Phones, in *2012 IEEE 11th International Conference on Trust, Security and Privacy in Computing and Communications* (IEEE, Liverpool, United Kingdom, 2012) pp. 1285–1292.
- [12] M. A. Alawami and H. Kim, LocAuth: A fine-grained indoor location-based authentication system using wireless networks characteristics, *Computers & Security* **89**, 101683 (2020).
- [13] R. A. Malaney, Location-dependent communications using quantum entanglement, *Phys. Rev. A* **81**, 042319 (2010).
- [14] A. Kent, W. J. Munro, and T. P. Spiller, Quantum tagging: Authenticating location via quantum information and relativistic signaling constraints, *Phys. Rev. A* **84**, 012326 (2011).
- [15] A. Bluhm, M. Christandl, and F. Speelman, A single-qubit position verification protocol that is secure against multi-qubit attacks, *Nature Physics* **18**, 623 (2022).
- [16] D. Unruh, Quantum Position Verification in the Random Oracle Model, in *Advances in Cryptology – CRYPTO 2014*, Vol. 8617, edited by J. A. Garay and R. Gennaro (Springer Berlin Heidelberg, Berlin, Heidelberg, 2014) pp. 1–18.
- [17] M. Liu, P. Niroula, M. DeCross, C. Foreman, W. Y. Kon, I. W. Primaatmaja, M. S. Allman, J. P. Campora, A. Isanaka, K. Singhal, O. Amer, S. Chakrabarti, K. Chakraborty, S. F. Cooper, R. D. Delaney, J. M. Dreiling, B. Estey, C. Figgatt, C. Foltz, J. P. Gaebler, A. Hall, Z. He, C. A. Holliman, T. S. Humble, S.-H. Hung, A. A. Husain, Y. Jin, F. Kaleoglu, C. J. Kennedy, N. Kotibhaskar, N. K. Lysne, I. S. Madjarov, M. Mills, A. R. Milne, K. Milner, L. Narmour, S. Omanakuttan, A. J. Park, M. A. Perlin, A. P. Reed, C. N. Self, M. Steinberg, D. T. Stephen, J. Sullivan, A. Chernoguzov, F. J. Curchod, A. Ransford, J. G. Bohnet, B. Neyenhuis, M. Foss-Feig, R. Otter, and R. Shaydulin, Certified randomness amplification by dynamically probing remote random quantum states (2025), arXiv:2511.03686 [quant-ph].
- [18] K. Kanneworff, M. Poortvliet, D. Bouwmeester, R. Allerstorfer, P. V. Lunel, F. Speelman, H. Buhrman, P. Steindl, and W. Löffler, Towards experimental demonstration of quantum position verification using true single photons (2025), arXiv:2502.04125 [quant-ph].
- [19] B. Qi and G. Siopsis, Loss-tolerant position-based quantum cryptography, *Physical Review A* **91**, 042337 (2015).
- [20] J. Ribeiro and F. Grosshans, A Tight Lower Bound for the BB84-states Quantum-Position-Verification Protocol (2015), arXiv:1504.07171 [quant-ph].

- [21] V. Zapatero, T. Van Leent, R. Arnon-Friedman, W.-Z. Liu, Q. Zhang, H. Weinfurter, and M. Curty, Advances in device-independent quantum key distribution, *npj Quantum Information* **9**, 10 (2023).
- [22] L. Lydersen, C. Wiechers, C. Wittmann, D. Elser, J. Skaar, and V. Makarov, Hacking commercial quantum cryptography systems by tailored bright illumination, *Nature Photonics* **4**, 686 (2010).
- [23] H. Weier, H. Krauss, M. Rau, M. Fürst, S. Nauerth, and H. Weinfurter, Quantum eavesdropping without interception: An attack exploiting the dead time of single-photon detectors, *New Journal of Physics* **13**, 073024 (2011).
- [24] L. K. Shalm, E. Meyer-Scott, B. G. Christensen, P. Bierhorst, M. A. Wayne, M. J. Stevens, T. Gerrits, S. Glancy, D. R. Hamel, M. S. Allman, K. J. Coakley, S. D. Dyer, C. Hodge, A. E. Lita, V. B. Verma, C. Lambrocco, E. Tortorici, A. L. Migdall, Y. Zhang, D. R. Kumor, W. H. Farr, F. Marsili, M. D. Shaw, J. A. Stern, C. Abellán, W. Amaya, V. Pruneri, T. Jennewein, M. W. Mitchell, P. G. Kwiat, J. C. Bienfang, R. P. Mirin, E. Knill, and S. W. Nam, Strong Loophole-Free Test of Local Realism, *Physical Review Letters* **115**, 250402 (2015).
- [25] M. Giustina, M. A. M. Versteegh, S. Wengerowsky, J. Handsteiner, A. Hochrainer, K. Phelan, F. Steinlechner, J. Kofler, J.-Å. Larsson, C. Abellán, W. Amaya, V. Pruneri, M. W. Mitchell, J. Beyer, T. Gerrits, A. E. Lita, L. K. Shalm, S. W. Nam, T. Scheidl, R. Ursin, B. Wittmann, and A. Zeilinger, Significant-Loophole-Free Test of Bell’s Theorem with Entangled Photons, *Physical Review Letters* **115**, 250401 (2015).
- [26] I. Šupić and J. Bowles, Self-testing of quantum systems: A review, *Quantum* **4**, 337 (2020).
- [27] I. W. Primaatmaja, K. T. Goh, E. Y.-Z. Tan, J. T.-F. Khoo, S. Ghorai, and C. C.-W. Lim, Security of device-independent quantum key distribution protocols: A review, *Quantum* **7**, 932 (2023).
- [28] G. Vidal and R. Tarrach, Robustness of entanglement, *Physical Review A* **59**, 141 (1999).
- [29] Ll. Masanes, A. Acin, and N. Gisin, General properties of nonsignaling theories, *Physical Review A* **73**, 012112 (2006).
- [30] N. Sastry, U. Shankar, and D. Wagner, Secure verification of location claims, in *Proceedings of the 2nd ACM Workshop on Wireless Security* (ACM, San Diego CA USA, 2003) pp. 1–10.
- [31] Y. Zhang, S. Glancy, and E. Knill, Asymptotically optimal data analysis for rejecting local realism, *Physical Review A* **84**, 062118 (2011).
- [32] Y. Zhang, S. Glancy, and E. Knill, Efficient quantification of experimental evidence against local realism, *Physical Review A* **88**, 052119 (2013).
- [33] G. A. Kavuri, J. Palfree, D. V. Reddy, Y. Zhang, J. C. Bienfang, M. D. Mazurek, M. A. Alhejji, A. U. Siddiqui, J. M. Cavanagh, A. Dalal, C. Abellán, W. Amaya, M. W. Mitchell, K. E. Stange, P. D. Beale, L. T. A. N. Brandão, H. Booth, R. Peralta, S. W. Nam, R. P. Mirin, M. J. Stevens, E. Knill, and L. K. Shalm, Traceable random numbers from a non-local quantum advantage, *Nature* **642**, 916 (2025).
- [34] L. K. Shalm, Y. Zhang, J. C. Bienfang, C. Schlager, M. J. Stevens, M. D. Mazurek, C. Abellán, W. Amaya, M. W. Mitchell, M. A. Alhejji, H. Fu, J. Ornstein, R. P. Mirin, S. W. Nam, and E. Knill, Device-independent randomness expansion with entangled photons, *Nature Physics* **17**, 452 (2021).
- [35] M. A. Rowe, D. Kielpinski, V. Meyer, C. A. Sackett, W. M. Itano, C. Monroe, and D. J. Wineland, Experimental violation of a Bell’s inequality with efficient detection, *Nature* **409**, 791 (2001).

- [36] P. H. Eberhard, Background level and counter efficiencies required for a loophole-free Einstein-Podolsky-Rosen experiment, *Physical Review A* **47**, R747 (1993).
- [37] S. Das and G. Siopsis, Practically secure quantum position verification, *New Journal of Physics* **23**, 063069 (2021).
- [38] C. Portmann and R. Renner, Security in quantum cryptography, *Reviews of Modern Physics* **94**, 025008 (2022).
- [39] J. Liu, Q. Liu, and L. Qian, Beating Classical Impossibility of Position Verification (2022), arXiv:2109.07517 [quant-ph].
- [40] W.-Z. Liu, M.-H. Li, S. Ragy, S.-R. Zhao, B. Bai, Y. Liu, P. J. Brown, J. Zhang, R. Colbeck, J. Fan, Q. Zhang, and J.-W. Pan, Device-independent randomness expansion against quantum side information, *Nature Physics* **17**, 448 (2021).
- [41] M.-H. Li, X. Zhang, W.-Z. Liu, S.-R. Zhao, B. Bai, Y. Liu, Q. Zhao, Y. Peng, J. Zhang, Y. Zhang, W. J. Munro, X. Ma, Q. Zhang, J. Fan, and J.-W. Pan, Experimental Realization of Device-Independent Quantum Randomness Expansion, *Physical Review Letters* **126**, 050503 (2021).
- [42] F. Kaleoglu, M. Liu, K. Chakraborty, D. Cui, O. Amer, M. Pistoia, and C. Lim, On the Equivalence between Classical Position Verification and Certified Randomness (2025), arXiv:2410.03982 [quant-ph].
- [43] G. Shafer, A. Shen, N. Vereshchagin, and V. Vovk, Test martingales, Bayes factors and p -values, *Statistical Science* **26**, 84 (2011).
- [44] Y. Zhang, S. Glancy, and E. Knill, Asymptotically optimal data analysis for rejecting local realism, *Phys. Rev. A* **84**, 062118/1 (2011), for supporting code, see arXiv:1108.2468.
- [45] Y. Zhang, S. Glancy, and E. Knill, Efficient quantification of experimental evidence against local realism, *Phys. Rev. A* **88**, 052119/1 (2013).
- [46] D. P. Nadlinger, P. Drmota, B. C. Nichol, G. Araneda, D. Main, R. Srinivas, D. M. Lucas, C. J. Ballance, K. Ivanov, E. Y.-Z. Tan, P. Sekatski, R. L. Urbanke, R. Renner, N. Sangouard, and J.-D. Bancal, Experimental quantum key distribution certified by Bell's theorem, *Nature* **607**, 682 (2022).
- [47] W. Zhang, T. van Leent, K. Redeker, R. Garthoff, R. Schwonnek, F. Fertig, S. Eppelt, W. Rosenfeld, V. Scarani, C. C.-W. Lim, and H. Weinfurter, A device-independent quantum key distribution system for distant users, *Nature* **607**, 687 (2022).
- [48] F. Xu, Y.-Z. Zhang, Q. Zhang, and J.-W. Pan, Device-Independent Quantum Key Distribution with Random Postselection, *Physical Review Letters* **128**, 110506 (2022).
- [49] A. Bluhm, M. Christandl, and F. Speelman, A single-qubit position verification protocol that is secure against multi-qubit attacks, *Nature Physics* **18**, 623 (2022).
- [50] D. Unruh, Quantum position verification in the random oracle model, in *Advances in Cryptology—CRYPTO 2014: 34th Annual Cryptology Conference, Santa Barbara, CA, USA, August 17–21, 2014, Proceedings, Part II 34* (Springer, 2014) pp. 1–18.
- [51] Y. Zhang, L. K. Shalm, J. C. Bienfang, M. J. Stevens, M. D. Mazurek, S. W. Nam, C. Abellán, W. Amaya, M. W. Mitchell, H. Fu, *et al.*, Experimental low-latency device-independent quantum randomness, *Physical review letters* **124**, 010505 (2020), arXiv:1812.07786.
- [52] Y. Zhang, E. Knill, and P. Bierhorst, Certifying Quantum Randomness by Probability Estimation, *Physical Review A* **98**, 040304 (2018), arXiv:1811.11928 [quant-ph].
- [53] T. Cooke, Coaxial Cables, in *The Global Cable Industry*, edited by G. Beyer (Wiley, 2021) 1st ed., pp. 331–349.
- [54] R. M. Wald, *General Relativity* (University of Chicago Press, Chicago, 1984).

- [55] H. Buhrman, N. Chandran, S. Fehr, R. Gelles, V. Goyal, R. Ostrovsky, and C. Schaffner, Position-based quantum cryptography: Impossibility and constructions, *SIAM Journal on Computing* **43**, 150 (2014), arXiv:1009.2490.
- [56] N. Chandran, V. Goyal, R. Moriarty, and R. Ostrovsky, Position based cryptography, in *Annual International Cryptology Conference* (Springer, 2009) pp. 391–407.
- [57] N. Brunner, D. Cavalcanti, S. Pironio, V. Scarani, and S. Wehner, Bell nonlocality, *Reviews of Modern Physics* **86**, 419 (2014).
- [58] L. Masanes, A. Acin, and N. Gisin, General properties of nonsignaling theories, *Phys. Rev. A* **73**, 012112 (2006).
- [59] P. H. Eberhard, Background level and counter efficiencies required for a loophole-free einstein-podolsky-rosen experiment, *Physical Review A* **47**, R747 (1993).
- [60] N. Brunner, N. Gisin, V. Scarani, and C. Simon, Detection loophole in asymmetric Bell experiments, *Physical Review Letters* **98**, 220403 (2007).
- [61] S. Pironio, J.-D. Bancal, and V. Scarani, Extremal correlations of the tripartite no-signaling polytope, *Journal of Physics A: Mathematical and Theoretical* **44**, 065303 (2011).
- [62] G. Vidal and R. Tarrach, Robustness of entanglement, *Physical Review A* **59**, 141 (1999).
- [63] O. Rudolph, Further results on the cross norm criterion for separability, *Quantum Information Processing* **4**, 219 (2005).
- [64] E. Knill, Y. Zhang, and P. Bierhorst, Quantum randomness generation by probability estimation with classical side information (2017), arXiv:1709.06159.

SUPPLEMENTARY INFORMATION

CONTENTS

I. Preliminaries		18
II. Protocol and assumptions		21
III. Experiment		24
A. Overview		24
B. Protocol Implementation		25
C. Hardware and Timing		28
IV. Classical Space-time Measurements		29
A. Physical Distances		30
B. Target Regions in the Spatial Dimensions		31
1. Experimental Parameters for Determining Target Regions		32
2. Computing Target Regions		33
3. Comparing Classical and Quantum Target Regions		34
V. Theory		35
A. Spacetime analysis		35
B. Reduction to 3-party non-signaling and connection to 2-party local realism		44
C. Test-factor construction		52
D. Test factors against small amounts of prior entanglement		53

VI. Analysis of experimental results	55
A. Parameter Determination	55
B. Calibration and Analysis	59

I. PRELIMINARIES

Our quantum position verification (QPV) protocol has three verifiers A , A' and B and a source of entangled pairs. One member of each entangled pair is sent to A' , who performs measurements on this member. The other member of the pair is sent to a target region E . Verifiers A and B send challenges and receive prover responses. In our experimental implementation, A and A' are co-located in the same lab, and we sometimes call A' a “measurement station”. We also employ the label A_{source} for the source of entangled photons, which is co-located with A' and A . The goal of the QPV protocol is to verify that a prover is in the target region E . The protocol consists of a sequence of n trials, and success of the verification and the protocol is determined by analyzing the statistics of the trial records. For provers whose movements are unrestricted, success of the protocol certifies that they are in the target region during at least one trial of the protocol. If the protocol succeeds for a prover, we say that the prover passes the protocol. Our analysis shows that to succeed, the prover must perform some non-trivial quantum operation in the target region. The honest prover P is in the target region during every trial of the protocol. The protocol is designed so that such an honest prover can ensure that the protocol succeeds with a reasonably high probability, while for any cooperating collection of provers who are never in the target region the protocol fails with high probability. Provers attempting to pass the QPV protocol without being in the target region are called adversaries. We demonstrate the honest prover strategy experimentally by implementing a measurement station P in a lab physically separated from the verifier A and B labs.

In each trial of the QPV protocol, a source at some position prepares two quantum systems $Q_{A'}$ and Q_P and sends $Q_{A'}$ to A' and Q_P to the target region. In spacetime, the target region E consists of a disjoint union of target regions E_k , where E_k is contained inside the time interval for the k 'th trial. For the k 'th trial, A and B choose challenges u_{A_k} and u_{B_k} from finite sets I_{u_A} and I_{u_B} according to a probability distribution specified by the protocol. In the experiment, the two challenges are bits and the distribution is uniform. When it is necessary to distinguish random variables (RVs) from their values, we use standard capitalization conventions for RVs and their values. For example, U_{A_k} and U_{B_k} are the random variables whose instances have values u_{A_k} and u_{B_k} , respectively. We use $\mathbb{P}(\dots)$ to denote probabilities of events and $\text{Exp}(\dots)$ to denote expectations of real-valued RVs. We assume that the values of random variables belong to finite sets of at least two elements. In the experiment, U_{A_k} and U_{B_k} are binary, independent and uniformly random. Unless explicitly stated, we do not assume that the trials are independent or identically distributed. Random variables without trial-index subscripts refer to the random variables of a generic trial and are used when the specific trial does not matter. In particular, for the remainder of this section, we consider a generic trial of the QPV protocol and drop the trial-index subscripts.

The honest prover receives u_A and u_B and computes an agreed-upon and publicly known prover settings function $f(u_A, u_B)$ with range $\{1, \dots, k_P\}$. In parallel, A' chooses a measurement setting $m_{A'} \in \{1, \dots, k_{A'}\}$. A' applies the measurement according to the setting $m_{A'}$ and obtains a measurement outcome $o_{A'} \in \{1, \dots, c_{A'}\}$. The honest prover chooses their

measurement setting m_P according to $m_P = f(u_A, u_B)$, applies the measurement accordingly and obtains measurement outcome $o_P \in \{1, \dots, c_P\}$. The honest prover then sends o_P to each of A and B. In general, A and B may receive responses from imperfect provers or adversaries, in which case the two responses may not agree. The responses actually received by A and B are denoted by z_A and z_B , where these values may belong to a larger set than o_P , for example, to account for absence of responses and invalid responses.

In the experiment $f(u_A, u_B) = (u_A - 1) \oplus (u_B - 1) + 1$, where u_A and u_B have values $u_A, u_B \in \{1, 2\}$ and \oplus denotes the exclusive OR operation. This is just the regular exclusive OR with inputs and outputs in $\{1, 2\}$. The measurement setting and outcomes of A' also have values $m_{A'} \in \{1, 2\}$ and $o_{A'} \in \{1, 2\}$. The prover outcome o_P is binary, and z_A and z_B are binned to be binary as well.

For each trial, the trial record R_{trial} consists of the verifier-visible random variables, which are $U_A, U_B, M_{A'}, O_{A'}, M_P, Z_A, Z_B$. These are the challenges from A' and B, the measurement setting and outcome at A', the computed measurement setting at the prover P, and the responses to the verifiers A and B, respectively. All random variables in play, including those involving multiple trials, are jointly distributed. To determine whether the prover passed the protocol successfully (“pass”) or failed (“fail”), the verifiers perform a statistical test on the sequence of trial records. The security of the protocol for a given class of adversaries is quantified by its soundness and completeness parameters. For $\delta \in [0, 1)$, the protocol is δ -sound if for adversaries in the given class, before the protocol starts, the probability that the protocol will succeed is at most δ . To ensure good security, the soundness parameter δ should be extremely small. For $\epsilon \in (0, 1]$, the protocol is ϵ -complete for the actual, honest prover if this prover succeeds with probability at least ϵ . The soundness parameter is established by proof. The completeness parameter for the actual, honest prover can only be estimated, but usefulness of the protocol requires that there exist honest provers with completeness much larger than the soundness. Since we cannot be sure of the value of the completeness parameter for the actual, honest prover, to interpret the security of the protocol, it is desirable to be conservative and assume that ϵ itself is very small. On the other hand, to ensure that the honest prover is securely distinguishable from adversaries, it is necessary that ϵ/δ is very large, requiring δ to be much smaller than the conservative value of ϵ . In our experimental implementation, there are non-trivial tradeoffs between the soundness, completeness, and the time required to run one instance of the protocol or the number of trials per instance. See Sect. VI.

The target region is determined by the positions of the verifiers and the timing of verifier events, see Sect. V A for details. In the experiment, the verifiers are stationary in a common inertial frame of a flat (Minkowski) spacetime \mathcal{M} . The spatial positions of verifiers A', A and B are $\mathbf{x}_{A'}$, \mathbf{x}_A and \mathbf{x}_B . Our spacetime and security analysis does not depend on stationary verifiers, but it simplifies the visualization of target regions and represents the situation implemented in the experiment. In the experiment, the honest prover P is at rest at position $\mathbf{x} = 0$. For simplicity, the theoretical analysis assumes that the relative timing of events in each trial is the same. In the experiment this is verified via indirect measurements during, and direct measurements after all the protocol runs. Let t be the time at which the trial starts. We let $t + s_A$ and $t + s_B$ be the times at which A and B begin to emit their challenges u_A and u_B toward the prover. The final times at which the verifiers accept the prover’s responses are $t + r_A$ and $t + r_B$. The verifiers determine a response value after these times based on the responses or their absence. The trial, including recording of the trial record, is complete at time $t + t_{\text{trial}}$. We require $0 \leq s_A \leq r_A \leq t_{\text{trial}}$ and $0 \leq s_B \leq r_B \leq t_{\text{trial}}$.

In principle, we can also specify the position of the source of the entangled pair of quantum systems and the time at which it sends the two systems. For our analysis this is subsumed by the constraints on prior entanglement of adversaries as explained below.

We use statistical tests based on the test-factor strategy [43–45] for testing the hypothesis that the responses are from adversaries in a given class. For our purposes, a trial’s test factor W for detecting a class of adversaries is a non-negative function of the trial record whose expectation is guaranteed to be at most 1 for all adversaries in the given class. To have completeness much larger than soundness, it is necessary that implementations of an honest prover strategy can achieve an expectation value $\text{Exp}(W) > 1$, as we experimentally demonstrate. In this work, we require that W is a function of $M_{A'}, O_{A'}, M_P, Z_A, Z_B$ only, so that it depends on U_A, U_B only through the settings function $M_P = f(U_A, U_B)$. The bound of 1 on the expectation of W must hold conditional on the past of the trial. The past includes all classical and quantum information available before the trial begins, as specified in the spacetime analysis below. In a generic trial, adversaries may either have no prior entanglement or pre-share bounded entanglement. We construct test factors for both scenarios. Test factors can be chained over multiple trials by multiplication. According to the theory of test factors, the product \mathcal{T} of test factors over the trials of the protocol has expectation at most 1 for all adversary strategies in the given class. A key property of such test-factor products is that the expectation of \mathcal{T} remains upper-bounded by 1 even when adversaries adapt their actions based on past information. By Markov’s inequality, \mathcal{T}^{-1} is a p -value for adversaries of the given class. For an experimental implementation of the protocol, an honest prover strategy that ensures $\text{Exp}(\mathcal{T}) \gg 1$ is desirable. We use the convention that a non-negative random variable R is a p -value against a composite null hypothesis if the probability that $R \leq p$ given a model in the null hypothesis is at most p . There is no requirement that there are models in the null hypothesis for which this bound is achieved, and we do not require p -values to be in the interval $[0, 1]$. We define the $\log(p)$ -value for the protocol as $\log(\mathcal{T})$. Note that the “ $\log(p)$ -value” is the negative of the logarithm of the p -value. The higher the $\log(p)$ -value, the stronger the evidence against the allowed adversaries. Given the desired soundness parameter δ , the protocol passes if the $\log(p)$ -value is at least $\log(1/\delta)$ and fails otherwise. Thus, the protocol passes only if the null hypothesis that the responses are from adversaries in the given class can be rejected according to the p -value \mathcal{T}^{-1} at significance level δ . Unless specified otherwise, the base of the logarithm is e .

Test factors can be chosen to maximize the trial gain for a specific honest prover P . The trial gain g is defined as the expectation $g = \text{Exp}(\log(W))$ for P of the logarithm of the test factor. The gain is the expected contribution per trial to the $\log(p)$ -value. The test factor is chosen by considering the honest prover that is implemented in the experiment. Since the implemented prover is designed to produce independent and identically distributed (i.i.d.) trial records, the value of $\log(\mathcal{T})$ after n trials has expectation ng with variance $O(n)$. Consequently, the number of trials required for P to succeed with reasonable probability can be estimated as $\log(1/\delta)/g$. Specific estimates based on asymptotic normality are used to determine protocol parameters, see Sect. VI.

II. PROTOCOL AND ASSUMPTIONS

Here is the abstract QPV protocol, a version of which was implemented in the experiment.

Protocol 1: Quantum Position Verification (QPV) Protocol

// See Sects. VC, VD and VIA for the required preparatory work for running this protocol.

Given:

- δ — desired soundness parameter.
- n — number of trials to be executed.
- ν_U — joint challenge distribution.
- $f(u_A, u_B)$ — settings function.
- $\mu_{A'}$ — measurement settings distribution of verifier A' .
- W — trial-wise test factor to be used.
- t_0 — initiation time.
- t_{trial} — trial duration.
- s_A, s_B, r_A, r_B — verifier send and receive times.

Let $t_1 \geq t_0$ be the first trial's start time;

for $k = 1$ **to** n **do**

Perform a QPV trial starting at time t_k :

1. The source prepares a joint state of $Q_{A'}$ and Q_P (event #4 in table I), and sends $Q_{A'}$ to A' and Q_P to the target region. This state preparation can be done before t_k , provided that Assumption 8 is satisfied.
2. A and B generate challenges u_A and u_B according to the joint distribution ν_U and A' chooses measurement setting $m_{A'}$ (event #5 in table I) according to probability distribution $\mu_{A'}$. The challenges and settings for this trial may be generated before t_k provided that Assumption 11 is satisfied.
3. A and B send the challenges u_A and u_B at times $t_k + s_A$ and $t_k + s_B$ from specified locations. See Assumption 4. These are events #1 & #2 in table I.
4. A' measures $Q_{A'}$ according to setting $m_{A'}$, producing outcome $o_{A'}$ (event #6 in table I). For device-independence based on causality, the period between applying the setting to recording the measurement outcome is space-like separated from the trial's target region.
5. A and B receive response values z_A and z_B from the provers at times $t_k + r_A$ and $t_k + r_B$ and at specified locations (events #13 & #14 in table I). See Assumption 4.
6. The verifiers save the reduced trial record $r_{\text{trial}k} = (m_{A'}, o_{A'}, f(u_A, u_B), z_A, z_B)$ and compute $w_k = W(r_{\text{trial}k})$. In the experiment w_k was computed later, after unblinding the data.

Let $t_{k+1} \geq t_k + t_{\text{trial}}$ be the next trial's start time;

end

Let $p = (\prod_{k=1}^n w_k)^{-1}$; // This is the p -value against adversaries

if $p \leq \delta$ **then**

return *success*; // Protocol succeeded

else

return *fail*; // Protocol failed

end

The assumptions required for the security of the protocol and to ensure that soundness is satisfied for the given soundness parameter δ are listed next.

Assumptions (see Sect. V A for definitions and terms):

- 1 **Classical computation and communication:** All classical computation is error-free and satisfies the protocol specifications. This is a standard assumption in device-independent quantum protocols [46, 47]. Classical communication between the verifiers is also error-free. Most classical communication between the verifiers can be deferred until after the protocol completed and can be implemented by authenticated classical channels.
- 2 **Classical spacetime and worldlines:** The background spacetime is Minkowski. Worldlines are classical. This means that the spacetime circuit of the relevant entities is determined in each trial given the past. In principle, the computations at the vertices could make choices of where to send the outputs. We assume that there is a finite, bounded number of such choices, in which case we can arrange for the fixed spacetime circuit to have edges and vertices for every possible combination of such choices. For this purpose, the systems on the edges may need to be enlarged by adding a “vacuum” state that indicates that the edge was not used. Vertex operations are extended accordingly.
- 3 **Classical timing and location:** For the theoretical analysis of the protocol we assume that trial timing and location measurements are error-free. The timing and location measurements determine the target region. In the experiment, timing and location measurements have uncertainties as described in Sect. III, which affect the boundaries of the target region. The effect of these uncertainties on localization is illustrated in Fig. IV.
- 4 **Verifier lab security:** The labs of the three verifiers are secured to disallow interaction with non-verifier entities except for those that are part of the protocol. In particular, the only outgoing edges from the labs of verifiers **A** and **B** to non-verifiers are those that jointly carry the classical challenges and are causally consistent with the challenge timing. In practice, this means that the classical challenges do not “leak” out of the verifier labs apart from the established exit points at the appropriate challenge exit time, see Fig. 6. In addition, there are no outgoing edges from **A'** to non-verifiers, which prevents information about the settings and outcomes at **A'** from leaking to adversaries during a trial. To ensure this condition, we assume that outgoing communications from **A'** other than to the verifiers are blocked during a trial. We further require that within a trial, there are no incoming edges from a non-verifier that causally precede edges from the verifiers to a non-verifier. For **A** and **B**, this can be enforced by blocking incoming communications before the challenges are sent. **A'** receives a quantum system from the source, which is treated as untrusted. We require that the verifiers’ processing of challenges and responses is completely classical. In particular, challenges are classical and the responses are immediately decohered in the computational basis at the moment they enter the lab. Such assumptions of lab security are standard in device-independent and other cryptographic protocols [46–48].
- 5 **Challenge and response events:** We identify specific events in spacetime where the challenges leave the labs and the responses enter the labs. The only requirement on these events is that the target region as defined in Sect. V A is non-empty. In the protocol and the experiment, these events have the specified space positions of **A** and

B (see Fig. 6), which are stationary with respect to the earth's surface. The challenges leave the lab at or after times $t_k + s_A$ and $t_k + s_B$. The responses enter the labs at or before times $t_k + r_A$ and $t_k + r_B$. All relevant experimentally measured timings are listed in table I.

- 6 **Adversary communication:** Except for space-time causality, there are no restrictions on adversary communication capabilities during a trial. The adversaries can communicate both classically and quantumly. Quantum communication and memory between trials is indirectly restricted by the constraints on adversary entanglement.
- 7 **Adversary entanglement:** The prior entanglement of adversaries for each trial is defined on a specific time slice determined by the trial timing as described in the spacetime analysis of Sect. V A. This time slice defines the trial boundary for the purpose of determining the prior adversary entanglement. The protocol assumes that this prior entanglement is zero or satisfies bounds described in Sect. V D. The test factors and the pass/fail decision depend on which assumption is used. The constraint on entanglement includes the source and the emitted or to be emitted entangled pair of quantum systems on the trial boundary.
- 8 **Quantum source:** We treat the source as an untrusted component that may be under the control of adversaries. This implies that the source cannot be in the target region. In addition, the restriction on prior entanglement of the adversaries implicitly constrains the source and the entangled system prepared and communicated by the source. To prevent the adversaries from exploiting the source for shared entanglement it is necessary to secure the location of source and the timing of the source emissions. Because the quantum system $Q_{A'}$ is treated as part of the adversary closer to A, the source needs to be located in the region closer to A. To prevent the source from contributing entanglement to the adversaries, it is desirable for the source emission of Q_P to the prover location to be constrained so that Q_P does not cross the trial boundary adjacent to the part of the adversary nearer B. If the protocol is secure against adversaries with prior entanglement greater than that available from the source, then there is no need to secure the source location or emission. Such security is expected to be satisfied with sufficiently complex challenges and settings functions. See Assumption 10 below.
- 9 **Quantum measurement:** A' uses a quantum apparatus in their lab to measure $Q_{A'}$. The apparatus is untrusted. Security of the protocol requires that the setting and the challenges are not known to the apparatus beforehand. For the analysis here, we assume that the only incoming message during a trial is the quantum system $Q_{A'}$ from the source. We assume that outgoing messages are blocked, except for the eventual message of the measurement outcomes to the other verifiers. We assume and ensure in the experiment (see Fig. 7) that the interval between applying a measurement setting and recording the measurement outcome is in the region where the challenge from B is not visible and from which no signal can reach B at or before the time point $t_k + r_B$. In particular this interval is space-like separated from the target region of a trial. In Fig. 7 and using the conventions introduced before Eq. 1, this region consists of the subregions labeled $*0*1$, where $*$ denotes either 0 or 1. An illustration of these subregions is provided in Fig. 9.
- 10 **Settings function:** There are no direct constraints on the settings function except for those implied by the assumptions on the settings and challenges in Assumption 11 below.

In QPV, increasing the complexity of the challenges and the settings function leads to higher bounds on the minimum prior entanglement required for adversaries to successfully pass the protocol [37, 49]. It can also be used to protect against computationally bounded adversaries without prior entanglement constraints [50]. Our inclusion of a challenge from A and use of the exclusive OR function anticipates the implementation of such strategies.

- 11 **Verifier settings and challenge distributions:** For our analysis, we assume that verifier settings and challenge distributions are fixed and independent of the state coming into the trial. In the spacetime circuit analysis given in Sect. V A below, this means that the probability distributions are independent of the state of the adversary including the source and the quantum systems that the source emitted on the time slice on which prior adversary entanglement is determined. For the reduction from general adversaries to two adversaries whose quantum messages to each other do not depend on the challenges, we require that 1) $M_{A'}$ and M_P are independent of U_A so that $\mathbb{P}(m_{A'}, m_P, u_A) = \mathbb{P}(m_{A'}, m_P)\mathbb{P}(u_A)$, and 2) $M_{A'}$ is conditionally independent of U_A and U_B given M_P so that $\mathbb{P}(m_{A'}, u_A, u_B | m_P) = \mathbb{P}(m_{A'} | m_P)\mathbb{P}(u_A, u_B | m_P)$. See Sect. V B for how these independence assumptions are used. The assumptions are satisfied if U_A and U_B are uniformly random, independent of $M_{A'}$, and the cardinality $|\{u_B | f(u_A, u_B) = m_P\}|$ does not depend on u_A or m_P . For simplicity of test-factor construction we choose uniform verifier and prover settings distributions for the experiment.

It is possible to relax the assumption that the joint distribution of the verifier settings $M_{A'}$ and the prover settings M_P is fixed and independent of the past. This can be done by allowing mixtures of products of incoming states and joint distributions of $M_{A'}$ and M_P , where the latter come from a fixed convex set of distributions near a target distribution. The chosen test factors then need to be designed to have worst-case expectation of 1 for adversaries over the convex set of distributions. See Ref. [51] for realizations of this strategy in the context of device-independent quantum randomness generation.

It is noteworthy that the assumptions on the settings and challenges can be satisfied with a settings function that does not depend on u_A , in which case the challenge u_A can be omitted. In this case, the role of s_A is to define the trial boundary and the target region. Because $Q_{A'}$ is attributed to the adversary nearer A, the restriction on entanglement requires that Q_P cannot reach the adversary nearer B before the trial boundary as defined by s_A . In the experiment this is satisfied by transmitting Q_P in fiber and accounting for the speed of light in the fiber. For future applications of the protocol it is necessary to strengthen the protocol to reject adversaries with prior entanglement significantly larger than that generated by the source, which we anticipated by having a nontrivial challenge u_A . Previous work [49] on related QPV protocols indicates that for n -bit challenges it is possible to exclude adversaries with prior entanglement of order n .

III. EXPERIMENT

A. Overview

Fig. 5 shows a schematic of the components of the experiment. In the experiment, verifier A that sends challenge bits and receives responses, verifier A' that measures one

of the entangled photons, and the entangled photon source A_{source} are in the same room. Verifier B is in another room of the National Institute of Standards and Technology (NIST) building that is about 200 m away.

The entangled photons $Q_{A'}$ and Q_P generated at A_{source} are distributed through single-mode optical fiber to measurement station A' and the honest prover, P. For the successful protocol runs presented here, the honest prover hardware is stationary and located in a room about 90 m from verifier A. Subsequently, verifier A' and the honest prover P measure the photons in one of two measurement bases, performing a Bell test. We label the measurement settings of A' and P determined by their measurement bases by $m_{A'}$ and m_P . Much of the hardware for this experiment builds on loophole-free Bell tests and device-independent random number generation (DIRNG) setups [34, 52]. For example, the measurements performed at A' are the same as at “Bob” in Ref. [33], with the measurement basis $m_{A'}$ chosen using the same source of local randomness as in that work. The resulting measurement outcomes are recorded to a timetagger. The measurement basis at the honest prover P, however is decided by the output of an exclusive OR (XOR) of random challenge bits $m_P = u_A \oplus u_B$ released by the verifiers A and B. The random bits are sent to the honest prover at high speed over specialized coaxial cables. The honest prover measures the photon and replies to verifiers A and B with the measurement outcome over fast coaxial cables. Verifiers A and B then record these signals z_A, z_B on their timetaggers.

Provided that the recorded signals violate a Bell inequality, the time difference between when the random inputs were provided and the measurement outcome was received by A and B allows the verifiers to perform a secure ranging based on round-trip communication times. Any excess latencies during transmission (i.e., transmission slower than the speed of light), or in the measurement process at the honest prover implies a larger target region E for localizing the prover. This highlights the importance of low-latency measurements at the implemented honest prover station and high-speed classical communication. In our experiment, this is enabled with the use of Pockels cells, custom high-speed electronics, and low-latency coaxial cables. The experimental realization of a QPV protocol requires careful design and optimization to minimize latency in electronics, measurement, and transmission.

With our protocol, much of the “quantum” hardware (such as the source and the measurement stations) need not be trusted, or even be within the secure verifier labs, allowing for more flexibility in configuration choices. A careful account of the assumptions involved in our demonstration can be found in Sect. II.

B. Protocol Implementation

The labs containing verifiers A and B are assumed to be trusted, in the sense that the equipment inside them is not under the influence of any adversaries. This is related to Assumptions 4 and 11 in Sect. II. Physically, this means the signals are assumed to be shielded from adversaries (in that they cannot be altered or read by adversaries) until they physically exit the labs, and that any signals coming in from the outside are similarly shielded once they enter the verifier labs.

All signals exit and enter the verifier labs via access points in the walls through which cables are laid. In all our analyses, we rely on the trusted lab assumption stated to use these physical access points to define the verifier A and B’s physical locations. Here, we are modeling a situation where the verifier labs are carefully shielded from external signals, while an opening allows transmission of signals in and out of the labs. The times when challenge

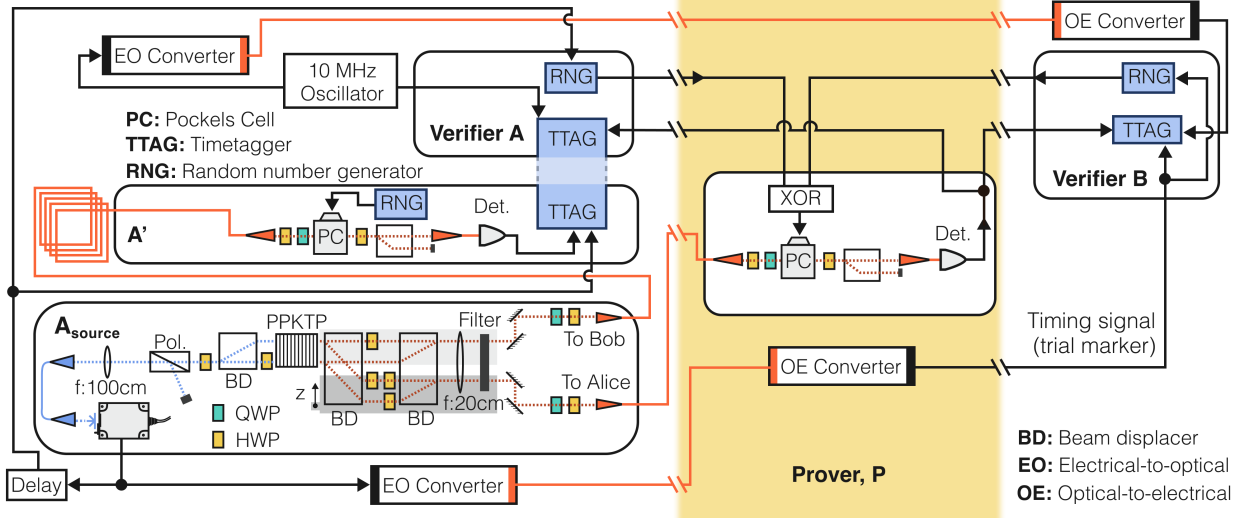


FIG. 5. Experimental diagram for the position verification demonstration. Verifiers A, A', and B, the honest prover P as implemented, and the entangled photon source A_{source} are indicated. The yellow shading around the honest prover P indicates the region prover hardware must be in to pass the protocol (target region E). The RNGs and timetaggers are associated with the verifiers. Electrical and optical cables carry information to and from the various experimental stations. The entangled photons are distributed via optical cables, and the measurement choice bits are transmitted via high-speed coaxial cables. Electrical cables are indicated in black, and optical cables in orange. Electrical-to-optical (OE) and optical-to-electrical (EO) converters convert information between electrical and optical encoding. These are used in the lines that transmit synchronization signals among the verifiers. A_{source} is the source of entangled photons, which produces entangled photons via spontaneous parametric downconversion with a periodically poled potassium titanyl phosphate (ppKTP) crystal placed inside a dual Mach-Zehnder interferometer formed with beam displacers (BD) [33]. For the measurements at A' and P, the pair of measurement bases are implemented with quarter-waveplates (QWP) and half-waveplates (HWP), and fast switching between the bases is performed with a Pockels cell.

(response) signals exit (enter) these openings are the earliest (latest) time at which they can be influenced or read by adversaries. From the adversarial point of view, it thus suffices to reduce the verifiers to the spatial points corresponding to the signal entry and exit. See Fig. 6 for photographs of the entry/exit points. Signals traveling to or from the verifier labs and crossing these physical thresholds at time ' t ' are considered to have been generated or detected at ' t '.

The protocol proceeds as a series of trials, with the number of trials performed in a single run of the protocol determined by previous calibration data and a desired threshold for soundness error (see Sect. I). Each trial starts with the creation of an entangled pair of photons at A_{source} . The photons are generated via spontaneous parametric downconversion. A solid-state pulsed laser at 775 nm pumps an entangled pair generation source that probabilistically downconverts the pump to generate entangled pairs of photons at 1550 nm.

The source of entangled photons is largely similar to the one employed in Ref. [33], and is based on a twin Mach-Zehnder interferometer constructed with beam displacers. The entangled photon source is tuned to produce a non-maximally entangled state, nominally



FIG. 6. Photographs of the physical entry/exit points of the classical and quantum signals that serve as the verifiers A and B in our demonstration. Any hardware and cabling inside the verifier labs is trusted. At verifier B, the lab houses a random number generator for deciding the challenge u_B , and a timetagger that records classical timing information and the response from provers z_B . All information exiting and entering the Verifier B lab is classical.

$0.383|HH\rangle + 0.924|VV\rangle$, conditional on a pair of photons being spontaneously generated, which happens with a probability of approximately $1/350$. This state (along with the measurement angles at the measurement stations) was chosen based on a numerical optimization maximizing the Bell violation. The optimization takes experimental losses, dark counts, and imperfect state fidelity into account. For comparison to bounds on prior entanglement by adversaries, the robustness of entanglement of the nominal state is $(0.383 + 0.924)^2 - 1 = 0.71$. Accounting for the probability of photon pair emission, this gives a robustness of entanglement per trial of 2×10^{-3} . The source sends one photon (Q_P) from each of the entangled photon pairs to P via optical fiber, and the measurement station A' makes measurements locally on its photon ($Q_{A'}$). The $Q_{A'}$ photon reaches the measurement station at A' after being delayed in a fiber spool. This delay ensures that the measurement basis choice at this station is space-like separated from the trial region, see Assumption 9 in Sect. II.

Following the release of entangled photons from A_{source} , the verifier A transmits a random bit (u_A). This bit is freshly generated via a hardware random number generator at A, and its value is immediately recorded on a timetagger located at A. The bit is then encoded as an electronic non-return-to-zero (NRZ) signal with about a 1 V amplitude and transmitted via a specialized coaxial fiber that has a central conductor surrounded by a foam dielectric. The air in the foam reduces the relative permittivity of the surrounding insulator and allows these cables to support a signal propagation velocity that is between 85-87% of the speed of light [53]. In traditional low-density polyethylene (LDPE) coaxial cables, the velocity of propagation is closer to 66%. This classical signal travels towards the prover faster than the 1550 nm photon Q_P , which travels through an optical fiber of roughly comparable length at approximately 66% of the speed of light. Some time after u_A is released, verifier B releases its bit (u_B), which is recorded on a timetagger at verifier B). In our configuration, with verifier

B situated closer to the honest prover P than verifier A, this delay is set so that the bits u_A and u_B reach the (known) location of the honest prover at approximately the same time. The classical challenge bits reaching the honest prover at the same time is optimal because any discrepancy in the arrival times would mean that the honest prover would have to wait for either u_A or u_B before computing their XOR. Waiting in this way would increase protocol latency at the honest prover hardware station and the size of the realizable target region of our protocol. In our realization, the synchronization is slightly imperfect and u_B arrives at the prover 9(2) ns after u_A . Once the bits u_A and u_B reach the prover, the prover computes the XOR of the bits $m_P = u_A \oplus u_B$ using an application-specific integrated circuit (ASIC). This computation takes only a few nanoseconds and does not contribute significantly to the latency at the honest prover P. The honest prover then sets the basis of the Pockels cell (see Fig. 5) so that incoming photons will be projectively measured in basis $a1 = 6.7^\circ$ or $a2 = -29.26^\circ$, depending on whether $m_P = 0$ or $m_P = 1$ respectively. Here, the angles represent the projective bases corresponding to rotations of a linear polarizer relative to the horizontal. The angles are the same as in Ref. [33]. An incoming photon Q_P arrives shortly after the Pockels cell is set. The photon is then measured in the appropriate basis with a superconducting nanowire single photon detector (SNSPD). The output is duplicated with a power splitter into z_A and z_B , which are sent to the verifiers over separate specialized coaxial cables. These are similar to those used for the transmission of u_A and u_B to the honest prover P.

Approximately at the same time as the photon Q_P is measured at the honest prover, its partner photon $Q_{A'}$ is measured at the measurement station A' using a local random bit produced at the station $m_{A'}$. The photon is measured in the basis $b1 = -6.7^\circ$ or $b2 = 29.26^\circ$ depending on if the value of $m_{A'}$ is 0 or 1. The result of this local measurement, $o_{A'}$, is recorded on the timetagger at verifier A. Finally, the returning outputs from the honest prover z_A to verifier A are recorded on verifier A's timetagger, and z_B on verifier B's timetagger. This concludes one trial in the experiment. Trials are repeated sequentially at a 250 kHz rate. The data recorded on the timetaggers, including the input random bits from the verifiers and the output bits back from any provers, constitutes the raw trial record. This raw trial record is then processed based on classical timing markers that are exchanged between the two verifiers via a trusted classical channel. A trusted classical channel is also used by the verifiers to exchange information used to align and process the collected data.

C. Hardware and Timing

As discussed above, the experiment has three physically distinct locations, shown in, Fig. 5. One lab, which we call “A’s lab”, contains A, A' , and A_{source} ; one contains B; and one contains P.

A number of optical and electrical cables carry information back and forth between the labs in our demonstration. Because the timetaggers that record this information are separated from each other, and recorded trial information must be reconciled to a common timebase, the timetaggers must exchange timing information between themselves. In our demonstration, timing information is derived from an electronic “sync” signal, which is divided down from the 775 nm pump laser pulsed at 80 MHz, and serves as the master clock for pulse generation. This signal is first converted to optical pulses, which are sent to the honest prover’s lab over optical fiber. The optical signal is then converted back to an electronic signal and propagated to verifier B. The sync signal is also used by the prover’s hardware

to sample the output of the XOR circuit correctly. In principle, the challenges can serve as sync signals, in which case sending separate sync signals is not required.

Another timing signal that the experiment uses is a 10 MHz clock that serves as a timebase for the remote timetagers. The “sync” signal serves as a trial marker, but it is not at the correct frequency to synchronize our remote timetagers. The 10 MHz clock is generated at verifier A, split off and supplied to the local timetagger, converted to an optical signal, and transmitted via optical fibers all the way to verifier B, where it is supplied to B’s timetagger.

The sync signal is divided down to 250 kHz from the electronic output monitor of the 80 MHz pump laser such that the laser emits 320 pulses during every sync period. The laser pulses then propagate through a set of beam displacers and optics to reach a periodically poled potassium titanyl phosphate crystal in two spatial modes to produce the entangled state, consisting of the Q_P and $Q_{A'}$ portions of the entangled state. The time of emission of the quantum state Q_P from the verifier A lab is much earlier than the emission of the classical bit u_A . This is to ensure that the photon traveling slowly through fiber arrives at the honest prover in time to be measured. Because the measurement station A’ is in the same room as the verifier A, the fiber is looped up into a spool to delay measurement by 791(1) ns, as mentioned in a previous section. These single mode optical fibers are each of length ≈ 160 m and have a transmission efficiency of over 99%.

Other processes are also clocked off of the electrical sync signal. In addition to the sync signal that is propagated to verifier B, it is also sent to verifier A after passing through a digital delay circuit. The sync signal triggers hardware random number generators at A and B to in-part determine when they each emit a random bit (u_A and u_B) to the prover P over custom coaxial cables. The delay at verifier A is then set so that the random bits u_A and u_B arrive at the prover at approximately the same time. The relative timing of the bits is decided so that there is sufficient time for the XOR of the bits to be computed and the Pockels cell to be set to either a high or low voltage based on the result of the XOR by the time the photon Q_P arrives.

The electronic sync signal is also provided to the measurement station A’, which measures its photon $Q_{A'}$ based on a random number generator that is triggered again by this sync signal. The output of this measurement is immediately recorded on a local timetagger. Finally, the prover P transmits the measurement outcome from its measurement of photon Q_P to A and B over electrical coax cables. These signals containing the measurement outcome are recorded on timetagers. Due to electronic errors, in about 2×10^{-6} of trials, A’s and B’s records of the prover’s measurement outcome disagree. Besides the outcomes, a local record of the RNG bits u_A and u_B is recorded on the timetagers every trial, along with the timetag of the sync signal to serve as a reference. Because the entire experiment is clocked on this sync signal, the timetagger records can be reconciled with one another using the trusted delay measurements. This allows the creation of a trial-by-trial timing record of all relevant events.

IV. CLASSICAL SPACE-TIME MEASUREMENTS

Determining the localization regions achieved by our protocol requires making measurements on the timing signals and the physical distances separating the verifiers. Here, we provide a summary of our space-time measurement techniques and results.

We define time $t = 0$ as when the synchronization signal exits the divider circuit, which electronically divides the monitor output of the 775 nm pump laser. Several techniques are

used to estimate the timing of various events relative to this reference during a trial. For instance, to establish the time when the sync signal reaches the prover P and the far verifier station B, we measure some electrical latencies directly with an oscilloscope, measure certain electrical cable latencies using electrical reflectometry, measure optical cable latencies using optical time domain reflectometry (OTDR), and perform relative delay measurements with timetaggers.

a. Direct Oscilloscope Measurements Where appropriate, we measure the electrical latency of components in a single-pass configuration. We split pulses produced by a pulse generator with a ≈ 1 ns rise time, and measure relative delays on a 1 GHz oscilloscope employing length-matched coaxial cables. For single-pass optical measurements (always in free-space), we employ physical measurements of the path lengths.

b. Time Domain Reflectometry When single-pass measurements were not appropriate, we use electrical and OTDR to measure component latencies. Here, a pulsed source is directed through one end of an electrical or optical path such that the reflections off the far end can be timed and divided by two to compute the component latency.

The results for key events in the experiment are listed in table I and depicted in Fig. 7. While provided here for completeness, not all of these times need to be characterized or measured for the execution of the position verification protocol by the verifiers. The only times that must remain constant during a protocol run are the times when the verifiers send the challenge bits and receive the response bits (numbered 1, 2, 13 and 14). The constancy of these times can be checked with the verifiers’ timetaggers during data runs. The timetaggers are assumed to be functioning correctly and outside adversarial influence (see assumptions 3 and 4). For our demonstration, we verify the timings on a few data sets, and assume that the timings remain constant during the actual data runs.

A. Physical Distances

The physical distance between the verifiers is assumed to be known and constant during the protocol, see Sect. II, assumption 5. We determine this distance with measuring tape by hand-measuring a set of orthogonal spans. The location of the prover hardware that we install for demonstrating successful runs of the protocol has a bearing on the choices of time delays used for the classical position verification. We measure these distances with measuring tape also. In a real-world implementation of this protocol, these distances must first be established using classical geomapping techniques before one could implement the position verification protocol.

The major contributors to uncertainty in the physical measurements is the uncertainty in the orthogonality of the various spans in the building, and the size of the exit points of the verifier labs. To estimate the effect of various uncertainties, we perform Monte-Carlo sampling based on the uncertainties of the individual spans, and the uncertainty in the solid angles connecting the various spans. Uncertainty in the solid angles shortens the best estimate for the separation between the verifiers because deviations from 90° for the angles between the orthogonal spans reduce the verifier separation. We estimate that the building is true to 1° , and employ a projected normal distribution to model angular uncertainty. The largest source of uncertainty is the 200 mm uncertainty in the size of the verifier locations (cable exit points) A and B, pictured in Fig. 6. A summary of the distance measurements is presented in table II.

Index	Parameter	Value
1.	Verifier A: random u_A out	1291.0(5) ns
2.	Verifier B: random u_B out	1429.1(6) ns
3.	Verifier A: photon Q_P exits laser	1023.3(3) ns
4.	Verifier A: photon Q_P emitted	1133(2) ns
5.	Verifier A': setting $m_{A'}$ created	1738.8(4) ns
6.	Verifier A': outcome $o_{A'}$ recorded	1874.5(3) ns
7.	Prover P: u_A in from A	1766(1) ns
8.	Prover P: u_B in from B	1769(1) ns
9.	Prover P: signal into Pockels cell	1798(1) ns
10.	Prover P: photon Q_P arrives at Pockels cell	1831(1) ns
11.	Prover P: photon Q_P arrives SNSPD	1858(2) ns
12.	Prover P: signals z_A, z_B created	1868(2) ns
13.	Verifier B: response z_B in	2207.7(6) ns
14.	Verifier A: response z_A in	2340.3(5) ns

TABLE I. A summary of the times events occur in a position verification trial, referenced to the time the synchronization signal exits the divider circuit as time $t = 0$ ns. Relevant events in the trial span about 1050 ns, if we consider the classical signal exiting the verifier A lab as the start time at verifier A. The protocol run time would increase with larger separations between the verifiers A and B. The trial rate is 4 μ s. See Fig. 7 for a visualization of these key events.

Distance	Value
Verifier A - Verifier B	195.1(3) m
Verifier A - Prover P (proj.)	92.8(1) m
Verifier A - Verifier A' TTAG (proj.)	192.2(3) m
Verifier A - Verifier A' RNG (proj.)	192.2(2) m

TABLE II. This table summarizes key measured distances and their associated uncertainties for our experimental layout. Because there are only two verifiers in our demonstration, the only relevant distances are those projected onto the line joining the verifiers, indicated by “(proj.)”.

B. Target Regions in the Spatial Dimensions

Using the distance and timing measurements, the verifiers can establish the target region that effectively localizes the successful prover. A formal treatment of the target region is presented in Sect. V A. In this section, we outline how the target region realized by the experimentally implemented protocol instance is calculated.

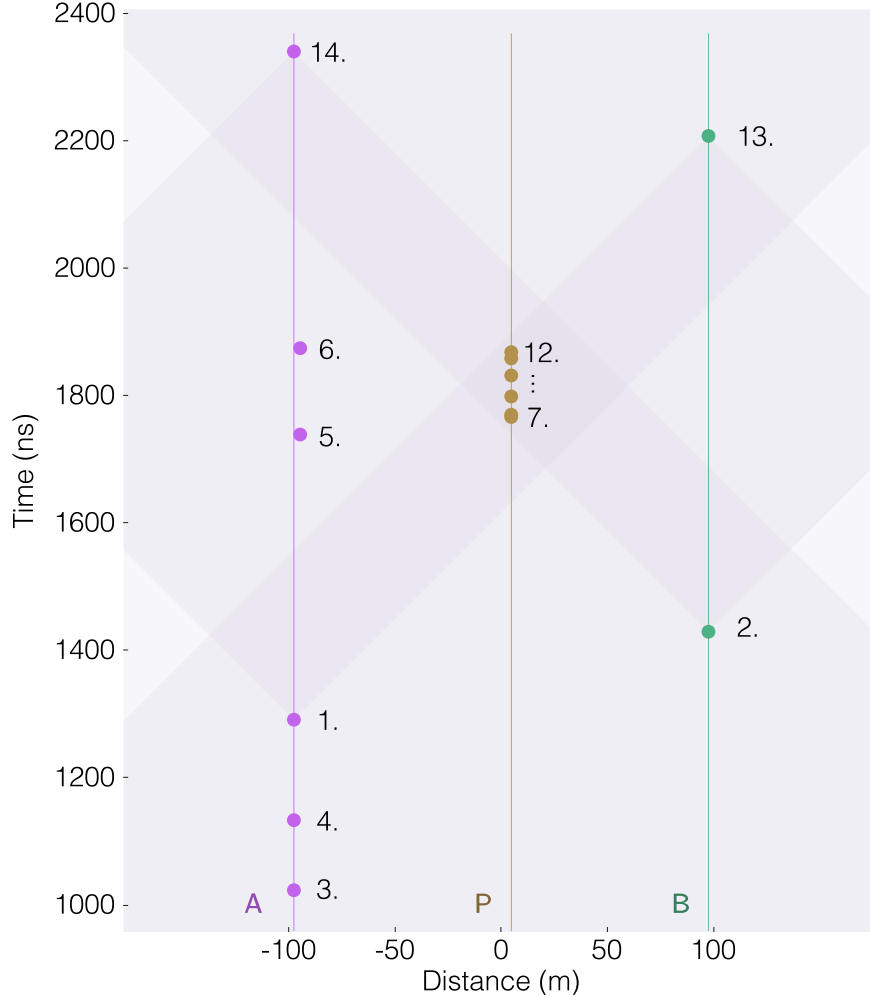


FIG. 7. Spacetime diagram of the position verification protocol. Important events during one trial of the protocol (listed in table I) are marked. The green lightcones are forward and backward lightcones from the times s_A , s_B , r_A , and r_B (labeled 1, 2, 14 and 13 respectively) when the verifiers send the challenge bits and receive the response bits (see Sect. IV B). The target region is the dark diamond that contains points 7 through 12. The events labeled 5 and 6 occur at A' , which is slightly offset from A. The origin (time $t = 0$) of both this figure and table I is when the sync signal corresponding to a particular trial exits the divider board. (see Sect. III C).

1. Experimental Parameters for Determining Target Regions

Our experiment is a series of trials, and times for trial k are described relative to the start time t_k for that trial. To compute the extent of the target region E in 3+1 dimensions, and lower-dimensional projections thereof, as in Fig. 3 of the main text, only four times are relevant. These are the times when the verifiers send classical challenge bits and the latest times they accept responses. Following the notation introduced in Sect. I, $t_k + s_A$ and $t_k + s_B$ are the times at which A and B emit their challenges u_A and u_B toward the prover. The verifiers agree beforehand that responses must be received by times $t_k + r_A$ and $t_k + r_B$ at A and B respectively. In our implementation, the verifiers time-tag when challenges are emitted, and when responses are received.

Parameter Description	Value
Sphere $S(A, c(r_A - s_A))$, radius	157.3(2) m
Sphere $S(B, c(r_B - s_B))$, radius	116.7(2) m
Ellipsoid $E(A, B; c(r_B - s_A))$, major axis	274.8(2) m
Ellipsoid $E(A, B; c(r_A - s_B))$, major axis	273.1(2) m
Focal distance for ellipsoids (verifier separation)	195.1(3) m

TABLE III. Extents of the geometric localization regions derived from the timing and distance measurements in the experimental setup. All values are presented with their associated uncertainties, rounded to two decimal places. The units for these measurements are meters.

A successful prover must simultaneously satisfy the following constraints related to the timing of signals in every trial (in addition to producing a Bell violation at the verifiers).

1. Receive challenge u_A (released at $t_k + s_A$) from **A** and reply with z_A to **A** (by $t_k + r_A$).
2. Receive challenge u_B (released at $t_k + s_B$) from **B** and reply with z_B to **B** (by $t_k + r_B$).
3. Receive challenge u_A (released at $t_k + s_A$) from **A** and reply with z_B to **B** (by $t_k + r_B$).
4. Receive challenge u_B (released at $t_k + s_B$) from **B** and reply with z_A to **A** (by $t_k + r_A$).

These constraints require that the prover measures Q_P with low enough latency to be able to respond in time and that the messages are transmitted to and from a prover over fast enough classical channels. As explained in the main text,

- Constraint 1 enforces a sphere of radius $\frac{c(r_A - s_A)}{2}$ centered around **A**, $S(A, c(r_A - s_A))$.
- Constraint 2 enforces a sphere of radius $\frac{c(r_B - s_B)}{2}$ centered around **B**, $S(B, c(r_B - s_B))$.
- Constraint 3 enforces an ellipsoid of rotation with foci at the verifiers and a major axis $c(r_B - s_A)$, $E(A, B; c(r_B - s_A))$.
- Constraint 4 enforces an ellipsoid of rotation with foci at the verifiers and a major axis $c(r_A - s_B)$, $E(A, B; c(r_A - s_B))$.

The dimensions of these shapes are indicated in table III. The target region for each trial is the intersection of these spheres and ellipsoids, which are all rotation ally symmetric about the axis joining the verifiers.

Because of the periodic nature of the trials, there is also a periodic constraint in the times that a prover must be located in these regions, which is not captured in the spatial projections.

2. Computing Target Regions

When projecting the target regions to the spatial dimensions (to perform position localization), the aforementioned two spheres and two ellipsoids are the only relevant geometries that verifiers need to estimate. Estimating these geometries requires measurement of the physical distance between the verifiers determined via the procedures outlined in table II, and the start and end transmission times determined by the verifiers' timetagger measurements (see table I).

For the QPV protocol, the target region E (where an honest prover must be located) projected to spatial dimensions is the intersection of the two spheres and two ellipses from Constraints 1-4 above, $E = S(A, c\Delta\tau_1) \cap S(B, c\Delta\tau_2) \cap E(A, B; c\Delta\tau_3) \cap E(A, B; c\Delta\tau_4)$. This is

shown in Sect. V A.

The target regions can also be projected into lower spatial dimensions (one and two dimensions). For a one-dimensional projection, the projection of interest is along the line joining the verifiers, and for two dimensions, it is the plane roughly parallel to the ground and containing the line joining the verifiers. Because of the rotational symmetry of the regions, projection onto any plane rotated along the line joining the verifiers yields an identical target region.

When projecting onto lower-dimensional regions, the spheres and ellipsoids reduce to lines in one dimension and circles and ellipses in two dimensions. The target region E can also be computed as a projection into these lower-dimensional regions. To perform these calculations, we use the known distances between the verifiers from table VI, and the timings from table I to numerically compute the lengths, areas and volumes of the target regions of the quantum protocol (quantum target region) in one, two and three dimensions. We also use the uncertainties in these quantities to run a Monte Carlo simulation to yield an estimate of the uncertainty in the length/area/volume of the target region.

3. Comparing Classical and Quantum Target Regions

An alternative protocol where the verifiers only require an honest prover to compute a classical function based on inputs u_A and u_B can be considered, see Sect. V A. Because such a protocol requires no quantum resources on the part of the prover or the verifiers, it serves as a useful comparison to our QPV protocol. If the target region achievable with the classical position verification protocol is comparable in size to the quantum target region E , we gain little by adding quantum resources to our protocol. On the other hand, if the quantum target region is significantly smaller than the classically achievable target region, we take our protocol to have demonstrated a quantum advantage. We note that the security of such a classical protocol is based on the impossibility of faster-than-light signaling and thus does not require restrictions on the entanglement shared between the adversaries that our quantum protocol requires (detailed in V D, also see Assumption 7).

We employ the following metric to quantify the advantage of using quantum resources,

$$\text{Quantum Advantage} = \frac{\text{size of classical target region}}{\text{size of quantum target region (E)}} \quad (1)$$

The “size” in the metrics may be a length, area, or volume when considering one, two or three-dimensional position verification. An ideal quantum protocol (without experimental latencies in transmission and processing) can achieve an infinite Quantum Advantage, as defined above. In general, the goal of a good quantum protocol is to maximize the Quantum Advantage.

In this work, we compare our quantum experiment to two classical protocols:

The ideal classical protocol involves the verifiers sending challenges at the speed of light, and the implemented prover replying back with zero latency, also at the speed of light. The target region is the point exactly at the midpoint of the line joining the verifier. This represents the classical protocol with the smallest possible target region.

The comparable classical protocol involves the verifiers sending challenges and receiving responses at the same times as our quantum protocol ($t_k + r_A, t_k + r_B, t_k + s_A, t_k + s_B$). The motivation here is to consider a practically implementable classical protocol. For any prover

Dimension	Quantum Advantage
1D (vs Ideal Classical)	2.47(2)
1D (vs Comparable Classical)	4.48(2)
2D (vs Comparable Classical)	4.02(3)
3D (vs Comparable Classical)	4.53(5)

TABLE IV. Comparison of localization ratios and quantum advantages for QPV protocols in different dimensions. The quantum protocol achieves zero quantum advantage compared to the ideal classical protocol in 2D and 3D because the ideal classical size is zero in 2D and 3D. Reported uncertainties are one standard deviation.

implementation, computing classical functions has lower latency than making quantum measurements. So it is reasonable that a classical protocol with the latencies we demonstrate here for the quantum protocol can be implemented.

For the classical protocols, a pair of provers can collude to pass the protocol as long as one of them is in $(S(A, c\Delta\tau_1) \cap E(A, B; c\Delta\tau_3))$, and the other in $(S(B, c\Delta\tau_2) \cap E(A, B; c\Delta\tau_4))$. This is shown in Sect. V A. We take this to mean that the classical target region is the union of these two regions for all our comparisons.

For **the ideal classical protocol**, the ellipsoids from Constraints 3 and 4 reduce to degenerate line segments. This is because the major axis is equal to the distance between the verifiers ($c(r_A - s_B) = c(r_B - s_A) = d_{AB}$). The classical target region is the line segment joining the verifiers. Because this is an *ideal* protocol, the target region is one-dimensional. The only uncertainty associated with the size of this region is in the distance between the verifiers. The quantum advantage for the ideal classical protocol is the ratio of its target region to the quantum target region projected along the line joining the verifiers. We performed Monte Carlo simulations to estimate the uncertainty in this ratio. The results are presented in table IV.

For **the comparable classical protocol**, the target regions in one, two and three dimensions all have non-zero sizes, and we compare these to the sizes of the quantum target region. This computation is similar to that done for the ideal classical protocol. The results of these comparisons are presented in table IV, Fig. 8 and in the main text.

V. THEORY

A. Spacetime analysis

For defining the target region and the restrictions on prior entanglement of adversaries, we use a version of the spacetime circuit formalism and adversary analysis introduced in Ref. [50] for QPV protocols with parties that have access to so-called random oracles for defining the settings function. The analysis of Ref. [50] applies to any number of verifiers and needs no restriction on the amount of prior entanglement of adversaries. However, the protocol depends on the purely theoretical tool of random oracles. We cannot use oracles for the settings function and therefore require a different version of this spacetime analysis

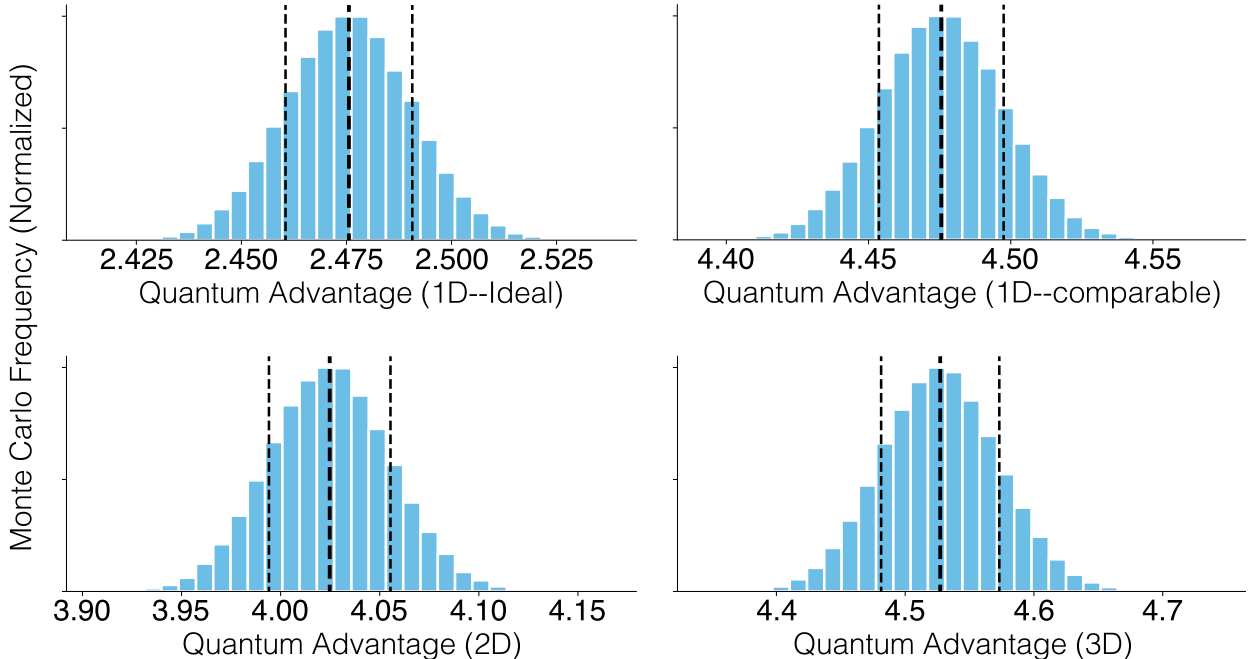


FIG. 8. Histograms showing the relative frequencies of the quantum advantage from 10^5 Monte Carlo simulations. The simulations sample the measured distances and timings based on estimated uncertainties to arrive at the quantum advantage distributions. The uncertainties on individual timing and distance measurements are modeled as Gaussian (with the exception of angular uncertainties, which use projected Gaussians). The largest source of uncertainty is the physical ambiguity in the definition of the verifier A and B positions, see Fig. 6. The mean and $\pm 1\sigma$ for each distribution are indicated with vertical black dashed lines. The top row plots the quantum advantage against ideal and comparable quantum protocols in 1 dimension, while the bottom row plots the advantage against the comparable protocol in 2 and 3 dimensions.

to identify the adversary capabilities and the time slice on which entanglement is restricted. For this purpose, we provide a self-contained description of the formalism and analysis. We first define the target region and the time slice on which adversaries' entanglement is restricted. We then reduce the problem of analyzing adversary capabilities without prior entanglement to the case of having two separate, initially unentangled adversaries that can each communicate to the other only once before committing to responses to the verifiers.

Spacetime circuits: We assume familiarity with the fundamental concepts of relativistic spacetime. Our theory applies to any time-oriented globally-hyperbolic Lorenzian manifold \mathcal{M} . Minkowski space is the most familiar example of such a manifold. For a comprehensive treatment of the relevant concepts see, for example, Ref. [54]. Here we give a brief overview of the concepts used here. An event or spacetime point in spacetime is identified by its position in the manifold. A worldline is a forward-directed light- or time-like path in spacetime. For our purposes, a worldline may be identified with the image of a differentiable function $\mathbf{r}(x)$ from an interval I on the reals to spacetime, where I may be open or closed on either end, and $d\mathbf{r}(x)/dx$ is forward-directed, light-like or time-like on the interior of I . The worldline is inextendible if it is not a proper subset of another worldline. Event \mathbf{r}' causally follows event \mathbf{r} if there is a worldline that contains both \mathbf{r} and \mathbf{r}' , and \mathbf{r}' follows \mathbf{r} on the worldline.

Because we assume global hyperbolicity, this defines the causal partial order on spacetime, and we write $\mathbf{r} \preceq \mathbf{r}'$ if \mathbf{r}' causally follows \mathbf{r} . The closed forward lightcone $C_{\mathbf{r},+}$ at \mathbf{r} consists of the events that causally follow \mathbf{r} , including \mathbf{r} . Similarly, the closed backward lightcone $C_{\mathbf{r},-}$ at \mathbf{r} consists of the events that causally precede \mathbf{r} , including \mathbf{r} . Lightcones have the property that no worldline can exit a forward lightcone or enter a backward lightcone. This means that the intersection of an inextendible worldline with a lightcone is either empty or a closed half-line. Backward lightcones are instances of past sets, which are defined as subsets J of spacetime such that if $\mathbf{r} \in J$ and $\mathbf{r}' \preceq \mathbf{r}$, then $\mathbf{r}' \in J$. Boundaries of past sets are instances of time slices, which we define to be closed space-like subsets of spacetime whose spacetime complement has two connected components, one consisting of the events that causally precede the time slice, and the other consisting of the events that causally follow the time slice. Space-like subsets satisfy that for every pair \mathbf{r} and \mathbf{r}' in the subset, neither $\mathbf{r} \preceq \mathbf{r}'$ nor $\mathbf{r}' \preceq \mathbf{r}$. Global hyperbolicity is equivalent to the existence of a time slices satisfying the property that every inextendible wordline intersects the time slice. In Minkowski space, the boundaries of light cones are examples of time slices that do not satisfy this property. A subset D of spacetime is causally convex if for every wordline that starts and ends in D , the wordline is contained in D . Equivalently, if $\mathbf{r} \preceq \mathbf{r}'$ are events in D and \mathbf{r}'' satisfies $\mathbf{r} \preceq \mathbf{r}'' \preceq \mathbf{r}'$, then $\mathbf{r}'' \in D$. A special case of a causally convex subset is a light diamond from one event \mathbf{r} to another \mathbf{r}' , which is defined as the intersection of the forward light cone $C_{\mathbf{r},+}$ at \mathbf{r} and the backward light cone $C_{\mathbf{r}',-}$ at \mathbf{r}' . Light diamonds are empty if \mathbf{r}' does not causally follow \mathbf{r} . The intersection of a worldline with a light diamond forms a time-bounded interval, which may be empty.

The following is a conceptual description of the behavior of entities such as verifiers and provers in spacetime: All entities exist on worldlines. The entities can interact with communications. Communications travel on worldlines starting on one entity's worldline and ending at another's. We refer to the events where an entity sends or receives a communication as interaction vertices and assume that there are finitely many such vertices in every compact region of spacetime.

Spacetime circuits abstract the conceptional description above. Spacetime circuits do not distinguish between worldlines of communications and entities connecting vertices, and confine the dynamics of systems to the vertices. In the conceptual picture, entities may perform operations along their worldlines. In the spacetime circuit, such operations are moved forward to the next interaction vertex along the line and combined into one operation.

Spacetime circuits \mathcal{S} are defined by the following: (1) A set of interaction vertices $\mathcal{V} = \mathcal{V}(\mathcal{S})$, which are events in spacetime. (2) A set of causally directed edges $\mathcal{E} = \mathcal{E}(\mathcal{S})$ representing worldlines connecting two events in spacetime, at least one of which is an interaction vertex in \mathcal{V} . The two events connected by an edge E are referred to as the source vertex $V_{\text{src}}(E)$ and the target vertex $V_{\text{tgt}}(E)$, where $V_{\text{tgt}}(E)$ causally follows $V_{\text{src}}(E)$. An edge E is internal if both endpoints are in the set \mathcal{V} . It is external if exactly one of the endpoints is in \mathcal{V} . (3) For each edge $E \in \mathcal{E}$ an assignment of a quantum system $Q(E)$ carried by E . (4) For each vertex $V \in \mathcal{V}$ a quantum operation $\mathcal{O}(V)$ that jointly transforms incoming quantum systems to outgoing quantum systems at V . For a vertex $V \in \mathcal{V}$, the incoming quantum systems are those associated with edges E whose target vertex is V , that is, $V_{\text{tgt}}(E) = V$. The outgoing quantum systems are those associated with edges E whose source vertex is V . The quantum operation at a vertex without incoming edges is a state preparation on the joint quantum systems of the outgoing edges. The operation at a vertex with no outgoing edges discards the quantum systems of the incoming edges. We refer to

the state of quantum systems of edges simply as the state of the edges.

Spacetime circuits describe the dynamics of the edge systems. Intuitively, for any time slice, the systems of edges crossing this time slice have a joint state, and the quantum operations on the vertices determine the joint state on a later time slice given the joint state on an earlier one. To treat this dynamics formally, we introduce a number of causal concepts for spacetime circuits. The vertices and edges of a spacetime circuit form a directed acyclic graph, which induces a partial order over the union of the vertex and edge sets. A directed path in the circuit is a sequence of alternating vertices and edges $(A_k)_{k=0}^m$ with $m \geq 0$ that starts with either a vertex or an edge, where the vertices and edges along the sequence are incident on each other and in causal order. Specifically, if A_k is an edge and A_{k+1} is a vertex, then $A_{k+1} = V_{\text{tgt}}(A_k)$, and if A_k is a vertex and A_{k+1} is an edge, then $A_k = V_{\text{src}}(A_{k+1})$. Topologically, we can associate to each edge its open worldline between its source vertex and its target vertex. Then the union of the vertices and edges on a directed path is a worldline. We use directed paths to define the circuit partial order. For two vertices or edges A and B , A precedes B in the circuit partial order, written $A \leq B$, iff there is a directed path starts with A and ends with B . This partial order is weaker than the partial order induced by spacetime causality, in the sense that we can have A causally precede B in spacetime but not $A \leq B$ in the circuit partial order.

A vertex subset \mathcal{V}' of \mathcal{V} is causally convex if for every directed path starting and ending in \mathcal{V}' , all vertices on the path are in \mathcal{V}' . We define the sets of in-edges and out-edges of \mathcal{V}' as $\text{in}(\mathcal{V}') = \{E \in \mathcal{E} : V_{\text{src}}(E) \notin \mathcal{V}', V_{\text{tgt}}(E) \in \mathcal{V}'\}$ and $\text{out}(\mathcal{V}') = \{E \in \mathcal{E} : V_{\text{src}}(E) \in \mathcal{V}', V_{\text{tgt}}(E) \notin \mathcal{V}'\}$. That is, $\text{in}(\mathcal{V}')$ includes all edges entering \mathcal{V}' from outside, while $\text{out}(\mathcal{V}')$ includes all edges exiting \mathcal{V}' to the outside. A causally convex set of vertices \mathcal{V}' defines a spacetime subcircuit $\mathcal{S}(\mathcal{V}')$ with vertex set \mathcal{V}' and edge set \mathcal{E}' consisting of the edges in \mathcal{E} with at least one endpoint in \mathcal{V}' . The external edges of $\mathcal{S}(\mathcal{V}')$ consist of the union of $\text{in}(\mathcal{V}')$ and $\text{out}(\mathcal{V}')$. A causally convex set of vertices \mathcal{V}' and its associated spacetime subcircuit $\mathcal{S}(\mathcal{V}')$ define a quantum operation $\mathcal{O}(\mathcal{V}')$ that maps the quantum systems of its in-edges to those of its out-edges. This quantum operation can be constructed recursively as follows: 1) Every set \mathcal{V}' consisting of a single vertex V is causally convex, and its quantum operation is given by $\mathcal{O}(\mathcal{V}') = \mathcal{O}(V)$. 2) If \mathcal{V}' consists of more than one vertex, choose a vertex $Z \in \mathcal{V}'$ that is maximal in the circuit partial order restricted to \mathcal{V}' . That is, no other vertex in \mathcal{V}' lies after Z along a directed path. Then the reduced set $\mathcal{V}'' = \mathcal{V}' \setminus \{Z\}$ is causally convex. Suppose that we have constructed the quantum operation $\mathcal{O}(\mathcal{V}'')$ of \mathcal{V}'' . The in-edges of Z partition into $\mathcal{Z}_1 = \text{in}(\{Z\}) \cap \text{out}(\mathcal{V}'')$ consisting of the in-edges of Z that are out-edges of \mathcal{V}'' , and $\mathcal{Z}_2 = \text{in}(\{Z\}) \cap \text{in}(\mathcal{V}')$ consisting of the in-edges of Z that are in-edges of \mathcal{V}' . The in-edges of \mathcal{V}' consist of the in-edges of \mathcal{V}'' and the edges of \mathcal{Z}_2 . The quantum operation of \mathcal{V}' is constructed by adjoining the quantum systems of edges in \mathcal{Z}_2 to those of the edges $\text{in}(\mathcal{V}'')$, applying $\mathcal{O}(\mathcal{V}'')$ to the latter, and then applying the $\mathcal{O}(Z)$ to both the systems of edges in \mathcal{Z}_2 and the systems of edges in \mathcal{Z}_1 that appeared at the output of $\mathcal{O}(\mathcal{V}'')$.

The spacetime circuit notion of a time slice and its state is captured by an antichain of edges and the joint state of their systems. A set of edges \mathcal{A} is an antichain if no pair of edges in \mathcal{A} is comparable in the circuit partial order, that is, there is no directed path connecting two edges in \mathcal{A} . For an antichain of edges \mathcal{A} , consider the set \mathcal{V}' of vertices V for which there exists an edge E in \mathcal{A} such that $V \leq E$. Intuitively, \mathcal{V}' consists of the vertices that lie in the causal past of the antichain \mathcal{A} . Then the set \mathcal{V}' is causally convex. To see this, consider a directed path from vertex $V_1 \in \mathcal{V}'$ to vertex $V_2 \in \mathcal{V}'$, and let V_3 be a vertex on the path. By definition of the circuit partial order, $V_3 \leq V_2$, and by construction of \mathcal{V}' , $V_2 \leq E$ for some

edge $E \in \mathcal{A}$. Therefore, $V_3 \leq E$, which implies that $V_3 \in \mathcal{V}'$. The state of the systems of the antichain is determined by the joint state of the quantum systems on the in-edges of \mathcal{V}' . The quantum operation $\mathcal{O}(\mathcal{V}')$ transforms this joint state into a joint state of the quantum systems of its out-edges. Because the source vertices of the edges in \mathcal{A} are in \mathcal{V}' , the edges in \mathcal{A} are among the out-edges of \mathcal{V}' . The state of \mathcal{A} is obtained by tracing out the systems on the out-edges of \mathcal{V}' that are not in \mathcal{A} .

For a spacetime circuit \mathcal{S} with vertex set \mathcal{V} and a subset D of spacetime, the intersection $\mathcal{V} \cap D$ consists of all vertices in \mathcal{V} that lie within the region D . If D is causally convex in spacetime, then $\mathcal{V} \cap D$ is causally convex in the spacetime circuit \mathcal{S} . This is because the circuit partial order on the vertices of \mathcal{V} is weaker than the partial order induced by spacetime causality. Consequently, If V and V' are vertices in $\mathcal{V} \cap D$ and V'' is a vertex of \mathcal{V} satisfying $V \leq V'' \leq V'$ in the circuit partial order for \mathcal{S} , then $V \preceq V'' \preceq V'$ in the causal partial order, so $V'' \in D$.

Spacetime circuit for verifiers and provers: We model verifiers and provers as a spacetime circuit \mathcal{S} that spans all trials of the QPV protocol. We consider a generic trial with start time t . We specify an event with the notation $\mathbf{r} = (\mathbf{x}, s)$, where \mathbf{x} is the spatial location, and s is the time. For $F = A, B$, let $C_{F,+}$ be the forward lightcone from $\mathbf{r}_{F,s} = (\mathbf{x}_F, t + s_F)$ and $C_{F,-}$ the backward lightcone from $\mathbf{r}_{F,r} = (\mathbf{x}_F, t + r_F)$, where $t + s_F$ and $t + r_F$ are the times at which the verifier F sends a challenge and receives a response, respectively. $C_{F,+}$ is the region within which the challenge sent by F is visible to provers, and $C_{F,-}$ is the region within which it is possible for a prover to send a response to F . Let $D_F = C_{F,+} \cap C_{F,-}$ be the light diamond from $\mathbf{r}_{F,s}$ to $\mathbf{r}_{F,r}$, representing the region in which a valid challenge–response interaction with the verifier F could occur. The target region for the trial is defined as $E = D_A \cap D_B$, which we assume to be non-empty. The target region for the QPV protocol is the union of the target regions for each trial. We analyze spacetime circuits in $d + 1$ -dimensional spacetime, where $d \geq 1$. For an illustration of the relevant regions in a $1 + 1$ -dimensional Minkowski cross-section containing the verifiers in the experiment, see Fig. 9. The labeling of the regions is introduced before Eq. (1), when we reduce the available adversary strategies to those achievable by two adversaries.

For each trial, the time slice on which entanglement of adversaries is restricted is defined as the boundary T of the set $\mathcal{M}_{\text{in}} = (C_{A,-} \cup C_{B,-}) \cap (\mathcal{M} \setminus (C_{A,+} \cup C_{B,+}))$, where \mathcal{M} is the spacetime manifold. See Fig. 9 for a visualization of T in the $1 + 1$ -dimensional cross-section containing the verifiers in the experiment. We refer to T as the trial boundary. The set \mathcal{M}_{in} is a past set. \mathcal{M}_{in} can be described as the set of events at which the trial’s challenges are not yet visible, but from which it is possible to send a response to at least one of the verifiers A or B . All events relevant to the trial occur in the union $C_{A,-} \cup C_{B,-}$. If \mathcal{M}'_{in} is the region defined in the same way as \mathcal{M}_{in} but for the next trial, then \mathcal{M}'_{in} contains $C_{A,-} \cup C_{B,-}$ of the current trial. This ensures that all events of the current trial occur before the trial boundary of the next one, and, similarly, all events of previous trials occur before the current boundary T . The restriction on adversarial entanglement is formulated in terms of the spacetime circuit’s edges that exit \mathcal{M}_{in} and is defined in terms of the systems listed at (3) after introducing the adversary spacetime circuit.

We now determine the adversary spacetime circuit, which by definition satisfies that there are no vertices in the trial’s target region E . Later we generalize the analysis by allowing a limited class of vertices in the target region E to prove that honest provers must employ quantum devices in the target region to successfully pass the protocol. The trial circuit \mathcal{C} is defined as the spacetime circuit associated with the vertices in the causally convex

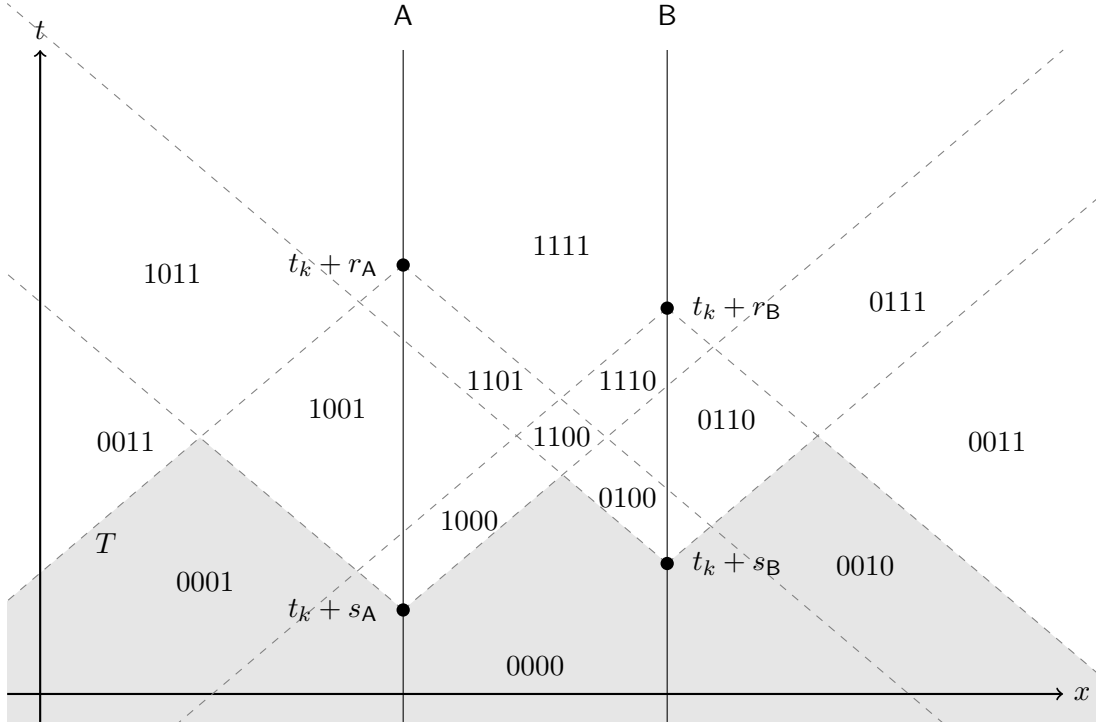


FIG. 9. Schematic 1 + 1-dimensional spacetime cross-section of a trial. The trial boundary T is the boundary of the grey-shaded region, which is the 1 + 1-dimensional cross-section of the region \mathcal{M}_{in} defined in the text. The k^{th} trial is shown and t_k is the trial's start time according to the protocol. The regions are labeled by 4-bit strings according to the convention introduced before Eq. (1), where bits 1 and 2 determine whether the points are causally after $t_k + s_{A'}$ and $t_k + s_B$, respectively; bits 3 and 4 determine whether the points are not causally before $t_k + r_{A'}$ and $t_k + r_B$, respectively. The region labeled with 0011 appears in two places, and regions labeled with 1010 and 0101 do not appear in this cross-section.

set $(C_{A,-} \cup C_{B,-}) \cap (C_{A,+} \cup C_{B,+})$. The trial record is determined by the trial circuit \mathcal{C} and the state on the in-edges of \mathcal{C} . The vertices of \mathcal{C} partition into verifier vertices and adversary vertices, where verifier vertices include any operations that are performed by verifier-owned devices and needed to implement the verifiers' protocol actions. The edges connecting verifiers and adversaries are restricted by Assumption 4. In particular, the only edges from verifiers to adversaries are those carrying the challenges. In addition, there are no edges from adversaries to verifiers that precede an edge from verifiers to adversaries. This restriction implies that no directed path starting and ending at adversary vertices can pass through a verifier vertex. Therefore, the set of adversary vertices is causally convex. Let \mathcal{A} be the spacetime subcircuit associated with the adversary vertices.

Reduction to two adversaries and one round of communication: Such a reduction is given for a protocol with idealized timing in Ref. [55] for one space dimension. Here we provide the reduction for any number of space dimensions. To analyze the capabilities of the adversary spacetime circuit \mathcal{A} , we partition the vertices of the circuit into causally convex subsets determined by the locations of vertices relative to the verifiers' sending and receiving vertices. For every event \mathbf{r} in spacetime, we assign a 4-bit string $l(\mathbf{r}) = b_1 b_2 b_3 b_4$ defined as follows: $b_1 = 1$ if $\mathbf{r} \in C_{A,+}$, $b_2 = 1$ if $\mathbf{r} \in C_{B,+}$, $b_3 = 1$ if $\mathbf{r} \notin C_{A,-}$, and $b_4 = 1$ if $\mathbf{r} \notin C_{B,-}$,

with $b_j = 0$ if the condition for $b_j = 1$ is not satisfied. Each bit encodes whether the event \mathbf{r} lies inside or outside an associated forward or backward lightcone. We form bit strings by concatenating the bit values. For two such bit strings \mathbf{b} and \mathbf{b}' , we define a partial order on bitstrings by bit-wise comparison and write $\mathbf{b} \leq \mathbf{b}'$ if each bit of \mathbf{b} is less than or equal to the corresponding bit of \mathbf{b}' . This partial order reflects the causal ordering of events: If an event \mathbf{r} causally precedes another event \mathbf{r}' , then $l(\mathbf{r}) \leq l(\mathbf{r}')$.

For each 4-bit string \mathbf{b} , the set $\mathcal{M}_{\mathbf{b}} = \{\mathbf{r} : l(\mathbf{r}) = \mathbf{b}\}$ is causally convex. This is because $\mathcal{M}_{\mathbf{b}}$ is the intersection of four causally convex sets specified by the values of the bits of \mathbf{b} . Since the intersection of causally convex sets is also causally convex, $\mathcal{M}_{\mathbf{b}}$ inherits this property. The set \mathcal{M}_{1100} is the target region E . This region is the intersection of the four closed lightcones $C_{A,\pm}$ and $C_{B,\pm}$, and is therefore also closed. For a subset B of 4-bit strings, let $\mathcal{M}_B = \cup_{\mathbf{b} \in B} \mathcal{M}_{\mathbf{b}}$. In general, a subset I of a partially ordered set P is called order-convex if for every $x, y \in I$ with $x \leq y$ and $z \in P$ with $x \leq z \leq y$, we have $z \in I$. In particular, causally convex sets of interaction vertices in a spacetime circuit are order-convex for the circuit partial order. If B is order-convex, then the set \mathcal{M}_B is causally convex. To see this, consider arbitrary events $\mathbf{r}, \mathbf{r}' \in \mathcal{M}_B$ and an event \mathbf{r}'' in \mathcal{M} with $\mathbf{r} \preceq \mathbf{r}'' \preceq \mathbf{r}'$. We have to show that $\mathbf{r}'' \in \mathcal{M}_B$. Be the relationship between the causal ordering and the partial order of bit strings, $l(\mathbf{r}) \leq l(\mathbf{r}'') \leq l(\mathbf{r}')$. Since B is order-convex, $l(\mathbf{r}'') \in B$ which implies that $\mathbf{r}'' \in \mathcal{M}_B$. We adopt the convention that the bit symbol “*” stands for either 0 or 1, and a bit string that has *’s denotes the set of bit strings obtained by replacing the *’s with 0 or 1. With this convention, the strings \mathbf{b} with alphabet $\{0, 1, *\}$ denote order-convex subsets of bitstrings and consequently, the corresponding the sets $\mathcal{M}_{\mathbf{b}}$ are causally convex. The regions that appear in the cross-section shown in Fig. 9 are labeled by bitstrings according to this convention. The regions \mathcal{M}_{1010} and \mathcal{M}_{0101} do not appear in the figure.

Let \mathcal{V} be the set of vertices of \mathcal{A} . For an order-convex set B of 4-bit strings, \mathcal{M}_B is causally convex in spacetime, from which it follows that $\mathcal{V} \cap \mathcal{M}_B$ is causally convex in \mathcal{A} . Since the set of vertices \mathcal{V} of \mathcal{A} are causally convex in the trial circuit \mathcal{C} , $\mathcal{V} \cap \mathcal{M}_B$ is also causally convex in \mathcal{C} . We define $\mathcal{A}_B = \mathcal{S}(\mathcal{V} \cap \mathcal{M}_B)$ to be the spacetime subcircuit of \mathcal{A} and of \mathcal{C} determined by the vertices in $\mathcal{V} \cap \mathcal{M}_B$. We partition \mathcal{A} into the following vertex-disjoint spacetime subcircuits:

$$\begin{aligned}
\mathcal{A}_{\text{in}} &= \mathcal{A}_{\{00*0,000*\}}, \\
\mathcal{A}_{A,\text{start}} &= \mathcal{A}_{\{100*,1010\}}, \\
\mathcal{A}_{B,\text{start}} &= \mathcal{A}_{\{01*0,0101\}}, \\
\mathcal{A}_{A,\text{end}} &= \mathcal{A}_{1101}, \\
\mathcal{A}_{B,\text{end}} &= \mathcal{A}_{1110}, \\
\mathcal{A}_{\text{out}} &= \mathcal{A}_{**11}.
\end{aligned} \tag{1}$$

We let \mathcal{A}_A be the part of the adversary that consists of $\mathcal{A}_{A,\text{start}}$ and $\mathcal{A}_{A,\text{end}}$, and \mathcal{A}_B the part that consists of $\mathcal{A}_{B,\text{start}}$ and $\mathcal{A}_{B,\text{end}}$:

$$\begin{aligned}
\mathcal{A}_A &= \mathcal{A}_{\{100*,1010,1101\}}, \\
\mathcal{A}_B &= \mathcal{A}_{\{01*0,0101,1110\}}.
\end{aligned} \tag{2}$$

Because \mathcal{A} contains no vertices in the target region, the bit-string suffixes in the above list do not include 1100. The partition of \mathcal{A} is shown in Fig. 10 with arrows indicating where there can be edges connecting the parts. \mathcal{A}_{in} is the part of the adversary in \mathcal{M}_{in} and consists

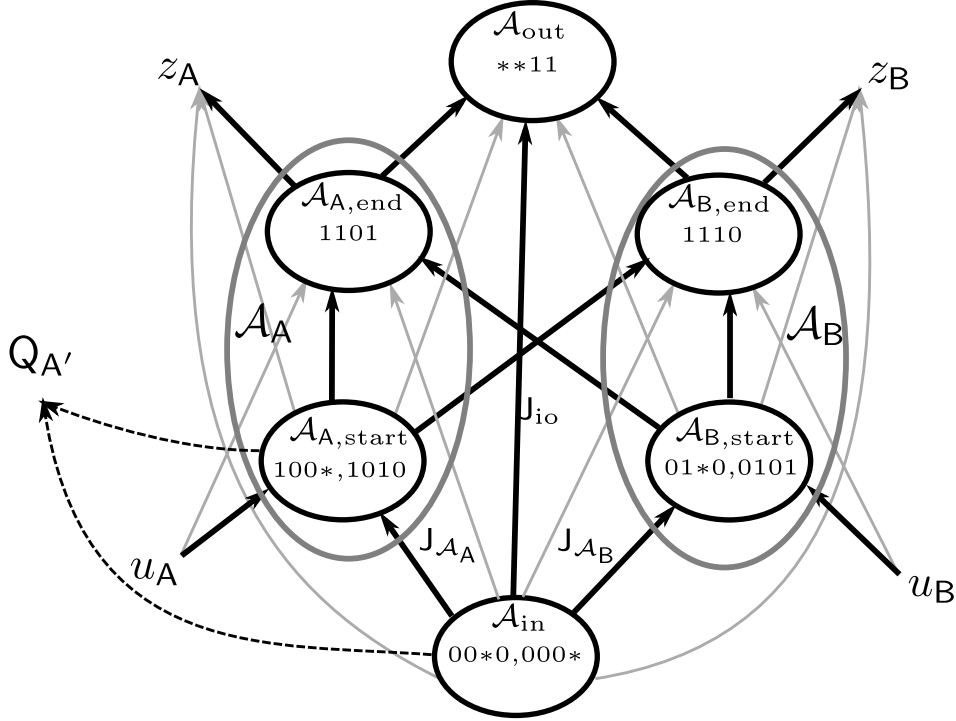


FIG. 10. Adversary spacetime circuit. The diagram depicts the adversary circuits and their interconnections. The circuit receives challenges u_A and u_B coming from the verifiers and delivers responses z_A and z_B to the verifiers. The adversary circuit partitions into six subcircuits indicated by the black ellipses. Each subcircuit enacts a quantum operation from its in-edges to its out-edges. The binary strings indicate the associated spacetime regions as described in the text. The entangled quantum systems prepared by the source are $Q_{A'}$ and Q_P . Because the source is treated as part of the adversary, Q_P is carried on the internal edges of the adversary circuit, while $Q_{A'}$ may be sent to A' from \mathcal{A}_{in} or from $\mathcal{A}_{A,start}$, where we show the edges that alternatively or jointly carry $Q_{A'}$ with dashed arrows. By Assumption 9, $\mathcal{A}_{A,end}$, $\mathcal{A}_{B,start}$ and $\mathcal{A}_{B,end}$ cannot send anything to A' before completion of A' 's measurement process. We therefore do not need to include edges from these subcircuits for producing $Q_{A'}$. The part of the circuit directly relevant to the protocol consists of two groups indicated by grey ellipses and labeled by \mathcal{A}_A on the left and \mathcal{A}_B on the right. The black arrows depict the principal circuit connections. The light-grey edges may be present in the spacetime circuit but are removed by passing them through one of the bypassed adversary circuits in the abstract analysis of adversary capabilities.

of the vertices of \mathcal{A} that do not yet have access to the challenges but are in principle able to send a response to at least one of the verifiers. \mathcal{A}_{out} consists of the adversary vertices that can no longer respond to either of the verifiers. The edges from $\mathcal{A}_{A,start}$ to $\mathcal{A}_{B,end}$ and from $\mathcal{A}_{B,start}$ to $\mathcal{A}_{A,end}$ allow for one-round communication between \mathcal{A}_A and \mathcal{A}_B . There is no edge connecting $\mathcal{A}_{A,start}$ and $\mathcal{A}_{B,start}$ or connecting $\mathcal{A}_{A,end}$ and $\mathcal{A}_{B,end}$, as the two parts are space-like separated from each other.

The restrictions on prior entanglement are expressed in terms of the joint state of the systems carried by the outgoing edges of \mathcal{A}_{in} , where we exclude direct edges to \mathcal{A}_{out} . These direct edges do not contribute to the current trial of the protocol. The systems carried by

edges that may contribute relevant entanglement partition into

- 1) the system on the edge from \mathcal{A}_{in} that may contribute to $\mathcal{Q}_{A'}$ and the system $J_{\mathcal{A}_A}$ carried by edges from \mathcal{A}_{in} to \mathcal{A}_A ,
 - 2) the system $J_{\mathcal{A}_B}$ carried by edges from \mathcal{A}_{in} to \mathcal{A}_B .
- (3)

After we eliminate the indirect edges in the abstract treatment of the circuit below, these edges go to A' and $\mathcal{A}_{A,\text{start}}$, and $\mathcal{A}_{B,\text{start}}$, respectively. In our analysis, we choose to restrict the entanglement between $\mathcal{Q}_{A'}J_{\mathcal{A}_A}$ and $J_{\mathcal{A}_B}$. Except for the untrusted measurement apparatus of A' , the verifiers may be assumed to be classical on exiting \mathcal{M}_{in} . Restrictions on communication by the measurement apparatus are described in Assumption 9.

Because of the absence of adversary vertices in the target region \mathcal{M}_{1100} , the vertices of \mathcal{A}_A and \mathcal{A}_B are causally convex in the circuit partial order, making \mathcal{A}_A and \mathcal{A}_B spacetime subcircuits of \mathcal{A} . In particular, because it would violate causality, there is no directed path that starts at a vertex in \mathcal{A}_A , enters \mathcal{A}_B , and returns to \mathcal{A}_A , or vice versa. Consequently, in the absence of the light-grey arrows in Fig. 10, the adversary actions in a trial can be viewed as follows: 1) An initial state preparation by \mathcal{A}_{in} , which is in the causal past of the trial, followed by local processing by $\mathcal{A}_{A,\text{start}}$ and $\mathcal{A}_{B,\text{start}}$. \mathcal{A}_{in} and $\mathcal{A}_{A,\text{start}}$ may contribute to the system $\mathcal{Q}_{A'}$ to be measured by A' . 2) A single round of communication consisting of one message from $\mathcal{A}_{A,\text{start}}$ to $\mathcal{A}_{B,\text{end}}$, and another from $\mathcal{A}_{B,\text{start}}$ to $\mathcal{A}_{A,\text{end}}$. 3) Responses sent from $\mathcal{A}_{A,\text{end}}$ to A and from $\mathcal{A}_{B,\text{end}}$ to B . After completing the trial, the adversaries pass a quantum state to \mathcal{A}_{out} for use in the next trial. The actions of the adversaries can therefore be represented by two adversaries \mathcal{A}_A and \mathcal{A}_B who prepare an initial joint state in their past, receive challenges locally, and communicate once in one round of communication before committing to responses to the verifiers. The light-grey arrows in Fig. 10 will be eliminated without weakening the capabilities of the adversary in the abstract analysis of the circuit in Sect. VB.

Projection of target region: A single trial's target region in spacetime is \mathcal{M}_{1100} . For visualization, it is helpful to project this region onto the space dimension of an inertial frame. In the experiment, both verifiers are stationary relative to the ground, so we use the inertial frame in which the verifiers are at rest. To determine the spatial projection of \mathcal{M}_{1100} , we find the set of space positions \mathbf{x} whose stationary worldlines intersect \mathcal{M}_{1100} . The stationary worldline for space position \mathbf{x} is given by $P = \{(\mathbf{x}, t)\}_{t \in \mathbb{R}}$. The distances from \mathbf{x} to the verifiers A and B are denoted by l_A and l_B . Let t_1, t_2, t_3 , and t_4 be the times at which the worldline P enters or leaves the lightcones $C_{A,+}$, $C_{B,+}$, $C_{A,-}$ and $C_{B,-}$. Then, with units where the speed of light is $c = 1$, we have

$$\begin{aligned}
 t_1 &= t + s_A + l_A \\
 t_2 &= t + s_B + l_B, \\
 t_3 &= t + r_A - l_A, \\
 t_4 &= t + r_B - l_B.
 \end{aligned}
 \tag{4}$$

To ensure that the stationary worldline P intersects the target region \mathcal{M}_{1100} , the condition $\max(t_1, t_2) \leq \min(t_3, t_4)$ must be satisfied. From the equivalent four inequalities $t_j \leq t_k$ for

$j \in \{1, 2\}$ and $k \in \{3, 4\}$, we get

$$\begin{aligned}
t_1 \leq t_3 &\leftrightarrow 2l_A \leq r_A - s_A, \\
t_2 \leq t_4 &\leftrightarrow 2l_B \leq r_B - s_B, \\
t_1 \leq t_4 &\leftrightarrow l_A + l_B \leq r_B - s_A, \\
t_2 \leq t_3 &\leftrightarrow l_A + l_B \leq r_A - s_B.
\end{aligned} \tag{5}$$

The first two inequalities constrain \mathbf{x} to lie within spheres centered at the verifiers A and B, while the last two constrain \mathbf{x} to ellipsoids with foci at the verifiers. Thus, the projection of \mathcal{M}_{1100} onto space in the verifiers' inertial frame is the intersection of these spheres and ellipsoids.

Classically achievable target region: Classical position[-based] verification with the two verifiers A and B involves the verifiers' sending challenges u_A and u_B and the prover responding to both verifiers with the value of $g(u_A, u_B)$ for some fixed function g . In the spacetime circuit picture, to succeed with probability 1 it is necessary and sufficient to have one prover vertex in the region where u_A and u_B are visible and there is sufficient time to send $g(u_A, u_B)$ to A, and another prover vertex in the region where u_A and u_B are visible and there is sufficient time to send $g(u_A, u_B)$ to B. These constraints are related to the analysis of adversaries for classical position verification in Ref. [56]. If either of these conditions is not met, the prover has a nonzero probability of failure. The first condition requires a prover vertex in $C_{A,+} \cap C_{B,+} \cap C_{A,-}$, while the second requires another prover vertex in $C_{A,+} \cap C_{B,+} \cap C_{B,-}$. We identify the union of these two spacetime regions as the effective target region E_c for classical position verification. Although this target region includes the locations of the verifiers themselves, it serves as a useful reference for comparing with our quantum protocol's target region E . The projection of E_c onto space in the verifiers' inertial frame can be determined in the same way as the projection of E . To determine the projection of the prover vertex in $C_{A,+} \cap C_{B,+} \cap C_{A,-}$, the inequalities that need to be satisfied are

$$\begin{aligned}
t_1 \leq t_3 &\leftrightarrow 2l_A \leq r_A - s_A, \\
t_2 \leq t_3 &\leftrightarrow l_B + l_A \leq r_A - s_B.
\end{aligned} \tag{6}$$

To determine the projection of the prover vertex in $C_{A,+} \cap C_{B,+} \cap C_{B,-}$, the inequalities to be satisfied are

$$\begin{aligned}
t_1 \leq t_4 &\leftrightarrow l_B + l_A \leq r_B - s_A, \\
t_2 \leq t_4 &\leftrightarrow 2l_B \leq r_B - s_B.
\end{aligned} \tag{7}$$

Both of these regions are intersections of an ellipsoid and a sphere. The projection of the target region E_c is the union of the two.

B. Reduction to 3-party non-signaling and connection to 2-party local realism

In the previous section, we reduced the adversary capabilities to two spacetime circuits \mathcal{A}_A and \mathcal{A}_B with limited inputs and restricted communication. We now assume that there is no entanglement between $Q_{A'}J_{A_A}$ and J_{A_B} , which implies that \mathcal{A}_A and \mathcal{A}_B share no prior entanglement. We relax this assumption in Sect. VD. The goal of this section is to characterize the probability distributions of the trial record achievable by the adversary in terms

of a three-party non-signaling scenario. Our use of test factors dictates that we characterize these probability distributions for any joint state of all entities' edges crossing the trial boundary T defining the start of the trial. This joint state includes the trial records of previous trials as well as all other information that can influence the trial. In the space-time analysis, this accounts for all possible dependencies on the past. To check that a test factor W has expectation at most 1 for all probability distributions achievable by the adversary, it suffices to consider extremal joint states as expectations cannot increase under convex combinations.

Before proceeding, we eliminate redundant edges in the high-level description of the adversary spacetime circuit depicted in Fig. 10. These are the edges associated with connections shown in light-grey. For this purpose, we detach the circuit from its specific space-time realization and consider it as an abstract quantum circuit with processing vertices $\mathcal{A}_{\text{in}}, \mathcal{A}_{\text{A,start}}, \mathcal{A}_{\text{A,end}}, \mathcal{A}_{\text{B,start}}, \mathcal{A}_{\text{B,end}}, \mathcal{A}_{\text{out}}$ that are directionally connected with inputs and outputs as shown in Fig. 10. In this abstract circuit, each of the redundant edges bypasses one or more intervening vertices. We can re-route the redundant edges by passing them through the intervening vertices, re-defining the process at these intervening vertices to copy the system carried by the redundant edge from the vertex input to the vertex output. The modified circuit contains no bypassing edges, and it preserves the power of the adversary.

The connection in Fig. 10 with system J_{io} in Fig. 10 is not re-routed because it does not contribute to the actions of the adversary during the trial. Entanglement between it and the systems on other edges into \mathcal{A}_{A} and \mathcal{A}_{B} is allowed, provided there is no entanglement between $Q_{\text{A}'}J_{\mathcal{A}_{\text{A}}}$ and $J_{\mathcal{A}_{\text{B}}}$ after tracing out J_{io} . The test factor W does not depend on J_{io} , since the trial record is independent of this system. In addition to J_{io} , we also need to consider the classical state of the verifiers on edges exiting the causal past \mathcal{M}_{in} of the trial. The classical state of the verifiers may include shared randomness that is kept secret from and therefore independent of other entities before the trial and that can help generate measurement settings and challenges. Such randomness is used to satisfy the independence requirements of Assumption 11. Accordingly, and because the reduced state on $Q_{\text{A}'}J_{\mathcal{A}_{\text{A}}}$ and $J_{\mathcal{A}_{\text{B}}}$ is separable, the adversary's expectation of the test factor W is maximized by some pure product state over the systems $Q_{\text{A}'}J_{\mathcal{A}_{\text{A}}}$ and $J_{\mathcal{A}_{\text{B}}}$. We now fix such a product state. This state may be assumed to be known by every component of the adversary.

The first half of the adversary strategy, executed by $\mathcal{A}_{\text{A,start}}$ and $\mathcal{A}_{\text{B,start}}$, can be described as follows: $\mathcal{A}_{\text{A,start}}$ transforms its input systems $J_{\mathcal{A}_{\text{A}}}$ into output systems $R_{\mathcal{A}_{\text{A}}}$ and $R_{\mathcal{A}_{\text{A}} \rightarrow \mathcal{A}_{\text{B}}}$, where $R_{\mathcal{A}_{\text{A}}}$ includes $Q_{\text{A}'}$. This transformation may depend on the classical challenge u_{A} , as it is an input to $\mathcal{A}_{\text{A,start}}$. The resulting systems $R_{\mathcal{A}_{\text{A}}}$ and $R_{\mathcal{A}_{\text{A}} \rightarrow \mathcal{A}_{\text{B}}}$ are then passed on to $\mathcal{A}_{\text{A,end}}$ and $\mathcal{A}_{\text{B,end}}$, respectively. Because the quantum inputs to \mathcal{A}_{A} and \mathcal{A}_{B} are in a product state, the quantum system $J_{\mathcal{A}_{\text{B}}}$, originally transmitted from \mathcal{A}_{in} to $\mathcal{A}_{\text{B,start}}$, can instead be treated as being internally prepared by $\mathcal{A}_{\text{B,start}}$ in a pure state. The operation by $\mathcal{A}_{\text{B,start}}$ is equivalent to transforming $J_{\mathcal{A}_{\text{B}}}$ into quantum systems $R_{\mathcal{A}_{\text{B}}}$ and $R_{\mathcal{A}_{\text{B}} \rightarrow \mathcal{A}_{\text{A}}}$. The joint state of these two systems may depend on the classical challenge u_{B} , which is an input to $\mathcal{A}_{\text{B,start}}$. The systems $R_{\mathcal{A}_{\text{B}}}$ and $R_{\mathcal{A}_{\text{B}} \rightarrow \mathcal{A}_{\text{A}}}$ are then passed on to $\mathcal{A}_{\text{B,end}}$ and $\mathcal{A}_{\text{A,end}}$, respectively. The communicated systems are shown in Fig. 11 with the bypassing edges removed. Without loss of generality, we may assume that the challenge u_{A} is separately passed on by $\mathcal{A}_{\text{A,start}}$ to both $\mathcal{A}_{\text{A,end}}$ and $\mathcal{A}_{\text{B,end}}$, and similarly, u_{B} is passed on by $\mathcal{A}_{\text{B,start}}$. The relevant second half of the strategy, which determines the classical challenge responses z_{A} and z_{B} recorded by the verifiers, can be treated as measurements performed by $\mathcal{A}_{\text{A,end}}$ and $\mathcal{A}_{\text{B,end}}$. Each of these measurements may depend on both challenges u_{A} and u_{B} . In the following, we modify

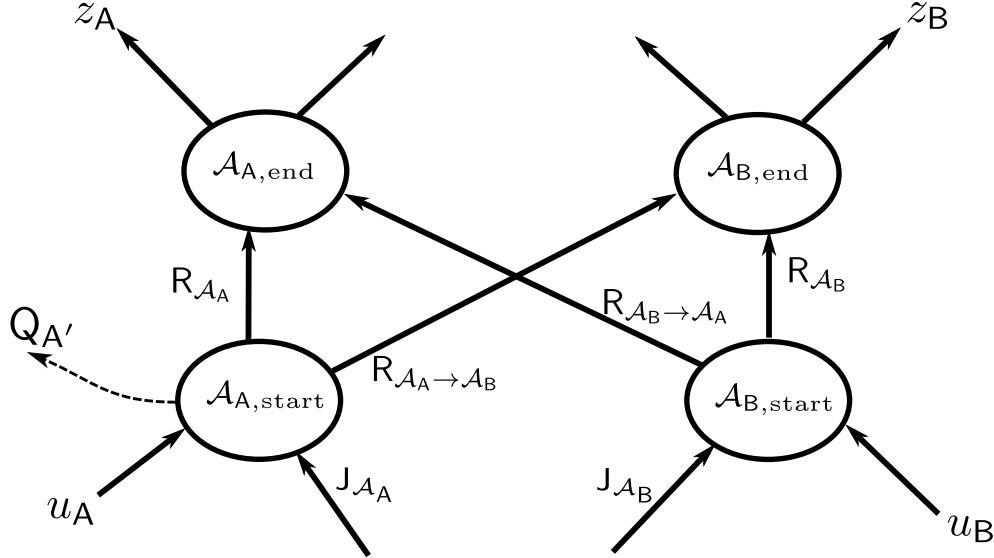


FIG. 11. Adversary spacetime circuit with bypassing edges removed and communicated systems labeled. The dashed arrow may contribute to $Q_{A'}$, see Fig. 10.

the adversary strategy while improving the corresponding expectation of the test factor W , and show that for the modified strategy the trial record follows a three-party non-signaling distribution.

We first show that the quantum messages $R_{A_B} R_{A_B \rightarrow A_A}$ from $\mathcal{A}_{B,start}$ can be eliminated without decreasing the expectation of the test factor W for the adversary strategy. Given that the initial state of J_{A_B} is a fixed pure state and considering the causal structure shown in Fig. 11, the state of $R_{A_B} R_{A_B \rightarrow A_A}$ depends on u_B but is independent of the other systems involved in the trial. $\mathcal{A}_{B,start}$ can therefore prepare it as a partial trace over an ancillary system of a u_B -dependent pure state $|\psi_{u_B}\rangle$. $\mathcal{A}_{B,start}$ can modify R_{A_B} so that it includes the ancillary system and let $\mathcal{A}_{B,end}$ remove or ignore it. We can therefore assume that $R_{A_B} R_{A_B \rightarrow A_A}$ is in state $|\psi_{u_B}\rangle$ when the challenge is u_B . Instead of $\mathcal{A}_{B,start}$ preparing and passing on R_{A_B} and $R_{A_B \rightarrow A_A}$, we can have $\mathcal{A}_{A,start}$ prepare independent systems $R_{A_B, u_B'} R_{A_B \rightarrow A_A, u_B'}$ for each possible value u_B' of U_B , where the state of $R_{A_B, u_B'} R_{A_B \rightarrow A_A, u_B'}$ is $|\psi_{u_B'}\rangle$. In addition to passing on the systems R_{A_A} and $R_{A_A \rightarrow A_B}$, $\mathcal{A}_{A,start}$ passes on all systems $R_{A_B \rightarrow A_A, u_B'}$ to $\mathcal{A}_{A,end}$ and all systems $R_{A_B, u_B'}$ to $\mathcal{A}_{B,end}$. Since both $\mathcal{A}_{A,end}$ and $\mathcal{A}_{B,end}$ know the actual challenge u_B used in the trial, they can discard all systems $R_{A_B, u_B'}$ and $R_{A_B \rightarrow A_A, u_B'}$ for $u_B' \neq u_B$. After this step, the joint state at $\mathcal{A}_{A,end}$ and $\mathcal{A}_{B,end}$ and $Q_{A'}$ relevant for the measurements producing the responses and the verifier measurement outcomes is identical to that in the original strategy. The trial-record probability distribution is therefore unchanged, and the edges leaving $\mathcal{A}_{B,start}$ only carry the classical message consisting of u_B to $\mathcal{A}_{A,end}$ and $\mathcal{A}_{B,end}$.

The action by which $\mathcal{A}_{A,start}$ creates the system $R_{A_A} R_{A_A \rightarrow A_B}$ may depend on u_A . Next we show that the adversary circuit can be modified so that this creation of $R_{A_A} R_{A_A \rightarrow A_B}$ becomes independent of u_A , without reducing the adversary's expectation $\text{Exp}(W)$ of the test factor W . Let $\bar{W}_{u_A} = \text{Exp}(W|U_A = u_A)$ be the expectation of W conditional on the challenge u_A . We have $\text{Exp}(W) = \sum_{u_A} \mathbb{P}(U_A = u_A) \bar{W}_{u_A}$, which is a convex combination of the \bar{W}_{u_A} . It follows that $\max(\bar{W}_{u_A}) \geq \text{Exp}(W)$. Let $u_{A0} = \arg \max_{u_A: \mathbb{P}(u_A) > 0} \bar{W}_{u_A}$. We now modify the adversary circuit so that $\mathcal{A}_{A,start}$ always prepares $R_{A_A} R_{A_A \rightarrow A_B}$ as if the challenge from A were $U_A = u_{A0}$, regardless of the actual u_A used in the trial. $\mathcal{A}_{A,end}$ and $\mathcal{A}_{B,end}$ modify

their measurements according to those that would have been performed if the challenge from \mathbf{B} were $u_{\mathbf{B}}'$, where they jointly choose $u_{\mathbf{B}}'$ from the probability distribution of the challenges from \mathbf{B} conditional on $U_{\mathbf{A}} = u_{\mathbf{A}0}$ and $M_{\mathbf{P}} = m_{\mathbf{P}} = f(u_{\mathbf{A}}, u_{\mathbf{B}})$, with $m_{\mathbf{P}}$ being the actual prover setting and $u_{\mathbf{A}}, u_{\mathbf{B}}$ the actual challenges in this trial. To see that this conditional probability distribution is well-defined, we note that by Assumption 11, $M_{\mathbf{P}}$ and $U_{\mathbf{A}}$ are independent. Since $m_{\mathbf{P}}$ is the actual prover setting, $\mathbb{P}(m_{\mathbf{P}}) > 0$. Similarly, $\mathbb{P}(U_{\mathbf{A}} = u_{\mathbf{A}0}) > 0$ by construction. Due to independence, the joint probability is simply the product $\mathbb{P}(m_{\mathbf{P}}, u_{\mathbf{A}0}) = \mathbb{P}(m_{\mathbf{P}})\mathbb{P}(u_{\mathbf{A}0})$, which is strictly positive. This ensures that the conditioning event $(U_{\mathbf{A}} = u_{\mathbf{A}0}, M_{\mathbf{P}} = m_{\mathbf{P}})$ has non-zero probability and the conditional distribution for choosing $u_{\mathbf{B}}'$ is well-defined. The method for choosing $u_{\mathbf{B}}'$ defines the random variable $U_{\mathbf{B}}'$ and ensures that $f(u_{\mathbf{A}0}, U_{\mathbf{B}}') = M_{\mathbf{P}} = f(U_{\mathbf{A}}, U_{\mathbf{B}})$. The joint choice of $u_{\mathbf{B}}'$ requires joint randomness, which can be shared by $\mathcal{A}_{\mathbf{A},\text{start}}$ as part of their classical message to $\mathcal{A}_{\mathbf{B},\text{end}}$. Although $\mathcal{A}_{\mathbf{A},\text{start}}$ does not know $m_{\mathbf{P}}$, $\mathcal{A}_{\mathbf{A},\text{start}}$ can generate the needed shared randomness for each possible value of $M_{\mathbf{P}}$ and pass on the shares to $\mathcal{A}_{\mathbf{A},\text{end}}$ and $\mathcal{A}_{\mathbf{B},\text{end}}$. $\mathcal{A}_{\mathbf{A},\text{end}}$ and $\mathcal{A}_{\mathbf{B},\text{start}}$ have both learned $m_{\mathbf{P}}$ and can choose from the shared randomness accordingly.

From now on, we abbreviate events and conditions of the form $R = r$ for RVs R by leaving out “ $R =$ ” inside probability and expectation expressions, provided that this does not introduce ambiguity. We claim that the expectation of W after the modifications of $\mathcal{A}_{\mathbf{A}}$ and $\mathcal{A}_{\mathbf{B}}$ is $\bar{W}_{u_{\mathbf{A}0}}$. To show this, let $O_{\mathbf{A}'}$ be the verifier \mathbf{A}' outcome RV and $Z_{\mathbf{A}'}$ and $Z_{\mathbf{B}'}$ the response RVs with the modifications. We compute the expectation of $W(M_{\mathbf{A}'}, O_{\mathbf{A}'}, m_{\mathbf{P}}, Z_{\mathbf{A}'}, Z_{\mathbf{B}'})$ below. By construction, and because $M_{\mathbf{A}'}$ is conditionally independent of $U_{\mathbf{A}}$ and $U_{\mathbf{B}}$ given $M_{\mathbf{P}}$ (see Assumption 11), the state being measured to obtain $O_{\mathbf{A}'}$, $Z_{\mathbf{A}'}$ and $Z_{\mathbf{B}'}$ and the measurements being performed are the same as if $U_{\mathbf{A}} = u_{\mathbf{A}0}$ and $U_{\mathbf{B}} = u_{\mathbf{B}}'$, where $M_{\mathbf{P}} = f(u_{\mathbf{A}}, u_{\mathbf{B}}) = f(u_{\mathbf{A}0}, u_{\mathbf{B}}')$. We first verify this equivalence by calculating the probability distribution of the settings and outcomes as follows. By assumption and then by construction,

$$\begin{aligned} \mathbb{P}(m_{\mathbf{A}'}, u_{\mathbf{B}}' | m_{\mathbf{P}}) &= \mathbb{P}(m_{\mathbf{A}'} | m_{\mathbf{P}}) \mathbb{P}(u_{\mathbf{B}}' | m_{\mathbf{P}}) \\ &= \mathbb{P}(m_{\mathbf{A}'} | U_{\mathbf{A}} = u_{\mathbf{A}0}, m_{\mathbf{P}}) \mathbb{P}(U_{\mathbf{B}} = u_{\mathbf{B}}' | U_{\mathbf{A}} = u_{\mathbf{A}0}, m_{\mathbf{P}}) \\ &= \mathbb{P}(m_{\mathbf{A}'}, U_{\mathbf{B}} = u_{\mathbf{B}}' | U_{\mathbf{A}} = u_{\mathbf{A}0}, m_{\mathbf{P}}). \end{aligned} \tag{8}$$

We apply this identity to determine

$$\begin{aligned} \mathbb{P}(m_{\mathbf{A}'}, o_{\mathbf{A}'}', m_{\mathbf{P}}, z_{\mathbf{A}'}', z_{\mathbf{B}'}') &= \sum_{u_{\mathbf{B}}'} \mathbb{P}(m_{\mathbf{A}'}, o_{\mathbf{A}'}', u_{\mathbf{B}}', m_{\mathbf{P}}, z_{\mathbf{A}'}', z_{\mathbf{B}'}') \\ &= \sum_{u_{\mathbf{B}}'} \mathbb{P}(o_{\mathbf{A}'}', z_{\mathbf{A}'}', z_{\mathbf{B}'}' | m_{\mathbf{A}'}, u_{\mathbf{B}}', m_{\mathbf{P}}) \mathbb{P}(m_{\mathbf{A}'}, u_{\mathbf{B}}' | m_{\mathbf{P}}) \mathbb{P}(m_{\mathbf{P}}) \\ &= \sum_{u_{\mathbf{B}}'} \mathbb{P}(O_{\mathbf{A}'} = o_{\mathbf{A}'}', Z_{\mathbf{A}} = z_{\mathbf{A}'}', Z_{\mathbf{B}} = z_{\mathbf{B}'}' | m_{\mathbf{A}'}, U_{\mathbf{A}} = u_{\mathbf{A}0}, U_{\mathbf{B}} = u_{\mathbf{B}}', m_{\mathbf{P}}) \\ &\quad \times \mathbb{P}(m_{\mathbf{A}'}, U_{\mathbf{B}} = u_{\mathbf{B}}' | U_{\mathbf{A}} = u_{\mathbf{A}0}, m_{\mathbf{P}}) \mathbb{P}(m_{\mathbf{P}}) \\ &= \sum_{u_{\mathbf{B}}'} \mathbb{P}(m_{\mathbf{A}'}, O_{\mathbf{A}'} = o_{\mathbf{A}'}', Z_{\mathbf{A}} = z_{\mathbf{A}'}', Z_{\mathbf{B}} = z_{\mathbf{B}'}', U_{\mathbf{B}} = u_{\mathbf{B}}' | U_{\mathbf{A}} = u_{\mathbf{A}0}, m_{\mathbf{P}}) \\ &\quad \times \mathbb{P}(m_{\mathbf{P}}) \\ &= \mathbb{P}(m_{\mathbf{A}'}, O_{\mathbf{A}'} = o_{\mathbf{A}'}', Z_{\mathbf{A}} = z_{\mathbf{A}'}', Z_{\mathbf{B}} = z_{\mathbf{B}'}' | U_{\mathbf{A}} = u_{\mathbf{A}0}, m_{\mathbf{P}}) \mathbb{P}(m_{\mathbf{P}}) \\ &= \mathbb{P}(m_{\mathbf{A}'}, O_{\mathbf{A}'} = o_{\mathbf{A}'}', m_{\mathbf{P}}, Z_{\mathbf{A}} = z_{\mathbf{A}'}', Z_{\mathbf{B}} = z_{\mathbf{B}'}' | U_{\mathbf{A}} = u_{\mathbf{A}0}), \end{aligned} \tag{9}$$

where in the first two lines, we calculate probabilities involving the RVs $O_{A'}$, Z_A , Z_B according to the modified adversary circuit, and in the last step we used $\mathbb{P}(m_P) = \mathbb{P}(m_P|U_A = u_{A0})$ by independence of M_P and U_A according to Assumption 11. We can now calculate the expectation of W for the modified adversary circuit.

$$\begin{aligned}
& \text{Exp}(W(M_{A'}, O_{A'}, M_P, Z_A, Z_B)) \\
&= \sum_{m_{A'}, o_{A'}, m_P, z_A, z_B} W(m_{A'}, o_{A'}, m_P, z_A, z_B) \mathbb{P}(m_{A'}, o_{A'}, m_P, z_A, z_B) \\
&= \sum_{m_{A'}, o_{A'}, m_P, z_A, z_B} W(m_{A'}, o_{A'}, m_P, z_A, z_B) \mathbb{P}(m_{A'}, O_{A'} = o_{A'}, m_P, Z_A = z_A, Z_B = z_B | U_A = u_{A0}) \\
&= \sum_{m_{A'}, o_{A'}, m_P, z_A, z_B} W(m_{A'}, o_{A'}, m_P, z_A, z_B) \mathbb{P}(m_{A'}, o_{A'}, m_P, z_A, z_B | U_A = u_{A0}) \\
&= \bar{W}_{u_{A0}}, \tag{10}
\end{aligned}$$

where we used Eq. (9) for the second identity and a change of variables for the third.

Because of Assumption 11, the incoming adversary state including that of the source and quantum systems being shared is independent of the verifier settings and challenge distribution. Consequently, with the above modifications to the adversary circuit, we have arrived at a situation where $\mathcal{A}_{A,\text{end}}$, $\mathcal{A}_{B,\text{end}}$ and A' receive a joint quantum state ρ that does not depend on the challenges u_A , u_B or the measurement setting $m_{A'}$ used by A' in the trial. The challenges and the measurement setting constitute classical inputs to $\mathcal{A}_{A,\text{end}}$, $\mathcal{A}_{B,\text{end}}$ and A' , and the measurements performed by $\mathcal{A}_{A,\text{end}}$ and $\mathcal{A}_{B,\text{end}}$ now depend only on $u_{B'}$. We can further modify the measurements so that they depend only on the actual prover setting m_P . For this additional modification, consider a particular m_P . Then we have, for the above modified adversary circuit and every $u_{B'}$ for which $f(u_{A0}, u_{B'}) = m_P$

$$\text{Exp}(W|m_P, u_{B'}) = \text{Exp}(W|u_{B'}) \leq \max_{u_{B''}} \{\text{Exp}(W|U_{B'} = u_{B''}) : f(u_{A0}, u_{B''}) = m_P\}, \tag{11}$$

where we define conditional expectations and probabilities to be zero whenever the conditioning event has zero probability. The adversary's expectation of W therefore improves if given $m_P = f(u_A, u_B)$, $\mathcal{A}_{A,\text{end}}$ and $\mathcal{A}_{B,\text{end}}$ always perform the measurements for an input $u_{A0}, u_{B''}$ that maximizes $\text{Exp}(W|u_{A0}, u_{B''})$ subject to $f(u_{A'}, u_{B''}) = m_P$. With this additional modification, $u_{B''}$ is determined by m_P , which implies that the joint randomness used for the first modification can now be omitted.

Instead of providing both u_A and u_B as inputs, it suffices to provide just m_P . The local measurement settings now depend only on the local inputs: $m_{A'}$ for A' , m_P for $\mathcal{A}_{A,\text{end}}$, and m_P for $\mathcal{A}_{B,\text{end}}$. Because the measurement settings are local to A' , $\mathcal{A}_{A,\text{end}}$ and $\mathcal{A}_{B,\text{end}}$, and the joint state ρ does not depend on the inputs, we can define the conditional distribution of the three measurement outcomes, namely, the outcome $O_{A'}$ of A' , the response Z_A from $\mathcal{A}_{A,\text{end}}$, and the response Z_B from $\mathcal{A}_{B,\text{end}}$. This conditional distribution can be defined not only for the case where the inputs for $\mathcal{A}_{A,\text{end}}$ and $\mathcal{A}_{B,\text{end}}$ are identical, but also when their inputs are different. Consequently, we constructed a modified adversary strategy that yields an expectation of W at least as high as the original, and for which the probability distribution of the trial record is derived from the full set of conditional distributions according to a three-party, necessarily non-signaling, scenario with a joint quantum state for the three parties, $k_{A'}$ settings and $c_{A'}$ outcomes for the first party, A' , and k_P settings and c_P outcomes for each of the second and third parties, $\mathcal{A}_{A,\text{end}}$ and $\mathcal{A}_{B,\text{end}}$. The expectation of W is evaluated

according to a distribution of inputs where the second and third party's inputs are always the same. It follows that to ensure that W is a test factor against adversaries without prior entanglement, it suffices to verify that its maximum expected value over all three-party non-signaling distributions does not exceed 1, where the three inputs are $m_{A'}$, m_P and m_P with probability distribution $\mathbb{P}(m_{A'}, m_P)$.

Existence of test factors for protocol completeness: The position verification protocol requires finding test factors against adversaries that ensure completeness of the protocol for an implementable honest prover. It suffices to consider non-negative candidate functions $W(m_{A'}, o_{A'}, m_P, z_A, z_B)$ that can be computed from the trial record and do not depend directly on u_A and u_B . To take advantage of the reduction to the three-party quantum scenario derived above, we write W in terms of a function $W'(o_{A'}, m_{A'}; z_A, b; z_B, b')$ according to

$$W(m_{A'}, o_{A'}, m_P, z_A, z_B) = W'(o_{A'}, m_{A'}; z_A, m_P; z_B, m_P). \quad (12)$$

The reduction implies that the conditional distributions accessible by adversary strategies for the QPV protocol can be written as

$$\mathbb{P}(o_{A'}, z_A, z_B | m_{A'}, m_P) = \mu(o_{A'}, z_A, z_B | m_{A'}, b = m_P, b' = m_P), \quad (13)$$

where the conditional distributions $\mu(o_{A'}, z_A, z_B | m_{A'}, b, b')$ satisfy both quantum and non-signaling constraints for three parties according to the configuration described in the previous paragraph. We use b and b' to refer to the inputs of parties $\mathcal{A}_{A,\text{end}}$ and $\mathcal{A}_{B,\text{end}}$ in the extended three party scenario where $\mathcal{A}_{A,\text{end}}$ and $\mathcal{A}_{B,\text{end}}$ may have different inputs determining their measurements. For a review of the quantum and non-signaling constraints, see Ref. [57]. We do not take advantage of the quantum constraints and instead consider all non-signaling conditional distributions. Let $\nu(m_{A'}, m_P)$ be the probability distribution of $m_{A'}, m_P = f(u_A, u_B)$ used in the position verification protocol, where $\nu(m_{A'}, m_P) > 0$ for each $m_{A'}, m_P$. Both conditional and unconditional probability distributions are denoted by μ, ν, \dots and treated as functions of their arguments, for which we avoid the use of RV conventions. The candidate function W' is a test factor against adversaries if for every three-party non-signaling conditional distribution $\mu(o_{A'}, z_A, z_B | m_{A'}, b, b')$, we have

$$\text{Exp}(W') = \sum_{m_{A'}, b, o_{A'}, z_A, z_B} W'(o_{A'}, m_{A'}; z_A, b; z_B, b) \nu(m_{A'}, b) \mu(o_{A'}, z_A, z_B | m_{A'}, b, b) \leq 1. \quad (14)$$

The construction and optimization of functions W' satisfying this condition is described in Sect. V C. We consider only W' that are symmetric under the exchange of parties $\mathcal{A}_{A,\text{end}}$ and $\mathcal{A}_{B,\text{end}}$, that is,

$$W'(o_{A'}, m_{A'}; z_A, b; z_B, b') = W'(o_{A'}, m_{A'}; z_B, b'; z_A, b) \quad (15)$$

for all values of the arguments. As a result, the expectation of W' is unchanged if we symmetrize the non-signaling conditional distribution $\mu(o_{A'}, z_A, z_B | m_{A'}, b, b')$ under the exchange of parties $\mathcal{A}_{A,\text{end}}$ and $\mathcal{A}_{B,\text{end}}$ according to

$$\mu'(o_{A'}, z_A, z_B | m_{A'}, b, b') = \frac{1}{2} (\mu(o_{A'}, z_A, z_B | m_{A'}, b, b') + \mu(o_{A'}, z_B, z_A | m_{A'}, b', b)). \quad (16)$$

Because the exchanged conditional distribution is also non-signaling, μ' is the mixture of two non-signaling conditional distributions. Since mixtures of non-signaling conditional distributions are non-signaling, μ' is non-signaling.

Consider the case $k_P = 2$ relevant for the experimental implementation. For any three-party non-signaling distribution $\mu'(o_{A'}, z_A, z_B | m_{A'}, b, b')$ that is symmetric under the exchange of parties $\mathcal{A}_{A,\text{end}}$ and $\mathcal{A}_{B,\text{end}}$, the two marginal conditional distributions $\mu'(o_{A'}, z_A | m_{A'}, b)$ for A' and $\mathcal{A}_{A,\text{end}}$, and $\mu'(o_{A'}, z_B | m_{A'}, b')$ for A' and $\mathcal{A}_{B,\text{end}}$, are identical. In the terminology of Ref. [58], this means that the marginal $\mu'(o_{A'}, z_A | m_{A'}, b)$ is 2-shareable. According to “Result 1” in this reference, any such 2-shareable probability distribution with $k_P = 2$ is local realistic. For the marginal conditional distribution $\mu'(o_{A'}, z_A | m_{A'}, b)$, the two parties are A' and $\mathcal{A}_{A,\text{end}}$ with inputs $m_{A'}$ and b , respectively. In the experiment, we directly sample according to $\mu(o_{A'}, z_A, z_B | m_{A'}, b, b)$ with probability $\nu(m_{A'}, b)$. From this we can in principle simulate samples from $\mu'(o_{A'}, z_A, z_B | m_{A'}, b, b)$ by swapping z_A with z_B with probability $1/2$ before recording the trial results. Because of symmetry of W' , it is not necessary to do this explicitly. That is, the value of W' is not affected by explicitly performing the probabilistic swap. By non-signaling of the distribution μ' , $\mu'(o_{A'}, z_A | m_{A'}, b, b') = \mu'(o_{A'}, z_A | m_{A'}, b, b)$. That is, the observed marginal for A' and $\mathcal{A}_{A,\text{end}}$ conditional on their inputs does not depend on which b' is given as input to $\mathcal{A}_{B,\text{end}}$. Consequently, although we cannot directly observe input combinations with $b \neq b'$, for the three-party non-signaling distribution implied by the best adversary strategies obtained above, after symmetrization the observable conditional marginal for A' and $\mathcal{A}_{A,\text{end}}$ is the 2-shareable and hence local-realistic marginal conditional distribution $\mu'(o_{A'}, z_A | m_{A'}, b)$ for all such adversary strategies.

Ideally, and with high probability in the experiment, the honest prover’s responses satisfy $z_A = z_B$. Let $\sigma(o_{A'}, z_A, z_B | m_{A'}, m_P)$ be the achieved conditional distribution for the honest prover, and $\sigma'(o_{A'}, z_A | m_{A'}, m_P) = (\sigma(o_{A'}, z_A | m_{A'}, m_P) + \sigma(o_{A'}, z_B | m_{A'}, m_P))/2$ its symmetrized marginal. By design, $\sigma'(o_{A'}, z_A | m_{A'}, m_P)$ violates a two-party Bell inequality with $k_P = 2$ values for input m_P . By the above argument, σ' is outside the local-realistic polytope. Given the conditional distribution $\sigma'(o_{A'}, z_A | m_{A'}, m_P)$ and the input distribution $\nu(m_{A'}, m_P)$, a test factor $W_{\text{LR}}(o_{A'}, m_{A'}; z_A, m_P)$ against local realism can be constructed that witnesses the Bell violation and has positive gain [44]. By the argument presented in the previous paragraph, if we set

$$W'(o_{A'}, m_{A'}; z_A, b; z_B, b') = \frac{1}{2}(W_{\text{LR}}(o_{A'}, m_{A'}; z_A, b) + W_{\text{LR}}(o_{A'}, m_{A'}; z_B, b')) \quad (17)$$

then W' is a test factor against three-party non-signaling conditional distributions, where the three inputs have probability distribution $\nu(m_{A'}, b)\delta_{b,b'}$. Here, $\delta_{b,b'}$ is the Kronecker delta. Consequently, W' satisfies Eq. (14) and so is a test factor against adversary strategies. Because W_{LR} has positive gain for the symmetrized marginal $\sigma'(o_{A'}, z_A | m_{A'}, m_P)$ introduced above, W' has positive gain for the honest distribution in the experiment, but expectation at most 1 for adversary strategies. Therefore, the completeness of the position verification protocol is ensured, provided that the number of trials is large enough.

The connection to the hypothesis test against local realism implies that our protocol is robust against experimental imperfections such as loss. In our experimental implementation, both the verifier A' and the prover P have two measurement settings, where under each setting there are two possible measurement outcomes. That is, $k_{A'} = k_P = 2$ and $c_{A'} = c_P = 2$. According to Ref. [59], it is possible to violate a two-party Bell inequality in this configuration for any photon loss less than $1/3$ for each party. In our experiment, the source is near A' ’s measurement apparatus, so A' can have substantially less loss than the honest prover. If A' has no loss, then any photon loss between the source and the honest prover of less than $1/2$ can be tolerated [60]. The test-factor construction described in Sect. V C below for position verification uses a test factor for two-party local realism as a starting point but

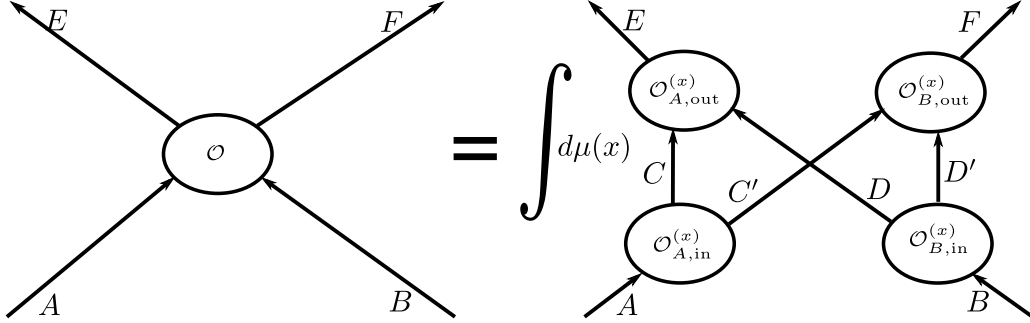


FIG. 12. Removable quantum operations.

exploits the greater flexibility of the three-party non-signaling constraints. In general, the test factors so constructed cannot be expressed in terms of Eq. (17).

Requirement for quantum vertices in the target region: Our position verification protocol fails if the honest prover uses only classical devices. We claim that no prover, either honest or adversarial, who uses only classical devices in the target region can successfully pass the protocol. Consider adversary circuits that include vertices in the target region \mathcal{M}_{1100} . According to our conventions, such vertices change the adversary into an honest prover. Here we show that if the joint action of the vertices in \mathcal{M}_{1100} satisfies the definition of being removable given below, then the adversary can not increase their expectation of the test factors used in the protocol over an adversary with no such vertices. We also show that if the vertices act classically as formally defined below, then they are removable. This is the sense in which an honest prover must have a quantum presence in the target region to pass the protocol.

The \mathcal{A}_{1100} subcircuit is now not empty and is part of the adversary circuit \mathcal{A} and needs to be added to the list of components of \mathcal{A} in Eq. (1). \mathcal{A}_{1100} receives inputs from \mathcal{A}_{in} , $\mathcal{A}_{A,start}$ and $\mathcal{A}_{B,start}$ and passes outputs to \mathcal{A}_{out} , $\mathcal{A}_{A,end}$ and $\mathcal{A}_{B,end}$. As in the analysis of \mathcal{A} given above, to simplify the circuit, without loss of generality, we can pass the input from \mathcal{A}_{in} through $\mathcal{A}_{A,start}$ or $\mathcal{A}_{B,start}$ and pass the output to \mathcal{A}_{out} through $\mathcal{A}_{A,end}$ or $\mathcal{A}_{B,end}$. With this simplification, the quantum operation of \mathcal{A}_{1100} can be viewed as an operation with two inputs, from $\mathcal{A}_{A,start}$ and $\mathcal{A}_{B,start}$, and two outputs, to $\mathcal{A}_{A,end}$ and $\mathcal{A}_{B,end}$.

Consider a general two-input two-output quantum operation $\mathcal{O} : \rho_{AB} \mapsto \mathcal{O}(\rho_{AB})_{EF}$, where A, B are the input quantum systems and E, F the output quantum systems. For \mathcal{A}_{1100} , the operation is implemented by \mathcal{A}_{1100} , and the inputs and outputs are the edges from $\mathcal{A}_{A,start}$ and $\mathcal{A}_{B,start}$, and to $\mathcal{A}_{A,end}$ and $\mathcal{A}_{B,end}$. We call \mathcal{O} removable if 1) there exist quantum systems C, C', D, D' , a probability distribution $\mu(x)$ over a classical variable x , and the following x -dependent quantum operations: $\mathcal{O}_{A,in}^{(x)}$ from A to C and C' , $\mathcal{O}_{B,in}^{(x)}$ from B to D and D' , $\mathcal{O}_{A,out}^{(x)}$ from C and D to E , and $\mathcal{O}_{B,out}^{(x)}$ from C' and D' to F . And 2) these quantum operations satisfy

$$\mathcal{O} = \int d\mu(x) \left(\mathcal{O}_{A,out}^{(x)} \otimes \mathcal{O}_{B,out}^{(x)} \right) \circ \left(\mathcal{O}_{A,in}^{(x)} \otimes \mathcal{O}_{B,in}^{(x)} \right). \quad (18)$$

The right-hand side is the replacement for the removable operation \mathcal{O} . The situation is illustrated in Fig. 12.

To make the correspondence between \mathcal{A}_{1100} and \mathcal{O} , let A be the system coming in from $\mathcal{A}_{A,start}$, B the system coming in from $\mathcal{A}_{B,start}$, E the system going to $\mathcal{A}_{A,end}$ and F the

system going to $\mathcal{A}_{B,\text{end}}$. To show that an adversary with removable \mathcal{A}_{1100} can do no better than an adversary with no vertices in the target region, with \mathcal{O} the quantum operation implemented by \mathcal{A}_{1100} , let $\mathcal{O}_{A,\text{in}}^{(x)}$, $\mathcal{O}_{A,\text{out}}^{(x)}$, $\mathcal{O}_{B,\text{in}}^{(x)}$ and $\mathcal{O}_{B,\text{out}}^{(x)}$ be the operations for the replacement in Eq. (18). We modify the other components of the adversary circuit to eliminate \mathcal{A}_{1100} . For this purpose, we modify \mathcal{A}_{in} and its outgoing edges so that \mathcal{A}_{in} randomly selects x with probability distribution $\mu(x)$ and sends x to both $\mathcal{A}_{A,\text{start}}$ and $\mathcal{A}_{B,\text{start}}$ by adding it to its outgoing edges. After completing their existing quantum operations, $\mathcal{A}_{A,\text{start}}$ and $\mathcal{A}_{B,\text{start}}$ apply $\mathcal{O}_{A,\text{in}}^{(x)}$ to A and $\mathcal{O}_{B,\text{in}}^{(x)}$ to B , respectively, producing systems C, C' and D, D' . They then send C and D to $\mathcal{A}_{A,\text{end}}$, and C' and D' to $\mathcal{A}_{B,\text{end}}$, along with x . Upon receiving these systems and x , $\mathcal{A}_{A,\text{end}}$ and $\mathcal{A}_{B,\text{end}}$ apply $\mathcal{O}_{A,\text{out}}^{(x)}$ to C and D , and $\mathcal{O}_{B,\text{out}}^{(x)}$ to C' and D' , which after averaging over x , reproduces the outputs they previously obtained from \mathcal{A}_{1100} in the original circuit.

Removable quantum operations include quantum routers that forward subsystems from the inputs to the outputs, and semiclassical operations that decohere the inputs in a product basis and map each basis element to a separable state. To implement the latter in the form given on the right-hand side of Eq. (18), decoherence is implemented by operations $\mathcal{O}_{A,\text{in}}$ and $\mathcal{O}_{B,\text{in}}$ that do not depend on the classical variable x introduced below. These operations implement the decoherence in their respective bases and copy their decohered states to their outputs. Let the basis elements of A and B be denoted by $|a\rangle_A$ and $|b\rangle_B$, where a and b range over finite index sets. The semiclassical operation produces, for each product state $|a\rangle_A |b\rangle_B$, a separable state. We express this separable state as an explicit mixture $\sum_{x_{a,b}} \mu_{a,b}(x_{a,b}) |\phi(x_{a,b})\rangle_E |\psi(x_{a,b})\rangle_F$, where for each a, b , $\mu_{a,b}(x_{a,b})$ is a probability distribution on a finite set depending on a, b . We let the variable x be a list $(x_{a,b})_{a,b}$, where each $x_{a,b}$ is independently distributed with probability distribution $\mu_{a,b}(x_{a,b})$. The operations $\mathcal{O}_{A,\text{out}}^{(x)}$ and $\mathcal{O}_{B,\text{out}}^{(x)}$ are then designed to independently prepare the states $|\phi(x_{a,b})\rangle_E$ and $|\psi(x_{a,b})\rangle_F$, given the inputs $|a\rangle_C |b\rangle_D$ and $|a\rangle_{C'} |b\rangle_{D'}$, respectively. After integrating over the probability distribution of x , this reproduces the original semiclassical operation. Such semiclassical operations include probabilistic classical computations and Markov processes that decohere the inputs in a product basis and perform probabilistic classical computation given the input basis elements to produce a random output, which is then encoded in a fixed output product basis.

C. Test-factor construction

Test factors for detecting adversaries without prior entanglement are constructed to maximize the gain per trial for the actual honest prover. This requires estimates of the conditional probabilities $\sigma(o_{A'}, z_A, z_B | m_{A'}, m_P)$ for the protocol with the actual prover. We obtain such estimates from calibration data obtained before runs of the protocol. Ideally, the prover always responds with $z_A = z_B$. However, in the experiment we observe trials where $z_A \neq z_B$. The method for estimating $\sigma(o_{A'}, z_A, z_B | m_{A'}, m_P)$ is described in Sect. VI. Here, we assume that $\sigma(o_{A'}, z_A, z_B | m_{A'}, m_P)$ is given. The associated trial-wise probability distribution is

$$\sigma(o_{A'}, z_A, z_B, m_{A'}, m_P) = \sigma(o_{A'}, z_A, z_B | m_{A'}, m_P) \mu_{\text{set}}(m_{A'}, m_P), \quad (19)$$

where $\mu_{\text{set}}(m_{A'}, m_P)$ is the probability of $m_{A'}$ and $m_P = f(u_A, u_B)$, which is determined by the joint distribution of settings and challenges. See Assumption 11. Let \mathcal{P} be the polytope of

conditional distributions $\mu(o_{A'}, z_A, z_B | m_{A'}, b, b')$ that are three-party non-signaling. See [61] for a detailed treatment of the geometry and extremal structure of \mathcal{P} . For such a $\mu \in \mathcal{P}$, define

$$\mu(o_{A'}, z_A, z_B, m_{A'}, b, b') = \mu(o_{A'}, z_A, z_B | m_{A'}, b, b') \mu_{\text{set}}(m_{A'}, b) \delta_{b, b'}. \quad (20)$$

We can maximize the gain by solving the following problem:

Gain optimization problem:

Given: Conditional probabilities $\sigma(o_{A'}, z_A, z_B | m_{A'}, m_P)$.

Maximize over W :

$$\begin{aligned} \text{Exp}_\sigma(\log(W)) = \\ \sum_{o_{A'}, z_A, z_B, m_{A'}, m_P} \log(W(m_{A'}, o_{A'}, m_P, z_A, z_B)) \sigma(o_{A'}, z_A, z_B, m_{A'}, m_P). \end{aligned} \quad (21)$$

Constraints:

$$\begin{aligned} W &\geq 0, \\ \text{Exp}_\mu(W) &= \sum_{o_{A'}, z_A, z_B, m_{A'}, m_P} W(m_{A'}, o_{A'}, m_P, z_A, z_B) \mu(o_{A'}, z_A, z_B, m_{A'}, m_P) \\ &\leq 1 \quad \text{for all } \mu \in \mathcal{P}. \end{aligned} \quad (22)$$

The gain optimization problem requires maximizing a concave function over the convex set \mathcal{P} of three-party non-signaling distributions. For the case of two settings per party and two outcomes for each setting, this can be done directly. To simplify the calculations, we restricted the test factor W to be symmetric under the exchange of z_A and z_B . In our experiment, the probability of $z_A \neq z_B$ is very low, on the order of 10^{-6} . If it is zero, then the probability distribution of $(o_{A'}, z_A, m_{A'}, m_P)$ conditional on $z_A = z_B$ for three-party non-signaling is local realistic, a consequence of the results of Ref. [58] discussed above. With this as motivation, we took advantage of existing strategies for optimizing the gain of test factors in two-party Bell tests against local realism [44]. From calibration data, we estimated the actual prover's probability distribution of $(o_{A'}, z_A, m_{A'}, m_P)$ conditional on $z_A = z_B$, and then determined the gain-optimizing test factor $W_{\text{LR}}(o_{A'}, m_{A'}; z_A, m_P)$ against local realism given this probability distribution. We then considered test factors W of the form

$$W(m_{A'}, o_{A'}, m_P, z_A, z_B) = \delta_{z_A, z_B} W_{\text{LR}}(o_{A'}, m_{A'}; z_A, m_P) + \lambda(1 - \delta_{z_A, z_B}), \quad (23)$$

where λ was chosen to have the largest value for which the resulting W is a test factor against three-party non-signaling, that is, for which W satisfies the constraints of the gain optimization problem. Although these test factors are not gain-optimal, they are robust against variations in the small probability that $z_A \neq z_B$. Empirical tests indicate that for the probability distributions encountered in our experiments, near-optimal gain is achieved.

D. Test factors against small amounts of prior entanglement

We can exclude small amounts of prior entanglement shared by adversaries, depending on the expectation of the chosen test factor that can be achieved by the actual prover. We

quantify entanglement in terms of the robustness of entanglement [62], see also Ref. [63]. For a density matrix ρ , we write $R(\rho)$ for the robustness of entanglement. $R(\rho)$ is an entanglement monotone. For separable states, $R(\rho) = 0$, and for entangled states, $R(\rho) > 0$. In particular, for a bipartite pure entangled state ρ with Schmidt coefficients a_j , we have $R(\rho) = \left(\sum_j a_j\right)^2 - 1$. The significance of robustness of entanglement is that for every bipartite entangled state ρ in finite dimensions, there exist separable states σ and τ such that $\rho = (1 + \xi)\sigma - \xi\tau$ with $\xi = R(\rho)$, and no such representation exists with $0 \leq \xi < R(\rho)$. These properties of robustness of entanglement can be found in Ref. [62]. We also remark that for a bipartite pure state ρ , the Rényi entropy of order 1/2 of its reduced density matrix is given by $S_{1/2} = \log(R(\rho) + 1)$, which establishes a direct connection between the robustness of entanglement and a conventional entropic measure.

Consider a test factor W for the position verification protocol against adversaries without prior entanglement. Let \bar{w}_{\min} be the average over settings and challenges of the minimum value of W conditional on the settings and challenges, that is

$$\bar{w}_{\min} = \sum_{m_{A'}, m_P} \mu_{\text{set}}(m_{A'}, m_P) \min_{o_{A'}, z_A, z_B} W(m_{A'}, o_{A'}, m_P, z_A, z_B). \quad (24)$$

Since the probability distribution of settings and challenges is fixed, the expectation of W is at least \bar{w}_{\min} . Without loss of generality, we may assume that $\bar{w}_{\min} < 1$, as the test factor is otherwise useless for the position verification protocol. If the entangled state ρ of the two subsystems $\mathcal{Q}_{A'}\mathcal{J}_{A_A}$ and \mathcal{J}_{A_B} on leaving the causal past \mathcal{M}_{in} of the trial satisfies $R(\rho) = \xi' \leq \xi$, then we represent the state as an affine combination of separable states σ and τ as $(1 + \xi')\sigma - \xi'\tau$. By construction, the expectation of W for each of σ and τ is between \bar{w}_{\min} and 1. By linearity over the affine combination of the expectation of W , the expectation of W for state ρ is at most $(1 + \xi') - \xi'\bar{w}_{\min} = 1 + \xi'(1 - \bar{w}_{\min}) \leq 1 + \xi(1 - \bar{w}_{\min})$. Let $\bar{w}_u = 1 + \xi(1 - \bar{w}_{\min})$. This implies that W/\bar{w}_u is a test factor against adversaries whose prior entanglement has robustness bounded from above by ξ . By using the test factor W/\bar{w}_u for each trial, we can effectively reject such adversaries.

We can also test the hypothesis that adversaries have prior entanglement with average robustness below some threshold, averaged over all trials. For this, suppose that at trial k , conditional on the past, the adversaries have prior entanglement with robustness Ξ_k . We treat Ξ_k as a random variable determined by the past of trial k . Let W_k denote the instantiation of the test factor W on the record of the k 'th trial. Conditional on the past, Ξ_k takes on a specific, determined value ξ_k , and the expectation of W_k given this past is at most $1 + \xi_k(1 - \bar{w}_{\min}) \leq e^{\xi_k(1 - \bar{w}_{\min})}$. Equivalently, the past-conditional expectation of $W_k e^{-\Xi_k(1 - \bar{w}_{\min})}$ is at most 1. By the law of total expectation, the product Z of $W_k e^{-\Xi_k(1 - \bar{w}_{\min})}$ over the trials also has expectation at most 1. By Markov's inequality, we have $\mathbb{P}(Z > 1/\delta) \leq \delta \text{Exp}(Z)$, where $\delta > 0$ is the desired soundness parameter. Rearranging the inequality in this expression, we conclude that the probability that

$$\frac{1}{n(1 - \bar{w}_{\min})} \left(\sum_k \log(W_k) - \log(1/\delta) \right) \geq \frac{1}{n} \sum_k \Xi_k \quad (25)$$

is at most δ . We can therefore take the left-hand side of this inequality as a lower bound on the average robustness of entanglement that the adversaries must share prior to each trial in order to pass the protocol with probability at least $1 - \delta$. We modify the protocol so that it succeeds when the lower bound on the average robustness certified at

soundness parameter δ exceeds a threshold chosen ahead of time. Let r_{th} be the chosen threshold for average robustness of entanglement per trial. Then, to pass the protocol we require $\frac{1}{(1-\bar{w}_{\text{min}})^n}(\sum_k \log(W_k) - \log(1/\delta)) \geq r_{\text{th}}$. We can rewrite this inequality as $\prod_k W_k e^{-r_{\text{th}}(1-\bar{w}_{\text{min}})} \geq 1/\delta$. Therefore, it suffices to replace the trial-independent test factor in Protocol 1 by $W e^{-r_{\text{th}}(1-\bar{w}_{\text{min}})}$ to test against adversaries with prior entanglement.

Before the run of the protocol, the verifiers determine, the values of the robustness threshold r_{th} for which the actual prover has a high probability of passing the protocol given enough trials. Suppose that the test factor W against adversaries without prior entanglement has gain $g = \text{Exp}(\log(W))$ for the actual prover, and define \bar{w}_{min} as above. For n trials with the actual prover, the expectation of the left-hand side in Eq. 25 is $g/(1-\bar{w}_{\text{min}}) - \log(1/\delta)/(n(1-\bar{w}_{\text{min}}))$. The term multiplying $\log(1/\delta)$ goes to zero as $n \rightarrow \infty$, so given sufficiently many trials, it is possible to reject adversaries with average robustness of entanglement per trial up to $g/(1-\bar{w}_{\text{min}})$.

Any test factor W for QPV against adversaries without prior entanglement can be used in the above expressions to also test against adversaries with prior entanglement. For the experiment, we modify W to minimize the number of trials required to ensure that the actual prover can pass the protocol with chosen threshold r_{th} and with sufficiently high probability. The modification consists of replacing W with $W' = \lambda W + (1-\lambda)$ and minimizing the required number of trials over $\lambda \in [0, 1/(1-w_{\text{min}})]$, where w_{min} is the minimum value that W can take. See Sect. VIA for details.

VI. ANALYSIS OF EXPERIMENTAL RESULTS

The data analysis consists of three main steps: parameter determination, calibration prior to each protocol instance, and execution of each instance. For the first step, parameter determination, we used data collected on September 19, 2024 and use this data to estimate the distribution of the trial records for the implemented prover. We refer to a prover for whom the trial records are i.i.d. according to the estimated distribution as the reference prover. This prover is honest. The second and third steps—calibration and analysis—were performed using data collected on September 20 and October 7, 2024. On each day, the data was saved across a varying number of files, with each file containing one minute of data. The trial rate in our experiment is approximately 250,000 trials per second.

A. Parameter Determination

The first step of data analysis is to determine key parameters necessary for evaluating the protocol. These parameters include:

1. The *soundness error* δ ,
2. The *target success probability* ϵ for the reference prover,
3. The *number of trials* n (the amount of data) to be used per protocol instance, and
4. The *success threshold* r_{th} on the certified average robustness of entanglement pre-shared by adversaries for implementing a successful attack.

We fixed the soundness error to $\delta = 2^{-64}$, which is considered sufficiently small for practical security purposes. In addition, we set the target success probability to $\epsilon = 0.97725$, corresponding to a two-sigma confidence level.

The procedure for determining the remaining parameters is as follows. In the case where the adversaries under consideration do not share prior entanglement, we examine the trade-off between the number of trials n and the soundness error δ (that is, the p -value threshold). We choose n such that for the reference prover, the observed p -value falls below δ with probability at least $\epsilon = 0.97725$. To consider adversaries with bounded prior entanglement, we analyze how n affects the achievable success threshold r_{th} , which serves as a lower bound on the entanglement per trial required for the adversaries to succeed. In this case, n and r_{th} are selected jointly to ensure that for the reference prover, the resulting p -value falls below δ with probability at least $\epsilon = 0.97725$. To estimate these probabilities, we proceed as follows: First, we use data collected on September 19, 2024 to estimate the conditional distribution of measurement outcomes given the settings. We refer to this data as the calibration data for parameter determination. Second, we determine a high-gain test factor for the estimated distribution. And finally, we analyze the statistical behavior of the logarithm of the test factor for the reference prover.

We begin by estimating the conditional distribution $\sigma(o_{A'}, z_A, z_B | m_{A'}, m_P)$ from calibration data. The calibration data can be summarized by counts $n(o_{A'}, z_A, z_B; m_{A'}, m_P)$. These counts are the number of trials for which the settings $(m_{A'}, m_P)$ and outcomes $(o_{A'}, z_A, z_B)$ were recorded. A representative example of the counts for each such combination of values for the trials obtained in one 5-minute run is shown in Tab. V, and this example is used as the calibration data for parameter determination. Ideally, we always have $z_A = z_B$, but in practice, due to technical imperfections, z_A and z_B occasionally differ. Such differences can also arise from adversarial manipulations, where an adversary may sacrifice the probability of returning identical responses to improve performance conditional on a match. In the experiment, the observed frequency of such differences was normally less than $d = 2 \times 10^{-6}$. Because differences occur rarely, we regularize the four conditional probabilities $\sigma(o_{A'}, z_A, z_B | m_{A'}, m_P)$ given settings $(m_{A'}, m_P)$ with $z_A \neq z_B$ by setting all of them to the fixed value $d/4 = 0.5 \times 10^{-6}$ for the purpose of constructing test factors and choosing protocol parameters. When constructing test factors, we constrain the test factor to take a constant value for all settings and outcomes with $z_A \neq z_B$. Consequently, all such events contribute identically to the logarithm of the test factor, and so the choice of a uniform distribution over these events in the regularization does not affect the gain calculation.

TABLE V. Calibration counts $n(o_{A'}, z_A, z_B; m_{A'}, m_P)$ for settings $(m_{A'}, m_P)$ and outcomes $(o_{A'}, z_A, z_B)$. All settings and outcomes are binary with two possible values denoted by 1, 2. The first four columns correspond to cases where $z_A = z_B$, while the last column aggregates all cases where $z_A \neq z_B$. These counts are based on 5 minutes of data collected on September 19, 2024. Random resampling suggests that this amount of data is sufficient for a reliable estimation of the underlying conditional distribution.

		$(o_{A'}, z_A, z_B)$				
		(1, 1, 1)	(2, 1, 1)	(1, 2, 2)	(2, 2, 2)	Others
$(m_{A'}, m_P)$	(1, 1)	18,764,031	2,339	2,390	4,794	16
	(2, 1)	18,751,159	9,481	1,647	5,474	29
	(1, 2)	18,752,299	1,527	6,879	5,730	32
	(2, 2)	18,745,211	14,655	12,333	364	35

Instead of directly determining the conditional distribution $\sigma(o_{A'}, z_A, z_B | m_{A'}, m_P)$ by fit-

ting the observed counts, we first restrict the counts to the events where $z_A = z_B$. We define the restricted counts as $\tilde{n}(o_{A'}, o_P; m_{A'}, m_P) = n(o_{A'}, o_P, o_P; m_{A'}, m_P)$ for each combination of settings $(m_{A'}, m_P)$ and outcomes $(o_{A'}, o_P)$. The counts $\tilde{n}(o_{A'}, o_P; m_{A'}, m_P)$ determine empirical conditional frequencies

$$\tilde{f}(o_{A'}, o_P | m_{A'}, m_P) = \tilde{n}(o_{A'}, o_P; m_{A'}, m_P) / \sum_{o_{A'}, o_P} \tilde{n}(o_{A'}, o_P; m_{A'}, m_P). \quad (1)$$

If the probability that $z_A \neq z_B$ is zero, the counts and frequencies are sampled according to some conditional distribution $\tilde{\sigma}(o_{A'}, o_P | m_{A'}, m_P)$, which must be in the set $\mathcal{Q}_{O_{A'}, O_P | M_{A'}, M_P}$ of two-party non-signaling distributions that satisfy Tsirelson's bounds. Here we do not consider other quantum constraints. The set $\mathcal{Q}_{O_{A'}, O_P | M_{A'}, M_P}$, as characterized in Sect. IX. A of Ref. [64], forms a convex polytope. We fit $\tilde{\sigma}(o_{A'}, o_P | m_{A'}, m_P) \in \mathcal{Q}_{O_{A'}, O_P | M_{A'}, M_P}$ to the frequencies $\tilde{f}(o_{A'}, o_P | m_{A'}, m_P)$ by maximum likelihood. That is, we obtain the estimate $\tilde{\sigma}(o_{A'}, o_P | m_{A'}, m_P)$ as the unique optimal solution of the following constrained maximum-likelihood problem:

$$\begin{aligned} \arg \max_{\mu(o_{A'}, o_P | m_{A'}, m_P)} & \sum_{o_{A'}, o_P, m_{A'}, m_P} \tilde{n}(o_{A'}, o_P; m_{A'}, m_P) \log \mu(o_{A'}, o_P | m_{A'}, m_P) \\ \text{subject to} & \mu(o_{A'}, o_P | m_{A'}, m_P) \in \mathcal{Q}_{O_{A'}, O_P | M_{A'}, M_P} \end{aligned} \quad (2)$$

The estimate obtained is shown in Tab. VI. We then determine the conditional probabilities $\sigma(o_{A'}, z_A, z_B | m_{A'}, m_P)$ as follows:

$$\sigma(o_{A'}, z_A, z_B | m_{A'}, m_P) = \delta_{z_A, z_B} (1 - d) \tilde{\sigma}(o_{A'}, O_P = z_A | m_{A'}, m_P) + (1 - \delta_{z_A, z_B}) d/4. \quad (4)$$

TABLE VI. The settings-conditional distribution of outcomes $\tilde{\sigma}(o_{A'}, o_P | m_{A'}, m_P)$ obtained by maximum likelihood using the calibration data in Tab. V. This probability distribution is used solely for determining key parameters in the position verification protocol and not intended to make a statement about the actual probability distribution during the calibration or analysis phase of each instance of the protocol. All displayed values are rounded to 10 digits after the decimal point.

		$(o_{A'}, o_P)$			
		(1, 1)	(2, 1)	(1, 2)	(2, 2)
$(m_{A'}, m_P)$	(1, 1)	0.9994906521	0.0001264110	0.0001261772	0.0002567597
	(2, 1)	0.9991117479	0.0005053152	0.0000885493	0.0002943876
	(1, 2)	0.9992478451	0.0000802128	0.0003689843	0.0003029579
	(2, 2)	0.9985476132	0.0007804446	0.0006526840	0.0000192581

Next, following the discussion in Sect. VC, we construct a test factor for the two-party Bell test using the strategy developed in Ref. [44]. This test factor is optimal for rejecting local realism [44] with respect to the settings-conditional distribution of outcomes $\tilde{\sigma}(o_{A'}, o_P | m_{A'}, m_P)$ shown in Tab. VI, given a uniform settings distribution $\mu_{\text{set}}(m_{A'}, m_P)$ defined as $\mu_{\text{set}}(m_{A'}, m_P) = 1/4$ for all $m_{A'}, m_P \in \{1, 2\}$. Building on this, we construct a family of test factors of the form given in Eq. (23), parameterized by λ . By maximizing λ , we obtain a well-performing test factor, as presented in Tab. VII, for the task of position verification against adversaries without prior entanglement. From now on, we refer to this

TABLE VII. Trial-wise test factor $W(m_{A'}, o_{A'}, m_P, z_A, z_B)$ for basic position verification, constructed using the calibration data in Tab. V. The four columns shown correspond to cases where $z_A = z_B$. For all other cases with $z_A \neq z_B$, which are not displayed in the table, the test factor takes a constant value of 0.9118409194, independent of the settings and outcomes. All displayed values are rounded to 10 digits after the decimal point.

		$(o_{A'}, z_A, z_B)$			
		(1, 1, 1)	(2, 1, 1)	(1, 2, 2)	(2, 2, 2)
(m_A, m_P)	(1, 1)	1.0000133425	0.8853069445	0.8825655759	1.0836976498
	(2, 1)	1.0000098326	0.9751727669	0.8016191273	1.0926205335
	(1, 2)	1.0000079803	0.7988759064	0.9699591897	1.0846655877
	(2, 2)	0.9999688446	1.0248059103	1.0300176352	0.7390162290

task as basic position verification and to the corresponding protocol as the basic protocol. In addition to its role in parameter determination below, this test factor could also be used to analyze future data for basic position verification.

Finally, we analyze the statistical behavior of the logarithm of the obtained test factor. According to our estimates of $\sigma(o_{A'}, z_A, z_B | m_{A'}, m_P)$ in Eq. (4), $\tilde{\sigma}(o_{A'}, o_P | m_{A'}, m_P)$ in Tab. VI, and the uniform settings distribution used in our implementation, the base-2 logarithm of the trial-wise test factor shown in Tab. VII, $\log_2(W)$, has a mean of $g_w = 3.79135 \times 10^{-6}$ and a variance of $v_w = 1.13029 \times 10^{-5}$. For the completeness analysis, we assume the reference prover so that the trials are i.i.d. and distributed according to the above estimates. We consider the case where the test factor W_k used in each trial k is identical to the one presented in Tab. VII. In view of the central limit theorem, we approximate the sum $\sum_{k=1}^n \log_2(W_k)$ over n i.i.d. trials as normally distributed with mean ng_w and variance nv_w . For a given soundness error δ , the condition $\sum_{k=1}^n \log_2(W_k) \geq \log_2(1/\delta)$ must be satisfied to ensure a p -value below δ . Accordingly, the success probability of obtaining a p -value less than δ after n trials is heuristically estimated to be $p_{\text{succ}} = Q(- (ng_w - \log_2(1/\delta)) / \sqrt{nv_w})$, where the function Q is the tail distribution function of the standard normal distribution. To ensure $p_{\text{succ}} \geq \epsilon$, the number of trials n must be above a certain threshold. By varying the values of δ and ϵ , we obtain the trade-off curves in Fig. 13. The trade-off curves show the value of δ that can be achieved at three different success probabilities as a function of the running time of the basic protocol. For the chosen values $\delta = 2^{-64}$ and $\epsilon = 0.97725$, the figure shows that 2 minutes of data is sufficient for basic position verification.

Similarly, we analyze the behavior of the test factor adapted for position verification in the presence of adversaries with bounded prior entanglement. Following Sect. VD, we consider trial-wise test factors of the form $W' = \lambda W + (1 - \lambda)$, where $\lambda \in [0, 1/(1 - w_{\min})]$ and w_{\min} is the minimum value of the test factor W for basic position verification. Let \bar{w}'_{\min} , defined analogously to \bar{w}_{\min} in (24), denote the average of the minimum values of the test factor W' conditioned on the measurement settings and challenges. Let W'_k represent the instantiation of the test factor W' used in the k 'th trial. Given n trials and a soundness error δ , the certified lower bound on the average robustness of prior entanglement is given by

$$\frac{1}{n(1 - \bar{w}'_{\min})} \left(\sum_k \log(W'_k) - \log(1/\delta) \right). \quad (5)$$

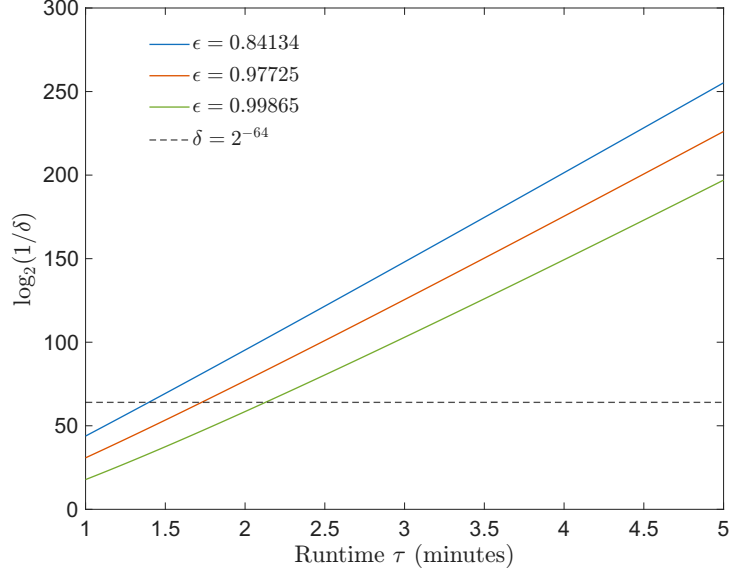


FIG. 13. Required runtime of the basic protocol (x -axis) to achieve a target soundness error δ (y -axis) with high probability. For a desired soundness error δ to be achieved with success probability at least ϵ , the experiment must run for at least the duration τ indicated on the x -axis. The three curves correspond to confidence levels of one-sigma ($\epsilon = 0.84134$), two-sigma ($\epsilon = 0.97725$), and three-sigma ($\epsilon = 0.99865$), respectively. In our experiment, we generate approximately 250,000 trials per second. For parameter determination, we assume that the trial generation rate is exact.

Thus, to ensure that the certified lower bound exceeds the threshold r_{th} , we must have

$$\sum_k \log(W'_k) \geq nr_{\text{th}}(1 - \bar{w}'_{\min}) + \log(1/\delta). \quad (6)$$

To characterize the statistical behavior of this condition, we compute the mean and variance of the random variable $\log(W')$. As before, we resort to the central limit theorem to estimate the success probability for the reference prover. For each desired success probability ϵ and each fixed value of the threshold r_{th} , we optimize over the parameter λ that characterizes the test factor W' . This optimization allows us to determine the minimum value of n required to satisfy the condition in Eq. (6) with success probability ϵ . This process also yields the corresponding optimized test factor W' , which could be used to analyze future data for position verification against adversaries with prior entanglement. Varying the values of ϵ and r_{th} yields the requirement curve illustrated in Fig. 14. Based on this figure, we set $r_{\text{th}} = 8 \times 10^{-6}$. For the chosen values of $\delta = 2^{-64}$ and $\epsilon = 0.97725$, the figure shows that 4 minutes of data is sufficient for position verification against adversaries with average robustness of prior entanglement at most r_{th} .

B. Calibration and Analysis

With the protocol parameters obtained above, we executed multiple instances of the protocol using data collected on September 20, 2024, for the case of adversaries without prior entanglement, and data collected on October 7, 2024, for the case involving adversaries with limited prior entanglement. On each day, trials were performed and recorded in successive

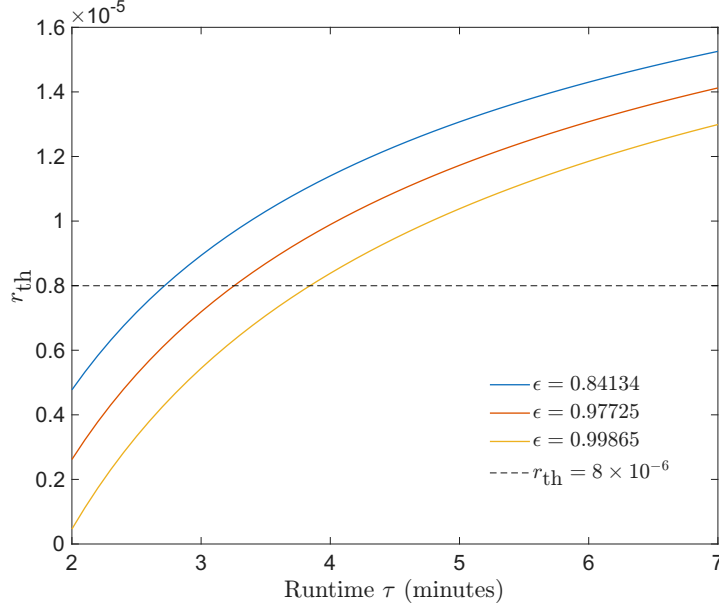


FIG. 14. Required runtime (x -axis) to ensure, with high probability, that the certified average robustness of entanglement pre-shared by adversaries reaches the target success threshold r_{th} (y -axis). The certification is performed with soundness error $\delta = 2^{-64}$. For a desired success threshold r_{th} to be reached with success probability at least ϵ , the experiment must run for at least the duration τ indicated on the x -axis. The three curves correspond to confidence levels of one-sigma ($\epsilon = 0.84134$), two-sigma ($\epsilon = 0.97725$), and three-sigma ($\epsilon = 0.99865$), respectively.

1-minute intervals, resulting in separate 1-minute data files with about 15 million trials each. The data was blinded until after the protocol parameters and analysis strategies were fixed. The protocol implementation and analysis are summarized in Protocol 2. Because the performance of the Bell test underlying the protocol varied in time, we optimized the test factor to be used for each instance of the protocol based on the 10 1-minute files immediately preceding the instance that are free of detection errors as described in the next paragraph. We refer to this data as the calibration data for the instance. For each instance, we used the calibration data to estimate the settings-conditional distribution of outcomes and to construct the corresponding test factor, following the approach described in Sect. VI A.

In our experiment, some 1-minute recording intervals experienced detector errors, an event that happened at most a few times per day. Such errors were recorded with the corresponding data files. At the beginning of each day, the first 10 1-minute files free of detector errors were used for calibration of the first protocol instance of the day. The next 2 or 4 files, regardless of whether or not detector errors happened, made up the first protocol instance, depending on whether the adversaries had no prior entanglement or bounded prior entanglement, respectively. Subsequent instances were processed sequentially using the next 2 or 4 files if available; otherwise the instance used all the remaining data files. For each such instance, calibration data consisted of the previous 10 files without detector errors.

Nominally, each 2-minute interval consists of 30 million trials, and each 4-minute interval consists of 60 million trials. However, due to clock synchronization and other uncertainties in our experiment, the actual number of recorded trials deviates from these nominal values. To ensure the validity of the analysis, we fixed the number of trials n processed to exactly

30 million for each 2-minute interval and 60 million for each 4-minute interval. If the actual number of trials exceeded n , the data were truncated and the excess trials were discarded. If it fell short, artificial trials were appended to reach n trials. In either case—whether testing for adversaries with prior entanglement or without—the appended artificial trials were analyzed using the trivial test factor that assigns a value of 1 to all possible measurement settings and outcomes, which is a valid choice. Consequently, the specific settings and outcomes assigned to each artificial trial are irrelevant. Since the logarithm of 1 is 0, these artificial trials did not contribute to the accumulated sum of the logarithms of the trial-wise test factors and thus did not influence the final analysis result. Therefore, in practice, it is not necessary to physically append artificial trials if the actual number of trials is less than n . This approach ensures the correctness of the analysis regardless of

fluctuations in the actual number of trials available for processing.

Protocol 2: Protocol Implementation and Analysis.

Input : Sequence of 1-minute data files collected in a day.

Given :

$\delta = 2^{-64}$ — soundness error (i.e., p -value threshold).

$\epsilon = 0.97725$ — target success probability for the reference prover.

n — number of analysis trials: 3×10^7 (nominally, 2-minute data) or 6×10^7 (nominally, 4-minute data), depending on the adversary model.

$r_{\text{th}} = 8 \times 10^{-6}$ — threshold on the certified average robustness of entanglement for adversaries with bounded prior entanglement.

Output: P — binary success flag: $P = 1$ (success) or $P = 0$ (failure).

Identify the 10th file in the sequence that is free of detector errors, and set the current file to the one immediately following it;

foreach *protocol instance* **do**

Set $P \leftarrow 0$;

Initialize the running number of calibration files: $K_{\text{calib}} \leftarrow 0$;

Initialize the running calibration counts for all settings $z = (m_{A'}, m_P)$ and outcomes $c = (o_{A'}, z_A, z_B)$: $\{\text{Data}_{\text{calib}}(cz)\}_{cz} \leftarrow 0$;

while *a previous 1-minute file exists* **do**

if *file has no detector error* **then**

 Load file; increment $K_{\text{calib}} \leftarrow K_{\text{calib}} + 1$;

 Increment $\{\text{Data}_{\text{calib}}(cz)\}_{cz}$ with counts from the file;

end

if $K_{\text{calib}} = 10$ **then**

break;

 // Load up to 10 files for calibration

end

end

Use $\{\text{Data}_{\text{calib}}(cz)\}_{cz}$ to estimate the settings-conditional distribution of outcomes for the purpose of test-factor construction (see Sect. VIA);

Construct test factor W (for adversaries without prior entanglement) or W' (for adversaries with bounded prior entanglement) as in Sect. VIA;

Load the trials from the next 2 or 4 1-minute files, if available. Otherwise, load from all remaining files. Truncate to n trials if necessary;

Compute the accumulated sum of the logarithms of test factors S_{run} . For adversaries with prior entanglement, return the certified lower bound r_{lb} on the average robustness of entanglement according to Eq. (5) with the replacement of $\sum_k \log(W'_k)$ with S_{run} ;

Calculate the success threshold $S_{\text{th}} = \log(1/\delta)$ for adversaries without prior entanglement and $S_{\text{th}} = \log(1/\delta) + nr_{\text{th}}(1 - \bar{w}'_{\text{min}})$ for adversaries with bounded prior entanglement;

if $S_{\text{run}} \geq S_{\text{th}}$ **then**

 Set $P \leftarrow 1$;

 // Protocol succeeded

end

Update the current file to the file immediately following the ones used for this protocol instance, if this is not the last instance;

end

The analysis procedure follows the implementation outlined in Protocol 2. Before unblinding the protocol instance data and conducting the final analysis, we validated that the protocol including the parameter determination functioned correctly using data collected on September 19, 2024. We then proceeded with the final analysis. Using 474 1-minute data files collected on September 20, 2024, we performed basic position verification, resulting in 232 instances, 8 of which failed. For position verification against adversaries with bounded prior entanglement, we used the 420 1-minute data files collected on October 7, 2024 to perform 103 instances. All but the final instance succeeded; the last one failed due to insufficient remaining data. Histograms of the analysis results are presented in Fig. 15. After completing the analysis of the protocol instances on the unblinded data, for diagnostic purposes, we reversed the data assignment for the two types of analyses. In the reversed analysis, using the data from September 20, 2024, we obtained 116 instances of position verification against adversaries with bounded prior entanglement, with 10 instances failing. Using the data from October 7, 2024, we obtained 205 instances of basic position verification, all of which succeeded. The results of the reversed analysis are shown in Fig. 16.

In the analysis described above, we certified a lower bound r_{lb} on the average robustness of prior entanglement to quantify the resources required for a successful adversarial attack. Alternatively, we can formulate this as a hypothesis-testing task: we aim to reject the null hypothesis that the average robustness of entanglement pre-shared by adversaries is bounded above by a specific threshold r_{th} . For this purpose, we introduce a modified test factor $W'' = W'e^{-r_{\text{th}}(1-\bar{w}'_{\text{min}})}$, where W' is the test factor used for certifying the average robustness, and \bar{w}'_{min} is the corresponding averaged minimum value (see Sect. VI A for details on determining W' and \bar{w}'_{min}). Let W''_k denote the instantiation of the modified test factor for the k 'th trial. Following the discussion below Eq. (25), we compare the accumulated product over all trials, $\prod_k W''_k$, against $1/\delta$ to determine whether the protocol instance successfully rejects the null hypothesis. When the number of available trials meets or exceeds the required number of trials n for the instance, we analyze exactly n trials. In this case, the rejection condition $\prod_k W''_k \geq 1/\delta$ is equivalent to satisfying Eq. (6). If the number of available trials is less than n , we virtually append artificial trials for which we set $W' = 1$. For each such artificial trial, $\text{Exp}(W'') = \text{Exp}(W'e^{-r_{\text{th}}(1-\bar{w}'_{\text{min}})}) \leq 1$ for adversaries with bounded average robustness, so the analysis according to the discussion below Eq. (25) in Sect. V D remains valid. Among the 103 instances using the data from October 7, 2024, there were 4 instances where the available number of analysis trial was less than n . The logarithm of the product $\prod_k W''_k$ for each instance using the data from October 7, 2024 is shown in the bottom panel of Fig. 4 of the main text.

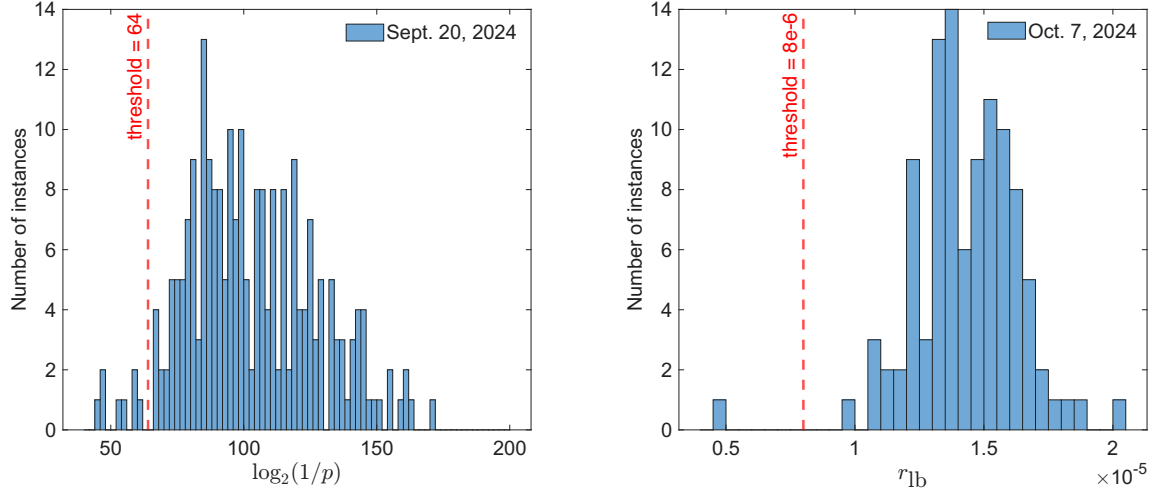


FIG. 15. Histograms of the final analysis results. The left panel shows the results for basic position verification, while the right is for position verification against adversaries with bounded prior entanglement. The histograms show the number of instances binned according to the $\log(p)$ -value and the certified lower bound r_{lb} on the average robustness of prior entanglement, respectively. These values are determined by the accumulated sum of the logarithms of the trial-wise test factors used in each instance. The value of r_{lb} is given by Eq. (5) for each instance.

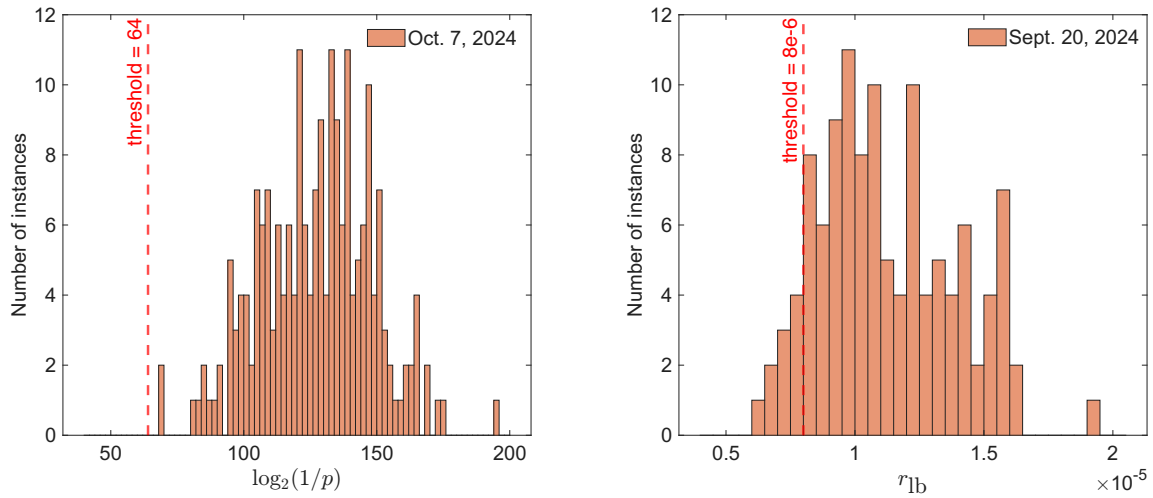


FIG. 16. Histograms of the reversed analysis results. The left panel shows the results for basic position verification, while the right is for position verification against adversaries with bounded prior entanglement. The plotted quantities are defined in the caption of Fig. 15.